CHAPTER 7

AERODYNAMICS OF BODIES FROM MOTION ANALYSIS

by

Gary T. Chapman, Donn B. Kirk,
and Gerald N. Malcolm

NASA – Ames Research Center

AERODYNAMICS OF BODIES FROM MOTION ANALYSIS

Gary T.Chapman, Donn B.Kirk,
and Gerald N.Malcolm

7.1 INTRODUCTION

The purpose of this chapter is to examine a number of techniques for determining the aerodynamic characteristics of bodies in free flight in a ballistic range. The measurements from which the aerodynamics are to be deduced usually consist of angular and linear position data from photographic records of a model in flight, such as shadowgraphs; they could conceivably be acceleration data obtained from onboard accelerometers, or velocity data obtained from onboard integrating accelerometers or rate gyros. With gun-launched models, the accelerations and velocities are not usually measured, since at the present state of development accelerometers and transmitters cannot withstand the launch loads imposed by the gun (see Chapter 12). The discussions in this chapter will therefore be restricted to the analysis of angular and linear position data as functions of either time or distance traveled.

There are basically two approaches to the problem of obtaining aerodynamics of bodies from such data. The first is to curve-fit the position and angular orientation data and differentiate the fitted curves twice to obtain the appropriate accelerations. These accelerations are directly related through Newton's laws of motion to the aerodynamic forces and moments acting on the body. This technique presents no problems in mathematics, but does require data of very high precision. The second approach is to consider the differential equations which govern the motion and perform the appropriate integrations to obtain solutions for the position and angular orientation as functions of time or distance. These solutions are then curve-fit to the data to yield the aerodynamic characteristics of the body. This approach does lead to problems in mathematics. The differential equations are highly nonlinear and in general cannot be solved in closed form.

Much work has been done by many people on this latter approach. The original contributions in this field were by Lanchester[7.1] at the turn of the century. His work was mainly restricted to the analysis of airplane-type motions in which he considered only small deviations from a steady-state glide-path, linear aerodynamics, and small roll rates. Since ballistics studies generally involved high roll rates and symmetric bodies, the ballistician had to take a somewhat different approach from Lanchester's. The original analysis of symmetric spinning bodies was conducted by Fowler and his associates in 1920 (References 7.2 and 7.3). Because the two areas, aerodynamics and ballistics, originally had so little in common, they developed independently. With the arrival of guided missiles, in particular, airplane-launched missiles, the aerodynamicist was confronted with the same problems as the ballistician and was not familiar with ballistics or ballistic terminology. Bolz[7.4], Nicolaides[7.5] and Charters[7.6] did much to alleviate this situation. They made an attempt to merge the approaches of the ballistician and the aerodynamicist and to clarify the differences in nomenclature between the two. All of this work was predominantly for linear aerodynamics. The introduction of nonlinear aerodynamics was done by such people as Murphy and Rasmussen in the early 1960's[7.7,7.8].

With the advent of the electronic computer, the application of many of the above procedures was greatly enhanced; but even more importantly a completely different approach to the problem was made possible. That approach is to curve-fit the position and angular orientation data using the differential equations directly by employing numerical integrations. A method for applying this technique is described in Section 7.8.2.

Much of the work in the field of dynamics, in particular, ballistics and aerodynamics, has been to describe the motion, given a set of aerodynamic coefficients. Although some attention will be directed to this problem, throughout most of this chapter emphasis will be placed on the inverse problem. That is, given the equations for the motion, determine the aerodynamic coefficients which best describe that motion. This problem is not nearly as unique since it is not known a priori what the functional relationships will be. For instance, it is necessary to assume either that the aerodynamics are linear or nonlinear, and if nonlinear, the form they take.

Because the discussions will be focused on ballistic range data reduction procedures, the derivations of the equations of motion will incorporate assumptions that are pertinent to this type of facility. For example, because ballistic ranges are normally short, the direction of the gravity vector can be assumed not to change. Major assumptions which are implicit in all of the material will be specifically pointed out.

The chapter begins with a discussion of the different coordinate systems used in analyzing free flight data. Once these have been established, the differential equations of motion are derived by considering several ways of writing the equations for flight dynamics and combining these with appropriate expressions for the applied forces and moments. With the equations of motion derived, the various techniques for deducing drag, static and dynamic stability, lift, and rolling moment coefficients (both linear and nonlinear) from the measured data are

discussed. Typical examples are presented and some of the results compared to conventional wind tunnel measurements. The chapter concludes with a section on error analysis and an appendix treating the method of least squares using differential corrections.

7.2 NOTATION

A reference area

C_i force or moment coefficient; i can take the values $x, y, z, \bar{x}, \bar{y}, \bar{z}, D, L, N, S, l, m,$ or n. Some particular coefficients that appear frequently are:

C_D drag coefficient, $\dfrac{\text{drag}}{\frac{1}{2}\rho V^2 A}$

C_L lift coefficient, $\dfrac{\text{lift}}{\frac{1}{2}\rho V^2 A}$

C_m pitching moment coefficient, $\dfrac{\text{moment}}{\frac{1}{2}\rho V^2 A l}$

C_{i_k} partial derivative of C_i with respect to a variable k; k can take the values $\alpha, \dot{\alpha}, \beta, \dot{\beta}, p, \dot{p}, q, \dot{q}, r,$ or $\dot{r}$ (refer to Equation (7.74)). Some particular derivatives that appear frequently are:

C_{L_α} lift-curve slope, $\partial C_L/\partial\alpha$

C_{m_α} moment-curve slope, $\partial C_m/\partial\alpha$

$C_{m_q} + C_{m_{\dot{\alpha}}}$ damping-in-pitch derivative, $\partial C_m/\partial(ql/V) + \partial C_m/\partial(\dot{\alpha}l/V)$

C_{N_α} normal-force-curve slope, $\partial C_N/\partial\alpha$

$C_{i_{kp}}$ partial derivative of C_{i_k} with respect to the roll rate p (Magnus terms)

C_{i_0} value of C_i at zero angle of attack

$\vec{F}$ force vector

F_c Coriolis force

F_i component of force

g gravitational constant

H_n damping moment coefficients, $n = 0, 1, 2, \ldots$.

H_{0_e} effective linear damping

$h_n = \dfrac{1}{2+n}\dfrac{H_n}{H_0}\alpha_a^n$ (Equation (7.201))

I moment of inertia: for an axially symmetric body, $I_{\bar{y}} = I_{\bar{z}} = I$; for a general body oscillating in one plane, I is the moment of inertia about an axis perpendicular to that plane

$I_{\bar{x},\bar{y},\bar{z}}$ roll, pitch, and yaw moments of inertia in body-fixed coordinates

$I_{\tilde{x}}$ roll moment of inertia in fixed-plane coordinates ($I_{\tilde{x}} = I_{\bar{x}}$)

$K = \rho A/2m$

$K_s = \rho Al/2I$

l reference length

$\vec{M}$ moment vector

M_n static moment coefficients, $n = 0, 1, 2, \ldots$.

$\hat{M}_n = -M_n/(\rho V^2 A l/2)$

$M_{l,m,n}$ moment components in body-fixed coordinates

$\tilde{M}_{l,m,n}$	moment components in fixed-plane coordinates
M_∞	Mach number
m	mass
m_n	$M_n\alpha_m^n/M_0$ or $M_n\alpha_a^n/M_0$
p, q, r	components of angular velocity in body-fixed coordinates
$\tilde{p}, \tilde{q}, \tilde{r}$	components of angular velocity in fixed-plane coordinates
P	roll-rate parameter, $(I_{\bar{x}}/I)p = (I_{\tilde{x}}/I)\tilde{p}$
Q_i	generalized force or moment
q_i	generalized coordinate
R_∞	Reynolds number
SD	standard deviation
T	total kinetic energy
$[T]_{A_1/A_2}$	transformation matrix from A_2 coordinate system to A_1 coordinate system
t	time
u, v, w	linear velocity components in earth-fixed coordinates
$\bar{u}, \bar{v}, \bar{w}$	linear velocity components in body-fixed coordinates
$\tilde{u}, \tilde{v}, \tilde{w}$	linear velocity components in fixed-plane coordinates
$\vec{V}$	velocity vector
V	magnitude of velocity vector, $\lvert\vec{V}\rvert$
x, y, z	earth-fixed coordinates
$\bar{x}, \bar{y}, \bar{z}$	body-fixed coordinates
$\tilde{x}, \tilde{y}, \tilde{z}$	fixed-plane coordinates
$\hat{x}, \hat{y}, \hat{z}$	trajectory coordinates
α, β	projection of resultant angle of attack onto x-z plane, onto x-y plane
$\bar{\alpha}, \bar{\beta}$	angle of attack and angle of sideslip in body-fixed coordinates
$\tilde{\alpha}, \tilde{\beta}$	angle of attack and angle of sideslip in fixed-plane coordinates
α_a	defined by $\alpha_a^2 = \frac{1}{2}[(\alpha_m)_k^2 + (\alpha_m)_{k+1}^2]$ where k denotes peak number
α_m	maximum angle of attack
α_R	resultant angle of attack
α_{rms}	root-mean-square angle of attack
Γ	gamma function
γ_1, γ_2	angles relating trajectory axes to earth-fixed axes
θ, ψ, ϕ	projected angles
θ_E, σ, ψ_E	Euler angles
$\theta_{ME}, \psi_{ME}, \phi$	modified Euler angles
θ_a, θ_l	the direction of flight with respect to the local meridian and the geographical latitude of a given facility (Equation (7.71b))

7.3.5 Trajectory Axes

Another useful coordinate system has one axis along the local velocity vector, ($\hat{x}$), and the other two perpendicular to the local velocity vector, ($\hat{y}, \hat{z}$). The $\hat{y}$ and $\hat{z}$ directions are chosen such that $\hat{y}$ lies in the x-y plane perpendicular to $\hat{x}$, and $\hat{z}$ forms a right-handed system. This system is illustrated in Figure 7.5. The angles locating these axes are γ_1 and γ_2, analogous to ψ_{ME} and θ_{ME}.

These coordinates are useful for axisymmetric bodies and/or planar motion in writing the aerodynamic forces and, in some cases, the equations of linear momentum. In tests in a ballistic range, the angles γ_1 and γ_2 are normally very small and hence certain simplifications are possible.

7.3.6 Relationships Between Systems

Since it is sometimes necessary to transform one coordinate system to another, we will give some transformation relations, both exact and approximate, before we proceed to the equations of motion.

The transformation matrix is that matrix which operates on a vector in one coordinate system to produce the vector in another system. For example, the forces in the body-fixed coordinates $\vec{F}_B$ transform to earth-fixed coordinates $\vec{F}_E$ by

$$\vec{F}_E = [T]_{E/B}\vec{F}_B , \tag{7.3}$$

where $[T]_{E/B}$ is the transformation matrix. This transformation matrix preserves the magnitude and direction of the vector; that is, it simply relates the vector to a different coordinate system. Hence, these matrices have the properties of a unitary matrix; that is, the inverse is equal to the transpose,

$$(T_{ij})^{-1} = (T_{ji}) = (T_{ij})^T . \tag{7.4}$$

Hence, it follows that $(T_{ij})_{A/B} = (T_{ij})^T_{B/A}$.

The transformation matrix for body-fixed to earth-fixed coordinates (using modified Euler angles) is

$$[T]_{E/B} = \begin{pmatrix} \cos\theta_{ME}\cos\psi_{ME} & \sin\theta_{ME}\cos\psi_{ME}\sin\phi - \sin\psi_{ME}\cos\phi & \sin\theta_{ME}\cos\psi_{ME}\cos\phi + \sin\psi_{ME}\sin\phi \\ \cos\theta_{ME}\sin\psi_{ME} & \sin\theta_{ME}\sin\psi_{ME}\sin\phi + \cos\psi_{ME}\cos\phi & \sin\theta_{ME}\sin\psi_{ME}\cos\phi - \cos\psi_{ME}\sin\phi \\ -\sin\theta_{ME} & \cos\theta_{ME}\sin\phi & \cos\theta_{ME}\cos\phi \end{pmatrix} . \tag{7.5}$$

For body-oriented fixed-plane coordinates to earth-fixed coordinates, it is

$$[T]_{E/FP} = \begin{pmatrix} \cos\theta_{ME}\cos\psi_{ME} & -\sin\psi_{ME} & \sin\theta_{ME}\cos\psi_{ME} \\ \cos\theta_{ME}\sin\psi_{ME} & \cos\psi_{ME} & \sin\theta_{ME}\sin\psi_{ME} \\ -\sin\theta_{ME} & 0 & \cos\theta_{ME} \end{pmatrix} \tag{7.6}$$

and for trajectory coordinates to earth-fixed coordinates, it is

$$[T]_{E/T} = \begin{pmatrix} \cos\gamma_1\cos\gamma_2 & -\sin\gamma_1 & \cos\gamma_1\sin\gamma_2 \\ \sin\gamma_1\cos\gamma_2 & \cos\gamma_1 & \sin\gamma_1\sin\gamma_2 \\ -\sin\gamma_2 & 0 & \cos\gamma_2 \end{pmatrix} . \tag{7.7}$$

It is possible to obtain relations between any combination of these systems using appropriate matrix multiplication.

These matrices will now be considered for small angles (except ϕ); that is

$$\sin(a) \doteq a$$

$$\cos(a) \doteq 1 .$$

Then the transformation matrices become

$$[T]_{E/B} = \begin{pmatrix} 1 & \theta_{ME}\sin\phi - \psi_{ME}\cos\phi & \theta_{ME}\cos\phi + \psi_{ME}\sin\phi \\ \psi_{ME} & \cos\phi & -\sin\phi \\ -\theta_{ME} & \sin\phi & \cos\phi \end{pmatrix} \tag{7.8}$$

$$[T]_{E/FP} = \begin{pmatrix} 1 & -\psi_{ME} & \theta_{ME} \\ \psi_{ME} & 1 & 0 \\ -\theta_{ME} & 0 & 1 \end{pmatrix} \tag{7.9}$$

$$[T]_{E/T} = \begin{pmatrix} 1 & -\gamma_1 & \gamma_2 \\ \gamma_1 & 1 & 0 \\ -\gamma_2 & 0 & 1 \end{pmatrix} . \tag{7.10}$$

Note that in these last three transformations, it would be consistent with the small-angle assumption to replace θ_{ME} and γ_2 by their projected values (on the x-z plane).

Another transformation matrix which is of interest is that between the trajectory coordinates and the body-oriented fixed-plane coordinates. This is obtained by the appropriate operations on Equations (7.6) and (7.7) (i.e., $[T]_{FP/T} = [T]_{FP/E} \cdot [T]_{E/T} = [T]^T_{E/FP} \cdot [T]_{E/T}$). The result to first order is

$$[T]_{FP/T} = \begin{pmatrix} 1 & \psi_{ME} - \gamma_1 & -\theta_{ME} + \gamma_2 \\ -\psi_{ME} + \gamma_1 & 1 & 0 \\ \theta_{ME} - \gamma_2 & 0 & 1 \end{pmatrix} . \tag{7.11}$$

The interpretation of the elements of this matrix is straightforward. If one calculates the components of velocity in the fixed-plane system using the first order matrix, the result is

$$\vec{V}_{FP} = [T]_{FP/T} \cdot \vec{V}_T$$

or

$$\begin{pmatrix} 1 & \psi_{ME} - \gamma_1 & -\theta_{ME} + \gamma_2 \\ -\psi_{ME} + \gamma_1 & 1 & 0 \\ \theta_{ME} - \gamma_2 & 0 & 1 \end{pmatrix} \cdot \begin{pmatrix} V \\ 0 \\ 0 \end{pmatrix} = \begin{pmatrix} V \\ (-\psi_{ME} + \gamma_1)V \\ (\theta_{ME} - \gamma_2)V \end{pmatrix} = \begin{pmatrix} \tilde{u} \\ \tilde{v} \\ \tilde{w} \end{pmatrix} . \tag{7.12}$$

Since the angle of attack and angle of sideslip are defined as

$$\left.\begin{aligned} \tilde{\alpha} &= \sin^{-1}\left(\frac{\tilde{w}}{V}\right) \approx \frac{\tilde{w}}{V} \\ \tilde{\beta} &= \sin^{-1}\left(\frac{\tilde{v}}{V}\right) \approx \frac{\tilde{v}}{V} . \end{aligned}\right\} \tag{7.13}$$

then to first order

$$\left.\begin{aligned} \tilde{\alpha} &= \theta_{ME} - \gamma_2 \\ \tilde{\beta} &= -\psi_{ME} + \gamma_1 . \end{aligned}\right\} \tag{7.14}$$

These angles are the off-diagonal elements in the transformation (7.11). They can be better visualized by referring to the lower portion of Figure 7.4. This is a view looking aft along the earth-fixed x axis at the y-z plane. A unit vector along the model axis, $\tilde{x}$, has a projection $0-A$, labeled $\vec{\Omega}$, with components θ_{ME} and ψ_{ME}. A unit vector along the total velocity vector appears as a projection $0-B$ and is called $\vec{\gamma}$. The components of $\vec{\gamma}$ are $\dot{y}/V$ and $\dot{z}/V$, which are essentially equal to γ_1 and $-\gamma_2$. The vector $B-A$ between the velocity vector and the model axis $\tilde{x}$ is called the resultant angle of attack, $\vec{\alpha}_R$, and has components $\tilde{\alpha}$ and $\tilde{\beta}$. Therefore

$$\vec{\alpha}_R = \vec{\Omega} - \vec{\gamma} . \tag{7.15}$$

This is an exact expression when velocity components are used. Also shown in this figure is the angle, ϕ, which one would observe between the coordinate axes and a canard on the nose of the body.

The coordinate systems necessary for motion analysis are now defined, and their relationships to one another have been given. We can now proceed to the development of the equations of motion for a body in free flight.

7.4 EQUATIONS OF MOTION

The equations of motion will be developed in three steps. First, the dynamics of a body in free-flight will be expressed in several forms. Second, expressions for the aerodynamic forces and moments will be obtained. Then the forces, moments, and flight dynamics will be combined to obtain the differential equations of motion.

7.4.1 Flight Dynamics

7.4.1.1 Introduction

The behavior of a rigid body in flight is governed by Newton's laws of motion. Although there are various ways of expressing these laws, the simplest is to write the equations of conservation of linear and angular momentum within an inertial reference frame

$$\frac{d(m\vec{V})}{dt} = \vec{F} \tag{7.16}$$

and

$$\frac{d([I]\vec{\omega})}{dt} = \vec{M} , \tag{7.17}$$

where m is the mass of the body, $\vec{V}$ is its velocity vector, $\vec{F}$ is the force vector acting on it, $[I]$ is the moment of inertia (a 2nd rank tensor), $\vec{\omega}$ is the angular velocity vector, and $\vec{M}$ is the moment vector. To apply these equations in a moving coordinate system one needs the transformation

$$\left(\frac{d\vec{A}}{dt}\right)_m = \left(\frac{d\vec{A}}{dt}\right)_f + \vec{\omega} \times \vec{A}_f , \tag{7.18}$$

where $\vec{A}$ is any vector quantity, m denotes the moving system and f the fixed system. An example of the type of quantity produced by the 2nd term is the Coriolis acceleration which appears in the equations of motion expressed in earth-fixed coordinates.

Another formulation of the momentum equations is that of Lagrange. It will be used more extensively in the following development than the basic form given above.

7.4.1.2 Lagrangian Equations

The Lagrangian equations of motion are derived in textbooks on dynamics[7-10]. These equations greatly simplify the handling of the pitching and yawing motion of a body in free flight. The Lagrangian equations are

$$\frac{d}{dt}\left(\frac{\partial T}{\partial \dot{q}_i}\right) - \frac{\partial T}{\partial q_i} = Q_i . \tag{7.19}$$

Here T is the total kinetic energy of the system; q_i is the i^{th} generalized coordinate; $\dot{q}_i$ is the time rate of change of q_i; Q_i is the force tending to change q_i; and t is time. There are as many such equations as there are degrees of freedom, the subscript i representing, therefore, the i^{th} degree of freedom. For free flight of a rigid body there are six degrees of freedom, three translational and three rotational.

The total kinetic energy of a rigid body in free flight is written as

$$T = \tfrac{1}{2}m(\dot{x}^2 + \dot{y}^2 + \dot{z}^2) + \tfrac{1}{2}I_{\bar{x}}p^2 + \tfrac{1}{2}I_{\bar{y}}q^2 + \tfrac{1}{2}I_{\bar{z}}r^2 , \tag{7.20}$$

where m is the model mass, $I_{\bar{x}}$, $I_{\bar{y}}$, and $I_{\bar{z}}$ are the moments of inertia about the three principal axes, p, q, and r are the angular rates about the principal axes and $\dot{x} = u$, $\dot{y} = v$, and $\dot{z} = w$ are the components of velocity in the earth-fixed axis system. Note that in using earth-fixed axes some energy has been ignored due to the non-inertial character of the earth-fixed coordinates. The only important term here is the Coriolis acceleration which we will discuss under the section on forces.

For a body with axial symmetry

$$I_{\bar{y}} = I_{\bar{z}} = I \tag{7.21}$$

and hence the total kinetic energy can be written as

$$T = \tfrac{1}{2}m(\dot{x}^2 + \dot{y}^2 + \dot{z}^2) + \tfrac{1}{2}I_{\bar{x}}p^2 + \tfrac{1}{2}I(q^2 + r^2) . \tag{7.22}$$

Note that any body which has a plane of mass symmetry and trigonal or greater rotational (mass) symmetry can be considered to be axially symmetric with respect to its moments of inertia ($I_{\bar{y}} = I_{\bar{z}}$).

7.4.1.3 Equations of Linear Momentum

The equations of motion in the x, y, and z directions can be obtained as follows: Let x be the first generalized coordinate,

$$\frac{d}{dt}\left(\frac{\partial T}{\partial \dot{x}}\right) - \frac{\partial T}{\partial x} = Q_x . \tag{7.23}$$

Using Equation (7.20),

$$m\frac{d^2x}{dt^2} = Q_x = F_x ; \tag{7.24}$$

similarly,

$$m \frac{d^2y}{dt^2} = F_y \tag{7.25}$$

and

$$m \frac{d^2z}{dt^2} = F_z \, . \tag{7.26}$$

In vector form these equations can be written

$$m \frac{d^2\vec{R}}{dt^2} = \vec{F} \, . \tag{7.27}$$

Note that the mass, m, has been taken outside the differential operator. This can be done not only if the mass is a constant, but also if the velocity (relative to the body) of the mass that leaves the body is very small. In that case, its contribution to the change in momentum can be neglected. Most of the problems to be treated will be for constant mass but some cases will be considered with variable mass where this momentum assumption is thought to be valid.

These equations can alternately be written in the trajectory coordinates described earlier. The result for the component of force along the velocity vector is

$$m \frac{d^2\hat{x}}{dt^2} = F_{\hat{x}} \tag{7.28}$$

and that normal to the velocity vector is

$$m \left(\frac{d\hat{x}}{dt} \right)^2 \vec{R}_c / R_c^2 = \vec{F} (F_{\hat{y}}, F_{\hat{z}}) \, . \tag{7.29}$$

The term on the left side of this equation is the centrifugal force term (R_c is the radius of curvature of the flight path) which arises from the non-inertial character of the trajectory coordinates.

7.4.1.4 Equations of Angular Momentum

The Lagrangian equations of angular motion can be written with each of the three sets of angles which have been introduced. The angular momentum equations will be written (at least in part) using all three sets so that similarities and differences can be seen. First, however, one must obtain the angular velocities in terms of the angles for each of the systems. They are listed in the following table.

Euler Angles	*Modified Euler Angles*	*Fixed-Plane Modified Euler Angles*
$p = \dot{\psi}_E + \dot{\theta}_E \cos\sigma$	$p = \dot{\phi} - \dot{\psi}_{ME} \sin\theta_{ME}$	$\tilde{p} = \dot{\phi} - \dot{\psi}_{ME} \sin\theta_{ME}$
$q = \dot{\sigma} \cos\psi_E + \dot{\theta}_E \sin\sigma \sin\psi_E$	$q = \dot{\theta}_{ME} \cos\phi + \dot{\psi}_{ME} \cos\theta_{ME} \sin\phi$	$\tilde{q} = \dot{\theta}_{ME}$
$r = -\dot{\sigma} \sin\psi_E + \dot{\theta}_E \sin\sigma \cos\psi_E$	$r = \dot{\psi}_{ME} \cos\theta_{ME} \cos\phi - \dot{\theta}_{ME} \sin\phi$	$\tilde{r} = \dot{\psi}_{ME} \cos\theta_{ME}$

Since the Euler angles and the modified Euler angles are more general in that they do not require axial symmetry, they will be considered first. The total kinetic energy using the Euler angles is

$$T = \tfrac{1}{2}m (\dot{x}^2 + \dot{y}^2 + \dot{z}^2) + \tfrac{1}{2} I_{\bar{x}} (\dot{\psi}_E + \dot{\theta}_E \cos\sigma)^2 + \tfrac{1}{2} I_{\bar{y}} (\dot{\sigma} \cos\psi_E + \dot{\theta}_E \sin\sigma \sin\psi_E)^2 + \tfrac{1}{2} I_{\bar{z}} (-\dot{\sigma} \sin\psi_E + \dot{\theta}_E \sin\sigma \cos\psi_E)^2 \tag{7.30}$$

and the total kinetic energy using the modified Euler angles is

$$T = \tfrac{1}{2}m (\dot{x}^2 + \dot{y}^2 + \dot{z}^2) + \tfrac{1}{2} I_{\bar{x}} (\dot{\phi} - \dot{\psi}_{ME} \sin\theta_{ME})^2 + \tfrac{1}{2} I_{\bar{y}} (\dot{\theta}_{ME} \cos\phi + \dot{\psi}_{ME} \cos\theta_{ME} \sin\phi)^2 + \tfrac{1}{2} I_{\bar{z}} (\dot{\psi}_{ME} \cos\theta_{ME} \cos\phi - \dot{\theta}_{ME} \sin\phi)^2 \, . \tag{7.31}$$

It is straightforward to substitute both of the above expressions for T into the Lagrangian equations (7.19) and arrive at the equations of angular momentum. However only those equations using modified Euler angles will be listed here. For the ψ_{ME} coordinate, we get

$$\frac{d}{dt} \left(\frac{\partial T}{\partial \dot{\psi}_{ME}} \right) = \frac{d}{dt} \left[I_{\bar{x}} (\dot{\phi} - \dot{\psi}_{ME} \sin\theta_{ME}) (-\sin\theta_{ME}) + I_{\bar{y}} (\dot{\theta}_{ME} \cos\phi + \dot{\psi}_{ME} \cos\theta_{ME} \sin\phi) (\cos\theta_{ME} \sin\phi) + I_{\bar{z}} (\dot{\psi}_{ME} \cos\theta_{ME} \cos\phi - \dot{\theta}_{ME} \sin\phi) (\cos\theta_{ME} \cos\phi) \right] = Q_{\psi_{ME}} \tag{7.32}$$

$$= [M_m \sin\phi + M_n \cos\phi] \cos\theta_{ME} \, .$$

for the θ_{ME} coordinate,

$$\frac{d}{dt}\left(\frac{\partial T}{\partial \dot{\theta}_{ME}}\right) - \frac{\partial T}{\partial \theta_{ME}} = \frac{d}{dt}\left[I_{\bar{y}}\left(\dot{\theta}_{ME}\cos\phi + \dot{\psi}_{ME}\cos\theta_{ME}\sin\phi\right)(\cos\phi) +\right.$$

$$+ I_{\bar{z}}\left(\dot{\psi}_{ME}\cos\theta_{ME}\cos\phi - \dot{\theta}_{ME}\sin\phi\right)(-\sin\phi)\Big] +$$

$$+ I_{\bar{x}}\left(\dot{\phi} - \dot{\psi}_{ME}\sin\theta_{ME}\right)\left(\dot{\psi}_{ME}\cos\theta_{ME}\right) +$$

$$+ I_{\bar{y}}\left(\dot{\theta}_{ME}\cos\phi + \dot{\psi}_{ME}\cos\theta_{ME}\sin\phi\right)\left(\dot{\psi}_{ME}\sin\theta_{ME}\sin\phi\right) +$$

$$+ I_{\bar{z}}\left(\dot{\psi}_{ME}\cos\theta_{ME}\cos\phi - \dot{\theta}_{ME}\sin\phi\right)\left(\dot{\psi}_{ME}\sin\theta_{ME}\cos\phi\right) = Q_{\theta_{ME}} = M_m\cos\phi - M_n\sin\phi \qquad (7.33)$$

and for the ϕ coordinate

$$\frac{d}{dt}\left(\frac{\partial T}{\partial \dot{\phi}}\right) - \frac{\partial T}{\partial \phi} = \frac{d}{dt}\left[I_{\bar{x}}\left(\dot{\phi} - \dot{\psi}_{ME}\sin\theta_{ME}\right)\right] +$$

$$+ I_{\bar{y}}\left(\dot{\theta}_{ME}\cos\phi + \dot{\psi}_{ME}\cos\theta_{ME}\sin\phi\right)\left(\dot{\theta}_{ME}\sin\phi - \dot{\psi}_{ME}\cos\theta_{ME}\cos\phi\right) +$$

$$+ I_{\bar{z}}\left(\dot{\psi}_{ME}\cos\theta_{ME}\cos\phi - \dot{\theta}_{ME}\sin\phi\right)\left(\dot{\psi}_{ME}\cos\theta_{ME}\sin\phi + \dot{\theta}_{ME}\cos\phi\right) = Q_{\phi} = M_l\ . \qquad (7.34)$$

These equations represent a set for the angular momentum. They are general in the sense that they apply to an arbitrary rigid body.

A more widely used form for the equations of angular momentum of an airplane-like configuration can be obtained from (7.17) and (7.18). First let $\vec{\omega} = \vec{\omega}(p,q,r)$. Then note that the cross-product needed in (7.18), $\vec{\omega} \times I\vec{\omega}$, can be represented by the determinant

$$\begin{vmatrix} \vec{l} & \vec{m} & \vec{n} \\ p & q & r \\ I_{\bar{x}}p & I_{\bar{y}}q & I_{\bar{z}}r \end{vmatrix}.$$

The resulting equations are:

$$\left.\begin{aligned} I_{\bar{z}}\dot{r} &= pq\left(I_{\bar{x}} - I_{\bar{y}}\right) + M_n \\ I_{\bar{y}}\dot{q} &= pr\left(I_{\bar{z}} - I_{\bar{x}}\right) + M_m \\ I_{\bar{x}}\dot{p} &= qr\left(I_{\bar{y}} - I_{\bar{z}}\right) + M_l\ . \end{aligned}\right\} \qquad (7.35)$$

In comparison to (7.32), (7.33), and (7.34), these equations are much simpler. Because (7.32) - (7.34) are so complicated, we will treat some specialized cases which result in many simplifications.

7.4.1.5 Planar Motion

For the case of planar motion (an oscillation confined to a single plane, here arbitrarily the x-z plane) ψ_{ME} is identically zero and since there can be no roll, $\dot{\phi} = 0$. Note that the results obtained will apply to any planar motion since in the absence of an important gravity force, the x-z plane can be rotated to the plane of motion. With these conditions (a single degree of rotational freedom) the equation for angular momentum is

$$I_{\bar{y}}\ddot{\theta}_{ME} = M_m\ . \qquad (7.36)$$

7.4.1.6 Small Angular Motion

There are a number of subcases in this category and several of them will be considered. First assume that the angles θ_{ME} and ψ_{ME} (but not necessarily ϕ) and the angular rates and accelerations are small. Hence,

$$\sin\psi_{ME} = \psi_{ME}$$

$$\sin\theta_{ME} = \theta_{ME}$$

$$\cos\psi_{ME} = \cos\theta_{ME} = 1\ .$$

With these restrictions and neglecting products of small terms, the equations of angular momentum in terms of the modified Euler angles reduce to the following:

$$I_{\bar{y}}\left(\ddot{\theta}_{ME}\sin\phi\cos\phi + \dot{\psi}_{ME}\sin^2\phi\right) + I_{\bar{z}}\left(\ddot{\psi}_{ME}\cos^2\phi - \ddot{\theta}_{ME}\sin\phi\cos\phi\right) = M_m\sin\phi + M_n\cos\phi \qquad (7.37)$$

$$I_{\bar{y}}\left(\ddot{\theta}_{ME}\cos^2\phi + \ddot{\psi}_{ME}\sin\phi\cos\phi\right) + I_{\bar{z}}\left(-\ddot{\psi}_{ME}\sin\phi\cos\phi + \ddot{\theta}_{ME}\sin^2\phi\right) = M_m\cos\phi - M_n\sin\phi \qquad (7.38)$$

$$I_{\bar{x}}\ddot{\phi} = M_l \,. \tag{7.39}$$

If, in addition, we assume there is no rolling torque ($M_l = 0$), (7.39) can be solved and

$$\phi = A + Bt \,. \tag{7.40}$$

If this result is substituted into (7.37) and (7.38) the result is

$$I_{\bar{y}}[\ddot{\theta}_{ME}\sin(A+Bt)\cos(A+Bt) + \ddot{\psi}_{ME}\sin^2(A+Bt)] + I_{\bar{z}}[\ddot{\psi}_{ME}\cos^2(A+Bt) - \ddot{\theta}_{ME}\sin(A+Bt)\cos(A+Bt)] = M_m \sin\phi + M_n \cos\phi \,. \tag{7.41}$$

and

$$I_{\bar{y}}[\ddot{\theta}_{ME}\cos^2(A+Bt) + \ddot{\psi}_{ME}\sin(A+Bt)\cos(A+Bt)] + I_{\bar{z}}[-\ddot{\psi}_{ME}\sin(A+Bt)\cos(A+Bt) + \ddot{\theta}_{ME}\sin^2(A+Bt)] = M_m \cos\phi - M_n \sin\phi \,. \tag{7.42}$$

The left hand sides of these two equations are linear with variable coefficients and are coupled.

Finally, if it is assumed that the angle ϕ is also small, the equations become

$$\left.\begin{aligned} I_{\bar{z}}\ddot{\psi}_{ME} &= M_n \\ I_{\bar{y}}\ddot{\theta}_{ME} &= M_m \,. \end{aligned}\right\} \tag{7.43}$$

All of the coupling has now been removed from the left hand sides.

7.4.1.7 Axially Symmetric Bodies

A more restricted but often encountered case will now be considered, namely, that of an axially symmetric body. Noting that $I_{\bar{y}} = I_{\bar{z}} = I$, the kinetic energy can be expressed in terms of Euler angles as

$$T = \tfrac{1}{2}m(\dot{x}^2+\dot{y}^2+\dot{z}^2) + \tfrac{1}{2}I_{\bar{x}}(\dot{\psi}_E+\dot{\theta}_E\cos\sigma)^2 + \tfrac{1}{2}I(\dot{\sigma}^2+\dot{\theta}_E^2\sin^2\sigma) \,. \tag{7.44}$$

The following equations of angular momentum can then be obtained.

$$\frac{d}{dt}[I_{\bar{x}}(\dot{\psi}_E+\dot{\theta}_E\cos\sigma)\cos\sigma + I\dot{\theta}_E\sin^2\sigma] = Q_{\theta_E} \tag{7.45}$$

$$\frac{d}{dt}[I\dot{\sigma}] + I_{\bar{x}}(\dot{\psi}_E+\dot{\theta}_E\cos\sigma)\dot{\theta}_E\sin\sigma - I\dot{\theta}_E^2\sin\sigma\cos\sigma = Q_\sigma \tag{7.46}$$

$$\frac{d}{dt}[I_{\bar{x}}(\dot{\psi}_E+\dot{\theta}_E\cos\sigma)] = Q_{\psi_E} \,. \tag{7.47}$$

These equations represent the most general case for an axially symmetric body. Noting that $\dot{\psi}_E + \dot{\theta}_E\cos\sigma = p$ and, defining a new parameter

$$P = \frac{I_{\bar{x}}}{I}p \,, \tag{7.48}$$

then (7.45), (7.46), and (7.47) can be written as

$$\frac{d}{dt}(IP\cos\sigma + I\dot{\theta}_E\sin^2\sigma) = Q_{\theta_E} \tag{7.49}$$

$$\frac{d}{dt}(I\dot{\sigma}) + IP\dot{\theta}_E\sin\sigma - I\dot{\theta}_E^2\sin\sigma\cos\sigma = Q_\sigma \tag{7.50}$$

$$\frac{d}{dt}(IP) = Q_{\psi_E} \,. \tag{7.51}$$

A special case using these equations is for zero roll torque ($Q_{\psi_E} = 0$) and for zero precession torque ($Q_{\theta_E} = 0$). With these restrictions, (7.49) and (7.51) become

$$IP\cos\sigma + I\dot{\theta}_E\sin^2\sigma = \text{constant} = Ib \tag{7.52}$$

$$IP = \text{constant} \,, \tag{7.53}$$

and hence, (7.50) becomes

$$\frac{d}{dt}(I\dot{\sigma}) + \frac{IP(b-P\cos\sigma)}{\sin\sigma} - \frac{I\cos\sigma(b-P\cos\sigma)^2}{\sin^3\sigma} = Q_\sigma \,. \tag{7.54}$$

Note that even for this restricted case the problem is highly nonlinear even if the right hand side of the equation is linear. This equation remains nonlinear even for small angles (i.e. σ small).

For the case of σ small, (7.54) reduces to

$$I\ddot{\sigma} + IP\frac{(b-P)}{\sigma} - I\frac{(b-P)^2}{\sigma^3} = Q_\sigma . \tag{7.55}$$

For planar motion $b = P = 0$ and (7.55) reduces to

$$I\ddot{\sigma} = Q_\sigma . \tag{7.56}$$

Note the left hand side of the equation is linear.

One other case that is of interest is that for which the moments are all conservative. Here the sum of the kinetic energy plus the potential energy is constant. This case is developed in Reference 7.8 and will not be discussed here.

Next the momentum equations using modified Euler angles in fixed-plane axes will be considered. Noting that $I_{\tilde{y}} = I_{\tilde{z}} = I$, the total kinetic energy is

$$T = \tfrac{1}{2}m(\dot{x}^2 + \dot{y}^2 + \dot{z}^2) + \tfrac{1}{2}I_{\tilde{x}}(\dot{\phi} - \dot{\psi}_{ME}\sin\theta_{ME})^2 + \tfrac{1}{2}I(\dot{\theta}_{ME}^2 + \dot{\psi}_{ME}^2\cos^2\theta_{ME}) . \tag{7.57}$$

Substituting into the Lagrangian Equations (7.19) one obtains for ψ_{ME}, θ_{ME}, and ϕ respectively

$$\frac{d}{dt}\left[-I_{\tilde{x}}(\dot{\phi} - \dot{\psi}_{ME}\sin\theta_{ME})\sin\theta_{ME} + I(\dot{\psi}_{ME}\cos^2\theta_{ME})\right] = \tilde{M}_n\cos\theta_{ME} \tag{7.58}$$

$$\frac{d}{dt}(I\dot{\theta}_{ME}) + I_{\tilde{x}}(\dot{\phi} - \dot{\psi}_{ME}\sin\theta_{ME})\dot{\psi}_{ME}\cos\theta_{ME} + I\dot{\psi}_{ME}^2\sin\theta_{ME}\cos\theta_{ME} = \tilde{M}_m \tag{7.59}$$

$$\frac{d}{dt}\left[I_{\tilde{x}}(\dot{\phi} - \dot{\psi}_{ME}\sin\theta_{ME})\right] = \tilde{M}_l . \tag{7.60}$$

These are the basic equations using modified Euler angles, and are similar to those with Euler angles. Consider the case where $\tilde{M}_l = 0$ (no roll torque). One obtains

$$(\dot{\phi} - \dot{\psi}_{ME}\sin\theta_{ME}) = \tilde{p} = \text{constant} = \frac{I}{I_{\tilde{x}}}P . \tag{7.61}$$

Substituting this in the remaining two equations yields

$$-IP\dot{\theta}_{ME}\cos\theta_{ME} + I\ddot{\psi}_{ME}\cos^2\theta_{ME} - 2I\dot{\psi}_{ME}\dot{\theta}_{ME}\sin\theta_{ME}\cos\theta_{ME} = \tilde{M}_n\cos\theta_{ME} \tag{7.62}$$

and

$$I\ddot{\theta}_{ME} + IP\dot{\psi}_{ME}\cos\theta_{ME} + I\dot{\psi}_{ME}^2\sin\theta_{ME}\cos\theta_{ME} = \tilde{M}_m . \tag{7.63}$$

If these equations are now linearized, the result is

$$I\ddot{\psi}_{ME} - IP\dot{\theta}_{ME} = \tilde{M}_n \tag{7.64}$$

$$I\ddot{\theta}_{ME} + IP\dot{\psi}_{ME} = \tilde{M}_m , \tag{7.65}$$

where it has been assumed that

$$\left.\begin{aligned}\cos\theta_{ME} &\approx 1\\ \sin\theta_{ME} &\approx \theta_{ME}\end{aligned}\right\} \tag{7.66}$$

and products of small terms have been neglected. Note that it is convenient to express (7.64) and (7.65) as a single equation in the complex plane (since $\dot{\theta}_{ME}$ and $\dot{\psi}_{ME}$ are orthogonal). This is done simply by multiplying (7.64) by $i\ (\sqrt{(-1)})$ and then collecting real and imaginary parts.

$$I\ddot{\vec{\Omega}} - iIP\dot{\vec{\Omega}} = \vec{M} , \tag{7.67}$$

where

$$\vec{\Omega} = \dot{\theta}_{ME} + i\dot{\psi}_{ME} \tag{7.68}$$

and

$$\vec{M} = \tilde{M}_m + i\tilde{M}_n . \tag{7.69}$$

There is another method (although not discussed here) of developing the dynamic equations of motion of a symmetric body which employs the nonrolling axes mentioned in Section 7.3.4 (Ref.7.9). This approach is advantageous in that a simple, exact differential equation for pitching motion can be obtained, but it is not as convenient to use since measured data must be expressed in an inconvenient reference frame.

With the above several formulations of the dynamic equations of motion available to us, it remains to consider the applied forces and moments which make up the right hand sides of these equations.

7.4.2 Forces and Moments

7.4.2.1 Introduction

The forces and moments acting on a body in flight can originate from a number of different sources, including pressure and shear forces, gravitational force, buoyancy force, Coriolis force, and electromagnetic force. In ballistic range tests, aerodynamic forces are usually dominant, and for tests of low flight velocity and/or long duration, gravity and Coriolis forces can become important. Buoyancy and electromagnetic forces are negligible and will not be considered. The bulk of the discussion in this chapter will be concerned with aerodynamic forces and moments. However, since gravity and Coriolis forces are sometimes considered, they will be described briefly now.

If the coordinate system is earth-fixed as described earlier, the gravity vector is always aligned with the z-axis and hence the gravity force can be written as

$$F_{z\ grav} = mg \ . \tag{7.70}$$

The Coriolis force is given by

$$\vec{F}_c = 2m(\vec{\omega}_E \times \vec{V}) \ , \tag{7.71a}$$

where $\vec{\omega}_E$ is the rotational velocity of the earth ($\omega_E = 7.3 \times 10^{-5}$ rad/sec), and m is the mass of the body in flight. Equation (7.71a) can be expanded to obtain

$$F_c = 2m\omega_E V(\sin\theta_l + i\cos\theta_l \sin\theta_a) \ , \tag{7.71b}$$

where the first term is along the y axis and the last term is along the z axis, θ_l is the geographical latitude of the facility (0^o at the equator) and θ_a is the direction of flight (i.e. the angle between the earth-fixed x axis and the local meridian - due east yields $\theta_a = 90^o$).

7.4.2.2 Aerodynamic Forces and Moments

The aerodynamic forces and moments are defined in body-fixed axes normally chosen to be principal axes through the center of mass. This coordinate system, with related forces and moments, is shown in Figure 7.6. The force components produce moments M_l, M_m, M_n about the $\bar{x}$, $\bar{y}$, and $\bar{z}$ axes, respectively.

The aerodynamic forces and moments are in general quite complicated. The aerodynamic force coefficients are expressed as $C_{force} = Force/\frac{1}{2}\rho V^2 A$ and the aerodynamic moment coefficients as $C_{moment} = Moment/\frac{1}{2}\rho V^2 A l$, where ρ is the density of the fluid through which the body is flying, V is the flight velocity, A is the reference area, and l is the reference length. They are functions of flight speed, conditions of the test gas, model scale, and geometry. They also depend to some degree on the flight history. If the dependence on history were strong, a correlation of results would be next to impossible. In practice this dependence is not strong. Therefore, the "aerodynamic hypothesis" will be invoked; that is, the forces on a body in free flight can be expressed in terms of the body's instantaneous motion. This can be done in two ways; in terms of velocity ratios $\bar{u}/V$, $\bar{v}/V$, $\bar{w}/V$, p, q, and r and derivatives thereof or, equivalently, in terms of the angles represented by the velocity ratios $\bar{u}/V$, $\bar{\beta}$, $\bar{\alpha}$, p, q, r. In the work to follow the latter will be used.

The aerodynamic hypothesis should apply when the flight distance in a cycle of oscillatory motion is many times the length of the body, the usual situation both in full-scale flight and in ballistic ranges. Despite this simplifying assumption, there remain many variables on which the forces may depend. We will write this functional dependence as

$$F_i = C_i(R_\infty, M_\infty, \bar{\alpha}, \bar{\beta}, \dot{\bar{\alpha}}, \dot{\bar{\beta}}, p, q, r \ldots)\tfrac{1}{2}\rho V^2 A \ , \tag{7.72}$$

where $C_i(R_\infty, M_\infty, \ldots\ldots)$ is the i^{th} force coefficient (for example, $i = \bar{x}, \bar{y}, \bar{z}$) and R_∞, M_∞ are Reynolds number and Mach number.

Similarly, for the moments

$$M_j = C_j(R_\infty, M_\infty, \bar{\alpha}, \bar{\beta}, \dot{\bar{\alpha}}, \dot{\bar{\beta}}, p, q, r \ldots)\tfrac{1}{2}\rho V^2 A l \ , \tag{7.73}$$

where C_j is the j^{th} moment coefficient (the subscript j becomes l,m,n for moments about the $\bar{x}$,$\bar{y}$, and $\bar{z}$ axes, respectively).

For well-behaved aerodynamic coefficients (i.e., smooth, continuous and single-valued functions) the coefficients can be expanded in a Taylor series as follows:

$$
\begin{aligned}
C_i = {} & C_{i_0} + C_{i_\alpha}\bar{\alpha} + C_{i_\beta}\bar{\beta} + \\
& + C_{i_{\dot\alpha}}\frac{\dot{\bar{\alpha}}l}{V} + C_{i_{\dot\beta}}\frac{\dot{\bar{\beta}}l}{V} + \\
& + C_{i_p}\frac{pl}{V} + C_{i_q}\frac{ql}{V} + C_{i_r}\frac{rl}{V} + \\
& + C_{i_{\dot p}}\frac{\dot p l^2}{V^2} + C_{i_{\dot q}}\frac{\dot q l^2}{V^2} + C_{i_{\dot r}}\frac{\dot r l^2}{V^2} + \\
& + C_{i_{\alpha p}}\bar{\alpha}\frac{pl}{V} + C_{i_{\beta p}}\bar{\beta}\frac{pl}{V} + \\
& + C_{i_{\dot\alpha p}}\frac{\dot{\bar{\alpha}}l}{V}\frac{pl}{V} + C_{i_{\dot\beta p}}\frac{\dot{\bar{\beta}}l}{V}\frac{pl}{V} + \\
& + C_{i_{pp}}\left(\frac{pl}{V}\right)^2 + C_{i_{qp}}\frac{ql}{V}\frac{pl}{V} + C_{i_{rp}}\frac{rl}{V}\frac{pl}{V} + \\
& + C_{i_{\dot p p}}\frac{\dot p l^2}{V^2}\frac{pl}{V} + C_{i_{\dot q p}}\frac{\dot q l^2}{V^2}\frac{pl}{V} + C_{i_{\dot r p}}\frac{\dot r l^2}{V^2}\frac{pl}{V} + \\
& + \text{higher order terms} .
\end{aligned}
\tag{7.74}
$$

Here i is used as a general subscript for both forces and moments (for example, $i = \bar{x}, \bar{y}, \bar{z}, l, m, n$). The second-order subscripts denote derivatives which have been nondimensionalized (e.g., $C_{i_\alpha} = \partial C_i/\partial\bar{\alpha}$, $C_{i_{\dot\alpha}} = \partial C_i/\partial(\dot{\bar{\alpha}}l/V)$, $C_{i_{\alpha p}} = \partial^2 C_i/\partial\bar{\alpha}\,\partial(pl/V)$, etc.). The terms involving $\dot p$, $\dot q$, and $\dot r$ are included for completeness since, under center of gravity translation, they are required to keep the force system invariant. They are neglected in practice, however, because they are small, and will not be carried along any further in this chapter.

The terms in the above equation can be interpreted as follows:

C_{i_0}	trim coefficients (e.g., the axial force $C_{\bar{x}_0}$)
C_{i_α}, C_{i_β}	initial static force or moment curve slopes (e.g. initial normal-force-curve slope)
$C_{i_{\dot\alpha}}$, $C_{i_{\dot\beta}}$	damping coefficient due to rates of change of angle of attack and sideslip
C_{i_p}, C_{i_q}, C_{i_r}	damping due to model roll, pitch, and yaw
$C_{i_{\alpha p}}$, $C_{i_{\beta p}}$, ...	Magnus terms. (A body traveling in, say, the x direction and spinning about the z axis experiences a force in the y direction due to the spin; forces of this type are called Magnus forces.)

These coefficients depend on Mach number, Reynolds number, and perhaps on other test conditions, but not on $\bar{\alpha}$, $\bar{\beta}$, p, q, r and their derivatives. In any ballistic range test there will be a change of Mach number, Reynolds number, etc., over the length of flight. One could expand the coefficients about the values at the center of the flight trajectory to yield a mean value.

$$
C_{i_K} = C_{i_K}\Big|_{mean} + \frac{\partial C_{i_K}}{\partial M_\infty}\Delta M_\infty + \frac{\partial C_{i_K}}{\partial R_\infty}\Delta R_\infty + \ldots
$$

For most of the material covered here, the following assumptions will be made:

$$
\frac{\partial C_{i_K}}{\partial M_\infty}\Delta M_\infty \ll C_{i_K}\Big|_{mean}
$$

$$
\frac{\partial C_{i_K}}{\partial R_\infty}\Delta R_\infty \ll C_{i_K}\Big|_{mean} .
$$

Therefore, for all flight conditions

$$C_{i_K} = C_{i_K}\big|_{mean}.$$

Note that these assumptions may be satisfied in two ways: either the derivatives are small (normally they are except at certain critical conditions such as in the transonic regime); or there is little change in conditions along the instrumented flight path. For example, the velocity loss is small.

In general, (7.74) states that there are 126 aerodynamic coefficients (first-order plus Magnus terms). However, depending on the degree of symmetry exhibited by the particular body under consideration many of the terms are zero or equal to other terms. The reader should be aware at this point that although these symmetry arguments are based on good mathematical and physical concepts, there are some recent experimental data[7.11] which show that under certain conditions an (apparently) axisymmetric body at some angle of attack and zero yaw experiences nonzero side forces. These forces are not understood at present. With this in mind conventional symmetry arguments will be presented.

7.4.2.3 Mirror Symmetry About One Plane (Airplane-like)

Mirror symmetry was considered in a very general mathematical fashion by Maple and Synge[7.12] and a good physical description is given by Charters[7.6]. Under the conditions of mirror symmetry many of the coefficients in (7.74) are zero. In addition Magnus terms can be ignored for airplane configurations because roll rates are normally of the order of pitching rates and hence the Magnus terms are 2nd order.

The force and moment coefficients can be written as*

$$\left.\begin{aligned}
C_{\bar{x}} &= -C_{\bar{x}_0} - C_{\bar{x}_\alpha}\bar{\alpha} - C_{\bar{x}_{\dot{\alpha}}}\frac{\dot{\bar{\alpha}}l}{V} - C_{\bar{x}_q}\frac{ql}{V} \\
C_{\bar{y}} &= C_{\bar{y}_\beta}\bar{\beta} + C_{\bar{y}_{\dot{\beta}}}\frac{\dot{\bar{\beta}}l}{V} + C_{\bar{y}_p}\frac{pl}{V} + C_{\bar{y}_r}\frac{rl}{V} + \left[C_{\bar{y}_0}\right] \\
C_{\bar{z}} &= -C_{\bar{z}_0} - C_{\bar{z}_\alpha}\bar{\alpha} - C_{\bar{z}_{\dot{\alpha}}}\frac{\dot{\bar{\alpha}}l}{V} - C_{\bar{z}_q}\frac{ql}{V} \\
C_l &= C_{l_\beta}\bar{\beta} + C_{l_{\dot{\beta}}}\frac{\dot{\bar{\beta}}l}{V} + C_{l_p}\frac{pl}{V} + C_{l_r}\frac{rl}{V} + \left[C_{l_0}\right] \\
C_m &= C_{m_0} + C_{m_\alpha}\bar{\alpha} + C_{m_{\dot{\alpha}}}\frac{\dot{\bar{\alpha}}l}{V} + C_{m_q}\frac{ql}{V} \\
C_n &= C_{n_\beta}\bar{\beta} + C_{n_{\dot{\beta}}}\frac{\dot{\bar{\beta}}l}{V} + C_{n_p}\frac{pl}{V} + C_{n_r}\frac{rl}{V} + \left[C_{n_0}\right].
\end{aligned}\right\} \tag{7.75}$$

These then represent the linear force and moment coefficients for airplane-like configurations. The minus signs on $\bar{x}$ and $\bar{z}$ are in conformity with standard practice. There remain 27 coefficients.

7.4.2.4 N-gonal Symmetry Plus Mirror Symmetry

This notation simply means that the configuration has a plane of symmetry and has N indistinguishable orientations of roll about its axis of symmetry located $2\pi/N$ radians apart. Magnus terms will be retained now since p can be large. Again Maple and Synge[7.12] have given the results which follow (as well as for the N-gonal case without mirror symmetry, e.g., canted fins), and a good physical description of a configuration with 90° roll symmetry (N = 4) has been given by Charters[7.6]. It will suffice here to state that for linear aerodynamics any model with trigonal or greater rotational symmetry can be considered axially symmetric. This additional symmetry allows many more coefficients to be set to zero and also yields

$$\left.\begin{aligned}
&C_{\bar{y}_\beta} = -C_{\bar{z}_\alpha}, \quad C_{\bar{y}_{\dot{\beta}}} = -C_{\bar{z}_{\dot{\alpha}}}, \quad C_{\bar{y}_r} = C_{\bar{z}_q}, \\
&C_{\bar{y}_{\alpha p}} = C_{\bar{z}_{\beta p}}, \quad C_{\bar{y}_{\dot{\alpha} p}} = C_{\bar{z}_{\dot{\beta} p}}, \quad C_{\bar{y}_{qp}} = -C_{\bar{z}_{rp}}, \\
&C_{n_\beta} = -C_{m_\alpha}, \quad C_{n_{\dot{\beta}}} = -C_{m_{\dot{\alpha}}}, \quad C_{n_r} = C_{m_q}, \\
&C_{n_{\alpha p}} = C_{m_{\beta p}}, \quad C_{n_{\dot{\alpha} p}} = C_{m_{\dot{\beta} p}}, \quad C_{n_{qp}} = -C_{m_{rp}}.
\end{aligned}\right\} \tag{7.76}$$

---

* The bracketed terms in (7.75) are ideally zero. In some sections of this chapter, however, they will be retained to account for small asymmetries.

Hence, due to trigonal symmetry or greater the force and moment coefficients become

$$\left.\begin{aligned}
C_{\bar{x}} &= -C_{\bar{x}_0} - C_{\bar{x}_{pp}}\left(\frac{pl}{V}\right)^2 \\
C_{\bar{y}} &= -C_{\bar{z}_\alpha}\bar{\beta} - C_{\bar{z}_{\dot{\alpha}}}\frac{\dot{\bar{\beta}}l}{V} + C_{\bar{z}_q}\frac{rl}{V} + C_{\bar{z}_{\beta p}}\bar{\alpha}\frac{pl}{V} + C_{\bar{z}_{\dot{\beta}p}}\frac{\dot{\bar{\alpha}}l}{V}\frac{pl}{V} - C_{\bar{z}_{rp}}\frac{ql}{V}\frac{pl}{V} + \left[C_{\bar{y}_0}\right] \\
C_{\bar{z}} &= -C_{\bar{z}_\alpha}\bar{\alpha} - C_{\bar{z}_{\dot{\alpha}}}\frac{\dot{\bar{\alpha}}l}{V} - C_{\bar{z}_q}\frac{ql}{V} - C_{\bar{z}_{\beta p}}\bar{\beta}\frac{pl}{V} - C_{\bar{z}_{\dot{\beta}p}}\frac{\dot{\bar{\beta}}l}{V}\frac{pl}{V} - C_{\bar{z}_{rp}}\frac{rl}{V}\frac{pl}{V} - \left[C_{\bar{z}_0}\right] \\
C_l &= C_{l_p}\frac{pl}{V} + \left[C_{l_0}\right] \\
C_m &= C_{m_\alpha}\bar{\alpha} + C_{m_{\dot{\alpha}}}\frac{\dot{\bar{\alpha}}l}{V} + C_{m_q}\frac{ql}{V} + C_{m_{\beta p}}\bar{\beta}\frac{pl}{V} + C_{m_{\dot{\beta}p}}\frac{\dot{\bar{\beta}}l}{V}\frac{pl}{V} + C_{m_{rp}}\frac{rl}{V}\frac{pl}{V} + \left[C_{m_0}\right] \\
C_n &= -C_{m_\alpha}\bar{\beta} - C_{m_{\dot{\alpha}}}\frac{\dot{\bar{\beta}}l}{V} + C_{m_q}\frac{rl}{V} + C_{m_{\beta p}}\bar{\alpha}\frac{pl}{V} + C_{m_{\dot{\beta}p}}\frac{\dot{\bar{\alpha}}l}{V}\frac{pl}{V} - C_{m_{rp}}\frac{ql}{V}\frac{pl}{V} + \left[C_{n_0}\right] .
\end{aligned}\right\} \qquad (7.77)$$

Again, the bracketed terms are ideally zero but are retained to allow for small asymmetries.

7.4.2.5 Drag and Lift Forces for Airplane-like Configurations

The expressions for aerodynamic forces and moments given so far have been in terms of the body-fixed coordinate system. Another frequently used set of aerodynamic force coefficients are those oriented relative to the velocity vector. For airplane-like configurations these are drag, lift, and side force. The drag component is along the velocity vector; the lift force is normal to the velocity vector and the $\bar{y}$ axis; and the side-force forms a right-hand system. These forces can be written by transformation of the forces in the body-fixed axis system:

$$\begin{aligned}
F_D &= -F_{\bar{x}}\cos\bar{\alpha}\cos\bar{\beta} - F_{\bar{y}}\sin\bar{\beta} - F_{\bar{z}}\sin\bar{\alpha}\cos\bar{\beta} \\
F_L &= F_{\bar{x}}\sin\bar{\alpha} \qquad\qquad - F_{\bar{z}}\cos\bar{\alpha} \\
F_S &= F_{\bar{x}}\cos\bar{\alpha}\sin\bar{\beta} \quad - F_{\bar{y}}\cos\bar{\beta} + F_{\bar{z}}\sin\bar{\alpha}\sin\bar{\beta} .
\end{aligned}$$

An alternative is to express them through their own expansions.

$$\begin{aligned}
F_D &= C_D\tfrac{1}{2}\rho V^2 A \\
&= \left(C_{D_0} + C_{D_\alpha}\bar{\alpha} + C_{D_{\dot{\alpha}}}\frac{\dot{\bar{\alpha}}l}{V} + C_{D_q}\frac{ql}{V}\right)\tfrac{1}{2}\rho V^2 A
\end{aligned} \qquad (7.78)$$

$$\begin{aligned}
F_L &= C_L\tfrac{1}{2}\rho V^2 A \\
&= \left(C_{L_0} + C_{L_\alpha}\bar{\alpha} + C_{L_{\dot{\alpha}}}\frac{\dot{\bar{\alpha}}l}{V} + C_{L_q}\frac{ql}{V}\right)\tfrac{1}{2}\rho V^2 A
\end{aligned} \qquad (7.79)$$

$$F_S = C_S\tfrac{1}{2}\rho V^2 A . \qquad (7.80)$$

7.4.2.6 Drag and Lift Forces for Axially Symmetric Bodies

For axially symmetric bodies, the drag force is again along the velocity vector, but the lift is now defined as being normal to the velocity vector and in a plane such that there is no side force. It is difficult to express these forces in terms of body-fixed forces because of the Magnus terms. Ignoring Magnus terms, the drag and lift are related to the body-fixed forces through the resultant angle of attack, α_R

$$\left.\begin{aligned}
F_D &= -F_{\bar{x}}\cos\alpha_R + F_N\sin\alpha_R \\
F_L &= F_{\bar{x}}\sin\alpha_R + F_N\cos\alpha_R \\
F_S &= 0
\end{aligned}\right\} \qquad (7.81)$$

where $F_N = |F_{\bar{y}} + iF_{\bar{z}}|$.

Note that F_N is frequently referred to as normal force and $F_{\bar{x}}$ as axial force.

The drag and lift forces can also be written with their own expansions, and to first order including the Magnus terms

$$F_D = C_D \tfrac{1}{2}\rho V^2 A = \left(C_{D_0} + C_{D_{pp}} \left(\frac{pl}{V} \right)^2 \right) \tfrac{1}{2}\rho V^2 A \tag{7.82}$$

$$F_L = \left[\left(C_{L_\alpha} + iC_{L_{\alpha p}} \frac{pl}{V} \right) (\bar{\beta} + i\bar{\alpha}) + \left(C_{L_{qp}} \frac{pl}{V} + iC_{L_q} \right) \frac{l}{V} (q + ir) + \left(C_{L_{\dot{\alpha}}} + iC_{L_{\dot{\alpha}p}} \frac{pl}{V} \right) \frac{l}{V} (\dot{\bar{\beta}} + i\dot{\bar{\alpha}}) \right] \tfrac{1}{2}\rho V^2 A \ . \tag{7.83}$$

7.4.2.7 Coordinate Transformation of Angular Rates

A question which has not been considered up to this point is what happens to the rate terms in the force and moment expressions when rotations about the $\bar{x}$-axis are required in transforming from one reference frame to another; for example, from body-fixed coordinates to fixed-plane coordinates. The complex angle, $(\bar{\beta} + i\bar{\alpha})$, when rotated to fixed-plane coordinates, is simply

$$e^{i\int \dot{\phi}\, dt} (\bar{\beta} + i\bar{\alpha}) = \tilde{\beta} + i\tilde{\alpha} \ .$$

Consider the rate terms by differentiating both sides with respect to time:

$$e^{i\int \dot{\phi}\, dt} (\dot{\bar{\beta}} + i\dot{\bar{\alpha}}) + i\dot{\phi} e^{i\int \dot{\phi}\, dt} (\bar{\beta} + i\bar{\alpha}) = \dot{\tilde{\beta}} + i\dot{\tilde{\alpha}} \ .$$

Rearranging and substituting $\tilde{\beta} + i\tilde{\alpha}$ for $e^{i\int \dot{\phi}\, dt} (\bar{\beta} + i\bar{\alpha})$ we get

$$e^{i\int \dot{\phi}\, dt} (\dot{\bar{\beta}} + i\dot{\bar{\alpha}}) = (\dot{\tilde{\beta}} + i\dot{\tilde{\alpha}}) - i\dot{\phi} (\tilde{\beta} + i\tilde{\alpha}) \ .$$

Note that we have generated an additional term. Murphy[7.9] "avoids" this by including a term of opposite sign $(+i\dot{\phi}(\bar{\beta} + i\bar{\alpha}))$ in the force and moment expressions in body-fixed coordinates, and hence the second term disappears after transformation. Nicolaides[7.5] neglects the second term in the above equation completely. An important conclusion is that when rate coefficients are quoted, one should indicate what coordinate system they are applicable to.

7.4.3 Differential Equations of Motion

The momentum equations and expressions for the forces and moments may now be combined to obtain the equations of motion for use in analyzing experimental data.

7.4.3.1 Airplane-like Configurations

The equations of motion of an airplane-like configuration can now be obtained by combining the momentum equations (7.24), (7.25), (7.26), and (7.35) with the forces and moments given by Equation (7.75). The linear momentum equations for small angles and angular rates (except roll), neglecting gravity and Coriolis forces, then become

$$m \frac{d^2x}{dt^2} = F_x \cong F_{\bar{x}} + F_{\bar{z}}\bar{\alpha} + F_{\bar{y}}\bar{\beta}$$

$$\cong - \left[C_{D_0} + C_{D_\alpha}\bar{\alpha} + C_{D_{\dot{\alpha}}} \frac{\dot{\bar{\alpha}} l}{V} + C_{D_q} \frac{ql}{V} \right] \tfrac{1}{2}\rho V^2 A \tag{7.84}$$

$$m \frac{d^2y}{dt^2} = F_y \cong - (F_{\bar{z}} - F_{\bar{x}}\bar{\alpha}) \sin\phi + (F_{\bar{y}} - F_{\bar{x}}\bar{\beta}) \cos\phi \tag{7.85}$$

$$m \frac{d^2z}{dt^2} = F_z \cong (F_{\bar{z}} - F_{\bar{x}}\bar{\alpha}) \cos\phi + (F_{\bar{y}} - F_{\bar{x}}\bar{\beta}) \sin\phi \tag{7.86}$$

where $(F_{\bar{z}} - F_{\bar{x}}\bar{\alpha}) \approx - F_L$ is given by (7.79) as

$$F_L = \left(C_{L_0} + C_{L_\alpha}\bar{\alpha} + C_{L_{\dot{\alpha}}} \frac{\dot{\bar{\alpha}} l}{V} + C_{L_q} \frac{ql}{V} \right) \tfrac{1}{2}\rho V^2 A \ . \tag{7.87}$$

Now using the angle relationships developed earlier for small angles (Equation (7.14)), the angle of attack and sideslip in body-fixed axes can be written as

$$\bar{\alpha} = (\theta_{ME} - \gamma_2) \cos\phi + (\psi_{ME} - \gamma_1) \sin\phi \tag{7.88}$$

$$\bar{\beta} = - (\psi_{ME} - \gamma_1) \cos\phi + (\theta_{ME} - \gamma_2) \sin\phi \ . \tag{7.89}$$

Differentiate these equations to get $\dot{\bar{\alpha}}$ and $\dot{\bar{\beta}}$; then substitute the small angle expressions of p, q, and r (see table in Section 7.4.1.4), note that $\dot{\gamma}_2 \cong - (1/V)\ddot{z}$ and $\dot{\gamma}_1 = (1/V)\ddot{y}$, and utilize (7.85) and (7.86) to arrive at

$$\dot{\bar{\alpha}} = q - p\bar{\beta} + \frac{F_{\bar{z}} - F_{\bar{x}}\bar{\alpha}}{mV} \tag{7.90}$$

$$\dot{\bar{\beta}} = -r + p\bar{\alpha} + \frac{F_{\bar{y}} - F_{\bar{x}}\bar{\beta}}{mV} . \tag{7.91}$$

Equations (7.35), (7.90), and (7.91) can be combined and after eliminating q and r and their derivatives, the following differential equations are obtained.

$$\left[C_{l_\beta}\bar{\beta} + (C_{l_{\dot\beta}} - C_{l_r})\frac{\dot{\bar{\beta}}l}{V} + C_{l_p}\frac{pl}{V} + C_{l_r}\frac{pl}{V}\bar{\alpha}\right]\frac{\rho V^2 Al}{2I_{\bar{x}}} +$$

$$+\left(\frac{I_{\bar{y}} - I_{\bar{z}}}{I_{\bar{x}}}\right)\left(\frac{\rho VA}{2m}\right)\left[C_{\bar{y}_p}(\dot{\bar{\alpha}} + p\bar{\beta})\frac{pl}{V} - C_{L_0}(\dot{\bar{\beta}} - p\bar{\alpha}) + C_{\bar{y}_0}(\dot{\bar{\alpha}} + p\bar{\beta})\right] = \dot{p} \tag{7.92}$$

$$\ddot{\bar{\alpha}} + C_1\dot{\bar{\alpha}} + C_2\bar{\alpha} + C_3\dot{\bar{\beta}} + C_4\bar{\beta} - \frac{\rho V^2 Al}{2I_{\bar{y}}}C_{m_0} + \dot{p}\bar{\beta} -$$

$$- \frac{I_{\bar{z}} - I_{\bar{x}}}{I_{\bar{y}}}p\frac{\rho VA}{2m}\left(C_{\bar{y}_p}\frac{pl}{V} + C_{\bar{y}_0}\right) = 0 \tag{7.93}$$

$$\ddot{\bar{\beta}} + C_5\dot{\bar{\beta}} + C_6\bar{\beta} + C_7\dot{\bar{\alpha}} + C_8\bar{\alpha} + \frac{\rho V^2 Al}{2I_{\bar{z}}}C_{n_0} - \dot{p}\bar{\alpha} +$$

$$+ \frac{I_{\bar{x}} - I_{\bar{y}}}{I_{\bar{z}}}p\frac{\rho VA}{2m}C_{L_0} + \frac{\rho V^2 Al}{2I_{\bar{z}}}C_{n_p}\frac{pl}{V} = 0 \tag{7.94}$$

where

$$C_1 = \frac{\rho VA}{2m}C_{L_\alpha} - \frac{\rho V^2 Al}{2I_{\bar{y}}}\frac{l}{V}(C_{m_q} + C_{m_{\dot\alpha}})$$

$$C_2 = -\frac{\rho V^2 Al}{2I_{\bar{y}}}C_{m_\alpha} - \frac{I_{\bar{z}} - I_{\bar{x}}}{I_{\bar{y}}}p^2$$

$$C_3 = \left(\frac{I_{\bar{z}} - I_{\bar{x}}}{I_{\bar{y}}} + 1\right)p$$

$$C_4 = \left[-\frac{\rho V^2 Al}{2I_{\bar{y}}}\frac{l}{V}C_{m_q} - \frac{I_{\bar{z}} - I_{\bar{x}}}{I_{\bar{y}}}\frac{\rho VA}{2m}(C_{\bar{y}_\beta} + C_{D_0})\right]p$$

$$C_5 = -\frac{\rho VA}{2m}(C_{\bar{y}_\beta} + C_{D_0}) - \frac{\rho V^2 Al}{2I_{\bar{z}}}\frac{l}{V}(C_{n_r} - C_{n_{\dot\beta}})$$

$$C_6 = \frac{\rho V^2 Al}{2I_{\bar{z}}}C_{n_\beta} + \frac{I_{\bar{x}} - I_{\bar{y}}}{I_{\bar{z}}}p^2$$

$$C_7 = \left(\frac{I_{\bar{x}} - I_{\bar{y}}}{I_{\bar{z}}} - 1\right)p$$

$$C_8 = \left[\frac{\rho V^2 Al}{2I_{\bar{z}}}\frac{l}{V}C_{n_r} + \frac{I_{\bar{x}} - I_{\bar{y}}}{I_{\bar{z}}}\frac{\rho VA}{2m}C_{L_\alpha}\right]p .$$

In the above coefficients the following types of terms were deleted:

(i) Products of aerodynamic coefficients (because they always appear with $(\rho Al/2I)^2$ or $(\rho A/2m)(\rho Al/2I)$ which are normally very small).

(ii) Certain rate terms which appear with other terms that are much larger; for example $(\rho Al/2m)(C_{L_q} + C_{L_{\dot\alpha}}) \ll 1$.

(iii) Terms involving products of angles and/or angular rates, like $\bar{\alpha}\bar{\beta}$ or $\dot{\bar{\alpha}}\bar{\beta}$.

Equations (7.84), (7.85), (7.86), (7.92), (7.93), and (7.94) are the equations of motion used for the analysis of airplane-like configurations. Note that for constant roll rate the right hand side of Equation (7.92) is zero as is the $\dot{p}$ term in (7.93) and (7.94). Note also that the last term in (7.93) and the last two terms in (7.94) are normally ignored.

Even for constant roll rate the coefficients C_1, C_2, C_4, C_5, C_6, and C_8 are not strictly constant since they contain velocity which will change because of drag. The coefficients can be made essentially constant by changing the independent variable from time to distance. This is accomplished as follows:

$$\frac{d}{dt} = u \frac{d}{dx}$$

$$\frac{d^2}{dt^2} = \frac{d}{dt}\left(u \frac{d}{dx}\right) = u^2 \frac{d^2}{dx^2} + \frac{du}{dt} \frac{d}{dx} ;$$

but $V \cong u$,

so $$\frac{du}{dt} = - C_D \frac{\rho V^2 A}{2m} ,$$

and hence $$\frac{d^2}{dt^2} = V^2 \frac{d^2}{dx^2} - C_D \frac{\rho A}{2m} V^2 \frac{d}{dx}$$

$$p(t) = Vp(x) .$$

Equations (7.85), (7.86), (7.93), and (7.94) now become

$$\frac{d^2y}{dx^2} = \frac{\rho A}{2m} C_D \frac{dy}{dx} + \frac{F_L}{mV^2} \sin\phi + \frac{F_{\bar{y}} - F_{\bar{x}}\bar{\beta}}{mV^2} \cos\phi \tag{7.95}$$

$$\frac{d^2z}{dx^2} = \frac{\rho A}{2m} C_D \frac{dz}{dx} - \frac{F_L}{mV^2} \cos\phi + \frac{F_{\bar{y}} - F_{\bar{x}}\bar{\beta}}{mV^2} \sin\phi . \tag{7.96}$$

Retaining the most dominant terms, the forces are given by

$$F_L = \frac{\rho V^2 A}{2} (C_{L_0} + C_{L_\alpha}\bar{\alpha}) , \qquad F_{\bar{x}} = - \frac{\rho V^2 A}{2} C_D ,$$

$$F_{\bar{y}} = \frac{\rho V^2 A}{2} (C_{\bar{y}_0} + C_{\bar{y}_\beta}\bar{\beta})$$

$$\bar{\alpha}'' + \bar{C}_1\bar{\alpha}' + \frac{1}{V^2} C_2\bar{\alpha} + \frac{1}{V} C_3\bar{\beta}' + \frac{1}{V^2} C_4\bar{\beta} - \frac{C_{m_q}\rho A l}{2I_{\bar{y}}} = 0 \tag{7.97}$$

$$\bar{\beta}'' + \bar{C}_5\bar{\beta}' + \frac{1}{V^2} C_6\bar{\beta} + \frac{1}{V} C_7\bar{\alpha}' + \frac{1}{V^2} C_8\bar{\alpha} + \frac{C_{n_q}\rho A l}{2I_{\bar{z}}} = 0 , \tag{7.98}$$

where

$$\bar{C}_1 = \frac{1}{V} C_1 - \frac{\rho A}{2m} C_D$$

$$\bar{C}_5 = \frac{1}{V} C_5 - \frac{\rho A}{2m} C_D .$$

The coefficients are now considered as constants, based on the assumption that the aerodynamic derivatives are invariant.

7.4.3.2 Axially Symmetric Bodies

To determine the differential equations of motion for axially symmetric bodies, we start with the Lagrangian dynamic equations. The Lagrangian equations for small angles and constant roll rate (Equation (7.67)), rotated to fixed-plane coordinates (and where $M_m = C_m \rho V^2 A l/2$ is obtained from Equation (7.77)), become

$$I\ddot{\vec{\Omega}} - iI_{\bar{x}}p\dot{\vec{\Omega}} = \tfrac{1}{2}\rho V^2 A l \left[\left(C_{m_{\alpha_p}} \frac{pl}{V} - iC_{m_\alpha}\right)(\tilde{\beta} + i\tilde{\alpha}) + \left(C_{m_q} - iC_{m_{qp}} \frac{pl}{V}\right)\frac{l}{V}(\tilde{q} + i\tilde{r}) + \right.$$

$$\left. + \left(C_{m_{\dot{\alpha}_p}} \frac{pl}{V} - iC_{m_{\dot{\alpha}}}\right)\frac{l}{V}(\dot{\tilde{\beta}} + i\dot{\tilde{\alpha}})\right] , \tag{7.99}$$

where $\dot{\vec{\Omega}} = \dot{\theta}_{ME} + i\dot{\psi}_{ME}$.

It should be noted that $C_{m_{\beta_p}}$ and $C_{m_{\dot{\beta}_p}}$ (Equation (7.77)) have been written here as $C_{m_{\alpha_p}}$ and $C_{m_{\dot{\alpha}_p}}$, which is the more common notation for those coefficients; for axisymmetric bodies, derivatives with respect to $\tilde{\alpha}$ or $\tilde{\beta}$ are equivalent. The same argument applies to writing $C_{m_{rp}}$ as $C_{m_{qp}}$.

Transforming the forces given by (7.82) and (7.83) into y and z directions and including gravity and Coriolis forces from (7.70) and (7.71), the linear momentum equations (7.24)-(7.26) become

$$\ddot{x} = -\frac{\rho V^2 A}{2m} C_D$$

$$\ddot{y} + i\ddot{z} = -\frac{\rho V^2 A}{2m}\left[\left(C_{L_\alpha} + iC_{L_{\alpha p}}\frac{pl}{V}\right)(\tilde{\beta} + i\tilde{\alpha}) + \right.$$

$$+ \left(C_{L_{qp}}\frac{pl}{V} + iC_{L_q}\right)\frac{l}{V}(\tilde{q} + i\tilde{r}) + \left(C_{L_{\dot{\alpha}}} + iC_{L_{\dot{\alpha}p}}\frac{pl}{V}\right)\frac{l}{V}(\dot{\tilde{\beta}} + i\dot{\tilde{\alpha}}) +$$

$$\left. + C_D(\gamma_1 - i\gamma_2)\right] + ig - 2\omega_E V(\sin\theta_l + i\cos\theta_l \sin\theta_a) \quad . \tag{7.100}$$

Here γ_1 and γ_2 are the projections of the local flight path angle γ on the x-y and x-z planes, g is the acceleration due to gravity, and the last term is the Coriolis acceleration. Combining (7.99), (7.100), and (7.15) and making the following assumptions:

(i) Products of aerodynamic derivatives are small and may be neglected.

(ii) Multiple-term coefficients preceding the various derivatives of $\vec{\alpha}_R$ which are of the form $(1 + a + b \ldots .)$, where a, b, etc. are $\ll 1$, are treated as just 1.

(iii) The quantity $(\rho A/2m)\, C_D L$ is much less than one. For cases with small roll rates where Magnus forces and moments are not important, this can be relaxed to $(\rho A/2m)(\lambda/2\pi) C_D \ll 1$. Here, λ is the wavelength of the oscillatory motion and L is the length of the facility.

the equations of motion for axially symmetric bodies become:

$$\ddot{\vec{\alpha}}_R - B_1\dot{\vec{\alpha}}_R - B_2\vec{\alpha}_R = 0 \quad , \tag{7.101}$$

where

$$\vec{\alpha}_R = \tilde{\beta} + i\tilde{\alpha}$$

$$B_1 = \frac{\rho VA}{2m}\left\{-C_{L_\alpha} + \frac{ml^2}{I}(C_{m_q} + C_{m_{\dot{\alpha}}}) + i\frac{pl}{V}\left[-C_{L_{\alpha p}} + \frac{ml^2}{I}(C_{m_{\dot{\alpha}p}} - C_{m_{qp}})\right]\right\} +$$

$$+ i\frac{I_{\tilde{x}}}{I}p$$

$$B_2 = \frac{\rho V^2 Al}{2I}\left(C_{m_\alpha} + iC_{m_{\alpha p}}\frac{pl}{V}\right) - \frac{\rho VA}{2m}\frac{I_{\tilde{x}}}{I}p\left(C_{L_{\alpha p}}\frac{pl}{V} - iC_{L_\alpha}\right),$$

$$\ddot{y} + i\ddot{z} = -\frac{\rho V^2 A}{2m}\left\{\left(C_{L_\alpha} + iC_{L_{\alpha p}}\frac{pl}{V}\right)(\tilde{\beta} + i\tilde{\alpha}) + \frac{l}{V}\left[(C_{L_q} + C_{L_{\dot{\alpha}}}) + \right.\right.$$

$$\left. + i(C_{L_{\dot{\alpha}p}} - C_{L_{qp}})\frac{pl}{V}\right](\dot{\tilde{\beta}} + i\dot{\tilde{\alpha}}) +$$

$$\left. + C_D(\gamma_1 - i\gamma_2)\right\} + ig - 2\omega_E V(\sin\theta_l + i\cos\theta_l \sin\theta_a) \quad . \tag{7.102}$$

For clarity, the definitions of the derivatives appearing in the last two equations are as follows:

$$C_{m_\alpha} = \frac{\partial C_m}{\partial \alpha} \quad , \qquad \text{static moment-curve slope}$$

$$C_{m_q} + C_{m_{\dot{\alpha}}} = \frac{\partial C_m}{\partial (ql/V)} + \frac{\partial C_m}{\partial (\dot{\alpha} l/V)} \quad , \qquad \text{damping-in-pitch derivative}$$

$$C_{m_{\alpha p}} = \frac{\partial^2 C_m}{\partial \alpha\, \partial (pl/V)} \quad , \qquad \text{static Magnus moment coefficient}$$

$$C_{m_{\dot{\alpha}p}} - C_{m_{qp}} = \frac{\partial^2 C_m}{\partial (\dot{\alpha} l/V)\, \partial (pl/V)} - \frac{\partial^2 C_m}{\partial (ql/V)\, \partial (pl/V)} \quad , \qquad \text{dynamic Magnus moment coefficient}$$

$$C_{L_\alpha} = \frac{\partial C_L}{\partial \alpha} \quad , \qquad \text{lift-curve slope}$$

$$C_{L_q} + C_{L_{\dot{\alpha}}} = \frac{\partial C_L}{\partial (ql/V)} + \frac{\partial C_L}{\partial (\dot{\alpha} l/V)} \quad , \qquad \text{lift derivative due to pitching and plunging}$$

$$C_{L_{\alpha p}} = \frac{\partial^2 C_L}{\partial \alpha \, \partial (pl/V)} , \qquad \text{static Magnus force coefficient}$$

$$C_{L_{\dot{\alpha} p}} - C_{L_{qp}} = \frac{\partial^2 C_L}{\partial (\dot{\alpha} l/V) \, \partial (pl/V)} - \frac{\partial^2 C_L}{\partial (ql/V) \, \partial (pl/V)} , \qquad \text{dynamic Magnus force coefficient.}$$

Distance again proves to be a more convenient independent variable than time, since it eliminates (to second order at least) the velocity from the equations. The transformation of (7.101) proceeds as follows:

$$\dot{\vec{\alpha}}_R = \dot{x} \vec{\alpha}'_R = V \cos\gamma \, \vec{\alpha}'_R \approx V \vec{\alpha}'_R \qquad (\cos\gamma \approx 1)$$

$$\ddot{\vec{\alpha}}_R = V \frac{d\vec{\alpha}'_R}{dt} + \vec{\alpha}'_R \frac{dV}{dt} = V \frac{d^2 \vec{\alpha}_R}{dx^2} \frac{dx}{dt} + \vec{\alpha}'_R \frac{d^2 x}{dt^2}$$

$$= V^2 \left(\vec{\alpha}''_R - C_D \frac{\rho A}{2m} \vec{\alpha}'_R \right)$$

$$p(t) = V p(x) .$$

Then (7.101) becomes

$$\vec{\alpha}''_R - \left\{ \frac{\rho A}{2m} \xi + i \frac{\rho A}{2m} pl \left[-C_{L_{\alpha p}} + \frac{ml^2}{I} \left(C_{m_{\dot{\alpha} p}} - C_{m_{qp}} \right) \right] + i \frac{I_{\tilde{x}}}{I} p \right\} \vec{\alpha}'_R -$$

$$- \left\{ \frac{\rho A l}{2I} \left(C_{m_\alpha} + i C_{m_{\alpha p}} pl \right) - \frac{\rho A}{2m} \frac{I_{\tilde{x}}}{I} p \left(C_{L_{\alpha p}} pl - i C_{L_\alpha} \right) \right\} \vec{\alpha}_R = 0, \qquad (7.103)$$

where ξ, which is called the dynamic stability parameter for unpowered flight at constant altitude, is defined as

$$\xi = C_D - C_{L_\alpha} + \frac{ml^2}{I} \left(C_{m_q} + C_{m_{\dot{\alpha}}} \right) . \qquad (7.104)$$

A similar transformation applied to (7.102), again assuming γ is small, leads to the following differential equation:

$$y'' + iz'' = -\frac{\rho A}{2m} \{ (C_{L_\alpha} + i C_{L_{\alpha p}} pl)(\tilde{\beta} + i\tilde{\alpha}) +$$

$$+ l [(C_{L_q} + C_{L_{\dot{\alpha}}}) + i (C_{L_{\dot{\alpha} p}} - C_{L_{qp}}) pl] (\tilde{\beta}' + i\tilde{\alpha}') \} +$$

$$+ \frac{ig}{V^2} - 2 \frac{\omega_E}{V} (\sin\theta_l + i \cos\theta_l \sin\theta_a) . \qquad (7.105)$$

We will now allow for the possibility of small asymmetries.

7.4.3.3 Small Asymmetries

For the axially symmetric body case just considered, but with slight asymmetries in forces and moments which are body fixed, we can, following Nicolaides[7-5], simply add to the force and moment equations a term which rotates the asymmetry into the fixed-plane coordinates. The appropriate term to add to the right-hand side of (7.103) is

$$\left[-\frac{\rho A l}{2I} C_{m_{\delta_\epsilon}} + i \frac{\rho A}{2m} \frac{p}{V} \left(1 - \frac{I_{\tilde{x}}}{I} \right) C_{L_{\delta_\epsilon}} \right] \delta_\epsilon e^{ipx} , \qquad (7.106)$$

while the term to add to the right-hand side of (7.105) is

$$-\frac{\rho A}{2m} C_{L_{\delta_\epsilon}} \delta_\epsilon e^{ipx} , \qquad (7.107)$$

where $C_{L_{\delta_\epsilon}}$ and $C_{m_{\delta_\epsilon}}$ are the trim force and moment coefficients due to small asymmetries from, for example, a flap deflection δ_ϵ. If the body is externally axisymmetric but has a center of mass not on the axis of external symmetry, then only $C_{m_{\delta_\epsilon}}$ would have a value.

Equations (7.103) and (7.105), along with the additional terms given by (7.106) and (7.107), represent the equations normally used for analysis of axisymmetric bodies with small asymmetries. They are often referred to as the tricyclic equations, a term which gives a physical description of the solution of (7.103) plus (7.106).

7.5 DRAG ANALYSIS

Consider that a test has been conducted in a ballistic range and that time and distance data have been obtained at a number of discrete observation stations. It is desired to determine the drag coefficient governing the test model. We start with the momentum equation along the flight path, which is (neglecting gravity)

$$m \frac{d^2\hat{x}}{dt^2} = F_{\hat{x}} = -D ,$$

where $\hat{x}$ is the distance traversed by the model c.g. and the drag, D, can be written

$$D = \frac{\rho A}{2}\left(\frac{d\hat{x}}{dt}\right)^2 C_D .$$

Note that the measured data are along the earth fixed axis, x, not along $\hat{x}$. However, x is related to $\hat{x}$ by

$$x = \int_0^{\hat{x}} \cos\gamma \, d\hat{x}$$

or

$$\hat{x} = \int_0^{x} \frac{dx}{\cos\gamma} ,$$

where γ is the angle between the x axis and the flight path. Extracting the drag coefficient from time and x-distance measurements using the above equations is a difficult task. In ballistic range testing, however, γ is normally less than a degree (1 ft swerve in 60 ft of travel). Hence, one can make the very good approximation that $\cos\gamma = 1$, and thus $\hat{x} = x$. The momentum equation can then be written

$$\frac{d^2x}{dt^2} = \frac{dV}{dt} = -\frac{\rho A}{2m} V^2 C_D \tag{7.108a}$$

or

$$\frac{dV}{dx} = -\frac{\rho A}{2m} V C_D . \tag{7.108b}$$

This is the basic equation for determining the drag coefficient.

7.5.1 Case with Constant Coefficients

When the density, reference area, mass, and drag coefficient (ρ, A, m, C_D) are all constants, (7.108) can be integrated in a straightforward manner. From (7.108a),

$$V = \frac{V_0}{1 + V_0 K C_D (t - t_0)} . \tag{7.109a}$$

Alternately from (7.108b)

$$\left.\begin{aligned} \log_e V &= \log_e V_0 - K C_D (x - x_0) \\ V &= V_0 e^{-K C_D (x - x_0)} , \end{aligned}\right\} \tag{7.109b}$$

where $K = \rho A/2m$, and the initial conditions are $t = t_0$, $V = V_0$ at $x = x_0$.

Integrating again yields

$$t = t_0 + \frac{1}{V_0 K C_D}\left[e^{K C_D (x - x_0)} - 1\right] . \tag{7.110}$$

Any of these equations can be used to determine the drag coefficient, and different simplifications are employed which lead to varying degrees of accuracy. The simplest approaches will be considered first since they are amenable to hand calculations and then more complicated ones suitable for high speed digital computers will be discussed. (A brief discussion of drag determination is also given in Chapter 10, Section 10.2.3).

Method 1: The simpler methods are based on (7.109) rather than (7.110), and begin by calculating the velocity. The average velocity between stations $i - 1$ and i is given as

$$V_{AV} = \frac{x_i - x_{i-1}}{t_i - t_{i-1}} . \tag{7.111}$$

For small velocity loss, this average velocity may be assumed to occur at the center of the distance interval, and the use of two adjacent intervals will give two velocities whose difference ΔV is a measure of the deceleration. Thus, data from two such intervals may be substituted into (7.108b) in difference form

$$\frac{\Delta V}{\Delta x} = -KV_{AV}C_D \tag{7.112}$$

to calculate C_D. Here V_{AV} is the average velocity over the double interval of three measuring stations.

Method 2: More accurately, the velocities calculated using (7.111) may be used in (7.109b) which may be written as

$$\log_e V = \log_e V_0 - KC_D x , \tag{7.113}$$

where x_0 has been arbitrarily set to zero. The slope of a plot of $\log_e V$ versus x is $-KC_D$. A least squares fit (see Section 7.12) of this linear equation to the $\log_e V$ versus x data will yield the drag coefficient.

This approach still retains a small error in that the average velocity does not occur at the center of the interval. The error can be almost entirely eliminated by a procedure suggested by Seiff[7.13]. This procedure is given next.

Method 3: First note that (7.109) and (7.110) can be combined to yield

$$\Delta t = \frac{1}{KC_D}\left(\frac{1}{V_f} - \frac{1}{V_0}\right), \tag{7.114}$$

where V_f is the velocity at the end of an interval, V_0 is the velocity at the beginning of an interval, and Δt is the time of flight over that interval. Next the average velocity for that interval is

$$V_{AV} = \frac{\Delta x}{\Delta t} = KC_D \Delta x \frac{1}{\left(\frac{1}{V_f} - \frac{1}{V_0}\right)} . \tag{7.115}$$

Now consider at what x position this average velocity occurs. Using (7.109),

$$V_{AV} = V_0 e^{-KC_D \kappa \Delta x} , \tag{7.116}$$

where $\kappa\Delta x$ is the x position in the interval (measured from the beginning of the interval) at which V_{AV} occurs ($\kappa = \frac{1}{2}$ for constant deceleration). Combining (7.115) and (7.116) yields κ as

$$\kappa = \frac{\log_e \left[\left(\frac{V_0}{V_f} - 1\right) \Big/ \log_e \frac{V_0}{V_f}\right]}{\log_e \frac{V_0}{V_f}} . \tag{7.117}$$

This then represents the fraction of the interval Δx at which the average velocity occurs and hence the point where V_{AV} should be plotted.

To apply this result, κ is first set equal to $\frac{1}{2}$. After the first approximation to the velocity-distance curve is obtained, κ can be evaluated for each interval and x positions adjusted accordingly. This new set of data can be treated as before and iterated to convergence. (Normally, a single iteration is sufficient.) This procedure is straightforward but requires precise calculation in evaluating κ from (7.117).

Method 4: Another approach is to use (7.110) to obtain the drag coefficient directly from the time-distance data. An approximate method for employing this equation is to expand the exponential and retain terms to order x^2. Thus, setting $x_0 = 0$, we obtain

$$t = t_0 + \frac{1}{V_0} x + \frac{KC_D}{2V_0} x^2 . \tag{7.118}$$

A least-squares fit will then yield the drag coefficient.

Method 5: Equation (7.110) could also be used without any expansion approximations even though C_D appears in an exponent by using either a differential correction procedure or some other numerical procedure to minimize the sum of the squares of the residuals of measured and calculated times at the given x locations. One method of minimizing residuals is to fix the value of the drag coefficient (use approximate value of C_D obtained from applying Equation (7.118) to start with) and fit (7.110) to the x-t data by least-squares (this is straightforward) and obtain values for V_0 and t_0. Next compute the sum of the squares of the time residuals, then change the drag coefficient a small amount and repeat the process. If the sum of the squares of the residuals increases, change the drag coefficient in the other direction and repeat the process. If the sum decreases continue to change C_D in the direction minimizing the sum of the squares of the residuals. Whenever the sum increases, C_D is changed in the other direction by a smaller increment. This process is assumed to converge when the increment becomes smaller than some prescribed value.

7.5.2 Cases with Variable Coefficients

7.5.2.1 Treatment of Drag Coefficient Dependent on Angle of Attack

At first glance it would appear that the drag coefficient determined assuming C_D constant (Section 7.5.1) would be of little value when C_D depends on angle of attack. However, this is not the case. Reference 7.14 showed that for axially symmetric bodies with drag coefficients which are quadratically dependent on angle of attack, i.e.,

$$C_D = C_{D_0} + C_{D_2}\alpha_R^2 , \tag{7.119}$$

a *mean line* (to be described) through a plot of $\log_e V$ versus x data determined an effective drag coefficient $C_{D_{eff}}$ given by

$$C_{D_{eff}} = C_{D_0} + C_{D_2}\alpha_{rms}^2 . \tag{7.120}$$

Here C_{D_0} is the zero-angle drag coefficient, α_R is the resultant angle of attack, and

$$\alpha_{rms} = \left(\frac{1}{x}\int_0^x \alpha_R^2\, dx\right)^{\frac{1}{2}} .$$

From (7.119) and (7.120) then, it is seen that $C_{D_{eff}}$ is that value of C_D which occurs at a resultant angle of attack equal to the root-mean-square resultant angle of attack of the flight in question. Therefore, for each flight or flight segment one obtains a value for $C_{D_{eff}}$ and α_{rms}. If these points are plotted as $C_{D_{eff}}$ versus α_{rms}^2 and a straight line is fit to them by least-squares, values for C_{D_0} and C_{D_2} are obtained and one then has an expression for C_D versus angle of attack.

If the drag coefficient cannot be expressed as a quadratic function of angle of attack but is instead of the form $C_D = C_{D_0} + C_{D_n}\alpha_R^n$, then the angle of attack at which to plot the effective drag coefficient is[7.15]

$$\alpha_{rmn} = \left(\frac{1}{x}\int_0^x \alpha_R^n\, dx\right)^{1/n}$$

and

$$C_{D_{eff}} = C_{D_0} + C_{D_n}\alpha_{rmn}^n .$$

The best value of n is found by a trial and error process.

A generalization of these ideas is possible. The drag coefficient is assumed to be monotonic (either increasing or decreasing with angle of attack) and can be represented by

$$C_D = C_{D_0} + C_{D_i}\alpha_R^i + C_{D_j}\alpha_R^j + \ldots \tag{7.121}$$

where the exponents i, j, etc. are arbitrary. If this is substituted for C_D in (7.108b) and integrated once, then

$$\log_e V = \log_e V_0 - K\int_0^x C_D\, dx . \tag{7.122}$$

With the definition

$$C_{D_{eff}} = \frac{1}{x}\int_0^x C_D\, dx = C_{D_0} + C_{D_i}(\alpha_{rmi})^i + C_{D_j}(\alpha_{rmj})^j + \ldots \tag{7.123}$$

where

$$\alpha_{rmi} = \left(\frac{1}{x}\int_0^x \alpha_R^i\, dx\right)^{1/i} \quad \text{etc.},$$

Equation (7.122) can be written

$$\log_e V = \log_e V_0 - KC_{D_{eff}}x . \tag{7.124}$$

Hence, a mean line through the $\log_e V$ versus x data would yield $C_{D_{eff}}$ and from several tests which had different values of angle of attack one could determine the coefficients C_{D_0}, C_{D_i}, etc. provided the angular motion had been analyzed and the appropriate angles determined. The quadratic and n^{th} power laws are special cases of this approach.

The term *mean line* has appeared several times and needs to be defined. It can best be visualized by considering the $\log_e V$ versus x plot in conjunction with an angle of attack versus x plot such as those shown in Figure 7.7. For a drag coefficient which is monotonic with angle of attack the mean line which yields the effective drag coefficient is that line which intersects the actual $\log_e V$ curve at x positions corresponding to maximum and minimum drag points and hence to the maximum and minimum angle-of-attack points as noted in the figure.

Note that in the present formulation the mean line is straight; hence, the pitching motion is assumed not to be excessively damped. Furthermore, in practice a least-square procedure is normally used to obtain $C_{D_{eff}}$ and this does not necessarily yield a mean line in the sense just described. It gives the mean line only if the angular motion is undamped and the least-squares fit extends over a flight path of many cycles of oscillation. For a half cycle of pitching motion, the result shown in Figure 7.8 occurs.

The deviations are normally small for cases of practical interest, however. Some examples of the error introduced by assuming that the least-squares line is the mean line have been obtained by numerical techniques. It was assumed that the drag coefficient was quadratically dependent on angle of attack and that the drag coefficient at zero angle of attack (C_{D_0}) was known exactly. The deduced value of C_{D_2} was found to depend on (i) the amount of damping present, (ii) the number of cycles of pitching motion, and (iii) the phase relation of the pitching motion to, say, a sine wave. The ratio C_{D_2} (deduced)/C_{D_2} (actual) is shown in the following table.

α_f/α_0	n = 0.5	n = 1	n = 2	n = 3	n = 5
0.9	0.70-1.30	0.92-1.08	0.98-1.02	0.99-1.01	0.99-1.00
0.7	0.70-1.30	0.90-1.07	0.96-1.01	0.97-1.00	0.98-1.00
0.5	0.67-1.29	0.86-1.06	0.92-0.99	0.93-0.98	0.95-0.97
0.1	0.54-1.22	0.58-0.98	0.65-0.83	0.68-0.79	0.71-0.78
	n = number of cycles of pitching motion α_f = angle-of-attack envelope at end of flight α_0 = angle-of-attack envelope at start of flight				

The quantity α_f/α_0 is proportional to the damping. The *range* of the numbers tabulated for the C_{D_2} ratio extends from the smallest to largest obtained as the phase relation was varied between 0^o and 90^o. Note that if 2 or more cycles of pitching motion are available and modest damping is present, the error introduced into C_{D_2} is at most a few percent.

When the least-square curve fitting procedure is applied directly to the time-distance data rather than to $\log_e V$ versus distance data, the situation is more complicated. It cannot be shown *exactly* that the $C_{D_{eff}}$ concept carries over to this case since (7.108) cannot be integrated twice in closed form when the drag coefficient depends on angle-of-attack. However, for planar motion and small velocity loss the $C_{D_{eff}}$ concept can be proved valid. For quadratic drag, it can be shown to apply for nonplanar motion again assuming a small velocity loss. Since in most cases of practical interest the velocity loss is small, the effective-drag-coefficient concept is valid within the limits imposed by the small damping restriction.

7.5.2.2 Treatment of Variable Ambient Density

In counter-flow facilities, the model may encounter density variations along its flight path. Usually the density variations encountered are not extreme, deviating perhaps ±20% from a given level. When this is the case, a very accurate estimate of the drag coefficient can be obtained exactly as before but using the *average* density over the length of the flight instead. That is

$$\rho_{AV} = \frac{1}{L}\int_0^L \rho(x)\, dx \,. \tag{7.125}$$

7.5.2.3 Treatment of Variable Model Mass

The problem of variable mass, which arises in the study of meteors, can also occur in the simulation of meteoric events in the laboratory by use of models. (To a lesser degree, mass variations occur with any model which ablates in flight.) The parameter of interest here is not the drag coefficient but rather the mass loss rate. If the mass loss rate is small, the drag coefficient and model reference area may be assumed constant. Further, it is assumed that the velocity of the mass leaving the body is small so that (7.108) is still applicable. Then differentiating (7.108) with respect to time and rearranging yields

$$\left.\begin{aligned} \dot{m} &= -\rho V A C_D - m\,\frac{d^2V}{dt^2}\Big/\frac{dV}{dt} \\ \text{or} \qquad \dot{m} &\approx \frac{2m}{V}\frac{dV}{dt} - m\,\frac{d^2V}{dt^2}\Big/\frac{dV}{dt} \,. \end{aligned}\right\} \tag{7.126}$$

If C_D is known from another source, the first of these equations should be used. These equations indicate that the distance versus time data must be differentiated three times to determine $\dot{m}$. Unless the data are very good, this procedure will not yield accurate information.

Given the functional dependence of the mass loss rate on velocity, one can obtain the mass loss rate more accurately. Consider the function

$$\dot{m} = -kV \,, \tag{7.127}$$

where k is a positive proportionality constant which depends on model material, size, and freestream density. (This function approximates ablators with good convective heat transfer blockage at very high speeds.) Equation (7.127) can be integrated, yielding

$$m - m_0 = -kx \,, \tag{7.128}$$

where at $x = 0$, $m = m_0$, $V = V_0$, and $t = t_0$.

By restriction to small mass loss, the reference area and drag coefficient are again assumed constant. Substituting the linear expression for m into (7.108) and integrating gives

$$\frac{V}{V_0} = \left(1 - \frac{k}{m_0} x\right)^{\rho AC_D/2k} \tag{7.129}$$

Integrating again yields

$$t = t_0 + \frac{m_0}{k\left(1 - \frac{\rho AC_D}{2k}\right)V_0} - \frac{\left(1 - \frac{k}{m_0} x\right)^{1-(\rho AC_D/2k)}}{\left(\frac{k}{m_0} - \frac{\rho AC_D}{2m_0}\right)V_0} . \tag{7.130}$$

For small mass loss this can be expanded as follows:

$$t = t_0 + \frac{1}{V_0} x + \frac{\rho AC_D}{2m_0V_0} \frac{x^2}{2} - \frac{\rho AC_D}{2m_0V_0}\left(\frac{\rho AC_D}{2m_0} + \frac{k}{m_0}\right)\frac{x^3}{6} + \ldots \tag{7.131}$$

Note that this equation is the same as that derived previously for constant mass (Equation (7.118)) to the order x^2. The information defining k occurs in the x^3 (and higher order) terms. Hence, well-defined data are again required, but less accuracy is needed than for the first method, since (7.131) uses the entire run to determine the coefficient k, while in the first method, the curvature in the velocity curve was considered locally.

In the event that the area changes importantly while the drag coefficient remains approximately constant (e.g., the case of an ablating meteor model with intermittent flange build-up and loss), one can deduce the mass-loss rate, provided the area change is known from shadowgraphs or other sources, by rearranging (7.108) to yield

$$m = \frac{-\rho A(x) C_D V(x)}{2\, dV/dx} . \tag{7.132}$$

Since all of the quantities on the right side of this equation are known or measurable at various points along the trajectory, one can plot the mass versus time. The slope of this curve is the mass loss rate. Again, this slope involves effectively a third derivative of the time-distance data.

7.5.3 Correction for Swerving Flight Path

The assumption that flight path distance, $\hat{x}$, is equal to the distance along the x axis can be removed if the swerving motion of the model center of gravity has been analyzed to yield a flight path distance. To first order, an average value of $1/\cos\gamma$ is computed over each data interval and applied as follows:

$$\Delta\hat{x}_i = \Delta x_{exp_i}\left(\frac{1}{\cos\gamma}\right)_{AV_i} , \tag{7.133}$$

where

$$\left(\frac{1}{\cos\gamma}\right)_{AV} = \frac{1}{\Delta x}\int_x^{x+\Delta x} \frac{dx}{\cos\gamma} . \tag{7.134}$$

A good approximation to the flight path distance is then

$$\hat{x} = \sum_i \Delta\hat{x}_i . \tag{7.135}$$

This correction is time consuming and usually unnecessary. It need be considered only in cases where the swerve is very large, enough to significantly increase the total distance traveled.

7.6 STATIC AND DYNAMIC STABILITY ANALYSIS

A model designed so that its center of gravity is ahead of the center of pressure of the aerodynamic forces will oscillate when in free-flight. Normally orthogonal shadowgraphs are taken at a number of stations along the trajectory to define this oscillation. Frequently, small pins are included on the base of the model so that the roll orientation (and hence roll rate) can also be determined.

The types of motions obtained from ballistic range tests are many and varied. The easiest way to visualize the motion is via a crossplot of the angle of attack versus the angle of sideslip (α versus β). This is equivalent to watching the path traced by the nose of the model on a plane normal to the velocity vector. Examples of typical motions are shown in Figure 7.9. The upper left motion has essentially zero roll rate, the lower right motion has a high roll rate. The roll rate present can be measured by the amount of precession of the peak amplitudes.

From a knowledge of the angle history experienced by the model, it is possible to deduce the static and dynamic stability coefficients which governed the flight. A number of methods are available for doing this and will be discussed in the following sections.

7.6.1 Determination from Wavelength and Amplitude Variation

The first method to be considered is not sophisticated, but does lead to a good physical understanding of the problem. The following assumptions will be made.

(i) Static restoring moment is linear with angle of attack.

(ii) Dynamic stability parameter is constant with angle of attack.

(iii) Aerodynamic coefficients are constant over the trajectory portion analyzed (small Mach number and Reynolds number changes or insensitivity of coefficients to Mach number and Reynolds number).

(iv) Motion is planar, which implies that the roll rate is zero. This assumption is introduced to simplify the discussion, and will be dropped presently.

The static and dynamic stability parameters, C_{m_α} and ξ, are determined from the wavelength and the change in the maximum amplitude of the motion, respectively. Consider the differential equation of angular motion that is appropriate under the assumptions listed (simplified version of Equation (7.103)):

$$\alpha'' - K\xi\alpha' - K_s C_{m_\alpha}\alpha = 0 , \tag{7.136}$$

where

$$K = \frac{\rho A}{2m}$$

ξ = dynamic stability parameter (or damping parameter) for unpowered flight at constant altitude

$$K_s = \frac{\rho A l}{2I}$$

$$C_{m_\alpha} = \frac{\partial C_m}{\partial \alpha} = \text{static moment-curve slope.}$$

Equation (7.136) is of the form

$$\alpha'' + 2\eta\alpha' + \omega^2\alpha = 0 , \tag{7.137}$$

which is the differential equation for damped simple harmonic motion. The solution to this equation is

$$\alpha = e^{-\eta x}\left[A_1 \cos (\omega^2 - \eta^2)^{\frac{1}{2}} x + A_2 \sin (\omega^2 - \eta^2)^{\frac{1}{2}} x\right] . \tag{7.138}$$

Normally $\eta \ll \omega$ so the frequency can be approximated $(\omega^2 - \eta^2)^{\frac{1}{2}} \approx \omega$.

From (7.136) and (7.137) we can write

$$\xi = \frac{-2\eta}{K} = \frac{-2\eta}{\rho A/2m} \tag{7.139}$$

and

$$C_{m_\alpha} = \frac{-\omega^2}{K_s} = \frac{-2\omega^2 I}{\rho A l} .$$

The wavelength is

$$\lambda = \frac{2\pi}{\omega}$$

and C_{m_α} in terms of the wavelength becomes

$$C_{m_\alpha} = \frac{-8\pi^2 I}{\lambda^2 \rho A l} . \tag{7.140}$$

Note that this equation specifies that for linear aerodynamics (i.e., C_{m_α} = constant) the wavelength of the motion does not depend on the amplitude.

Making use of (7.138) and Figure 7.10, it is seen that

$$\text{at} \quad x_1 = 0, \quad \alpha_1 = A_1$$

$$\text{at} \quad x_2 = \lambda, \quad \alpha_2 = e^{-\eta\lambda}(A_1 \cos\omega\lambda + A_2 \sin\omega\lambda) ;$$

but $\lambda = 2\pi/\omega$,

so $$\alpha_2 = e^{-\eta\lambda}(A_1 \cos 2\pi + A_2 \sin 2\pi) = A_1 e^{-\eta\lambda}$$

$$\frac{\alpha_2}{\alpha_1} = \frac{A_1 e^{-\eta\lambda}}{A_1} = e^{-\eta\lambda} .$$

Hence $\log_e\left(\frac{\alpha_2}{\alpha_1}\right) = -\eta\lambda$ (logarithmic decrement in amplitude)

$$\eta = -\frac{1}{\lambda}\log_e\frac{\alpha_2}{\alpha_1} . \tag{7.141}$$

In terms of ξ, from (7.139),

$$\xi = \frac{\log_e \frac{\alpha_2}{\alpha_1}}{(\rho A/4m)\lambda} , \tag{7.142a}$$

which can also be written as

$$\alpha_2 = \alpha_1 e^{(\rho A/4m)\xi\lambda} . \tag{7.142b}$$

Hence, knowing the wave length and the amplitude ratio, the static and dynamic stability parameters can be determined from (7.140) and (7.142).

Note that the dynamic stability parameter could also be determined using, for example, the ratio $|\alpha_3/\alpha_1|$ together with the distance between these peaks. This is not as accurate as using the ratio from every other peak due to the possibility that the model is oscillating about a trim angle of attack other than zero.

Assume next that the motion is not planar but the roll rate is small. The static and dynamic stability parameters can be determined exactly as before except now the wave length and amplitude ratio are determined from a plot of the resultant angle of attack (α_R) versus flight distance (note $\alpha_R \approx \sqrt{(\alpha^2 + \beta^2)}$).

Now assume in addition an arbitrary (but near-constant) roll rate which is presumed known. The expression for the static stability parameter is then given by the following equation, the first term of which is the same as (7.140):

$$C_{m_\alpha} = \frac{-8\pi^2 I}{\lambda^2 \rho A l} + \frac{2I}{\rho A l}\left(\frac{p}{2}\frac{I_x}{I}\right)^2 .$$

In this case, however, there is no simple expression like (7.142) for obtaining the dynamic stability parameter.

7.6.2 Determination from Angle of Attack Variation Near a Peak

The pitching moment coefficient (C_m) and damping parameter (ξ) can also be determined by applying directly the differential equation of motion and determining the angular accelerations from the angle of attack history. This method can be applied to motions at all amplitudes (including tumbling motions) and is not limited to linear aerodynamics. While the method of the previous section requires that more than a cycle of oscillatory motion be defined, with three peak amplitudes to get dependable results, the method we will now present requires instead as many data points as possible in a quarter to half cycle of motion, preferably containing a peak amplitude near its center. The assumptions made in this approach are:

(i) The Mach number or Reynolds number variations in the aerodynamic coefficients may be neglected.

(ii) The angular motion is accurately defined on both sides of a peak.

(iii) The motion is nearly planar. This assumption will be relaxed later.

The general differential equation of angular motion for planar flight is

$$\alpha'' = K(C_m)_D + K_S(C_m)_S , \tag{7.143}$$

where

$(C_m)_D$ = dynamic pitching moment coefficient

$(C_m)_S$ = static pitching moment coefficient

$$K = \frac{\rho A}{2m}$$

$$K_S = \frac{\rho A l}{2I} .$$

The half cycle of motion to be analyzed is represented in Figure 7.11 and can be considered as two segments, divided by the peak, where $\alpha' = 0$. If there is damping in the system, the $\alpha(x)$ curves on either side of

center will not be identical. The difference between the two curves is a measure of the damping. The shape of the curves $\alpha_1(x)$ and $\alpha_2(x)$ will reveal the nature of the pitching moment which produced the resulting motion.

We proceed as follows. Define

$$\alpha = \alpha_1(x), \qquad x_1 \leq x \leq x_c$$

$$\alpha = \alpha_2(x), \qquad x_c \leq x \leq x_2$$

and at $x = x_c$

$$\alpha' = 0, \quad \alpha_1(x) = \alpha_2(x) = \alpha_m .$$

From (7.143)

$$\left.\begin{aligned} \alpha_1'' &= K(C_m)_{D_1} + K_S(C_m)_{S_1} \\ \alpha_2'' &= K(C_m)_{D_2} + K_S(C_m)_{S_2} . \end{aligned}\right\} \tag{7.144}$$

At any given α the static moments are identical, that is

$$(C_m)_{S_1} = (C_m)_{S_2} = (C_m)_S .$$

From (7.144) then, at points of equal α,

$$\alpha_1'' + \alpha_2'' = K\left[(C_m)_{D_1} + (C_m)_{D_2}\right] + 2K_S(C_m)_S$$

or

$$(C_m)_S = \frac{\alpha_1'' + \alpha_2''}{2K_S} - \frac{K}{2K_S}\left[(C_m)_{D_1} + (C_m)_{D_2}\right] . \tag{7.145}$$

Thus, from values of the angular accelerations α_1'' and α_2'', if we could either evaluate or neglect $(C_m)_{D_1}$ and $(C_m)_{D_2}$, we could readily compute values for $(C_m)_S$. When the damping contributions to the total moment are zero or negligible, that is $(C_m)_{D_1} = (C_m)_{D_2} = 0$, then

$$\alpha_1'' = \alpha_2'' = \alpha''$$

and (7.145) reduces to

$$(C_m)_S = \frac{\alpha''}{K_S} . \tag{7.146}$$

An expression for $\alpha = \alpha(x)$ can be obtained by fitting a polynomial in x to the α versus x data. Differentiation of this expression twice yields values of $\alpha''(x)$ which lead directly to $C_{m_S}(x)$ through (7.146). By plotting C_{m_S} versus α for common values of x, $C_{m_S}(\alpha)$ is obtained.

Real systems have some damping, which is in general proportional to the angular rate,

$$(C_m)_D = \xi\alpha' ,$$

where ξ is again the dynamic stability parameter.

On substituting $(C_m)_{D_1} = \xi\alpha_1'$ and $(C_m)_{D_2} = \xi\alpha_2'$ into (7.144) we get

$$\left.\begin{aligned} \alpha_1'' &= K\xi\alpha_1' + K_S(C_m)_{S_1} \\ \alpha_2'' &= K\xi\alpha_2' + K_S(C_m)_{S_2} . \end{aligned}\right\} \tag{7.147}$$

Subtracting these equations for points at a common value of α, remembering that $(C_m)_{S_1} = (C_m)_{S_2}$ at a given α, we get

$$\alpha_1'' - \alpha_2'' = K\xi(\alpha_1' - \alpha_2') ,$$

so that

$$\xi = \frac{\alpha_1'' - \alpha_2''}{K(\alpha_1' - \alpha_2')} . \tag{7.148}$$

Thus, the damping parameter can be calculated from the first and second derivatives of the angle of attack variations with x at points of common amplitude on both sides of the peak, α_m.

When the damping terms are retained, the static pitching moment is calculated as follows:

Equation (7.145) is written with the damping coefficients proportional to angular rate

$$(C_m)_S = \frac{\alpha_1'' + \alpha_2''}{2K_S} - \frac{K\xi}{2K_S}(\alpha_1' + \alpha_2') .$$

But ξ is defined by (7.148) so

$$(C_m)_S = \frac{\alpha_1'' + \alpha_2''}{2K_S} - \frac{\alpha_1'' - \alpha_2''}{2K_S(\alpha_1' - \alpha_2')}(\alpha_1' + \alpha_2')$$

and we obtain

$$(C_m)_S = \frac{\alpha_2''\alpha_1' - \alpha_1''\alpha_2'}{K_S(\alpha_1' - \alpha_2')} . \tag{7.149}$$

The static and dynamic pitching moment coefficients can be obtained over a large angle of attack range by this technique if the observed motion of α versus x can be well represented mathematically. A polynomial of the form $\alpha = A_1 + A_2x + A_3x^2 + \ldots + A_Nx^{N-1}$ is fitted by least squares to the α versus x data. At each value of α, there will be two (meaningful) values of α' and α'', one for each side of the peak. Substituting these values in (7.148) and (7.149) gives the desired results. The method is least accurate in the low-angle portion of the α versus x curve where the acceleration is small and consequently the curvature approaches zero. An improvement to the results can be made by first locating the point of $\alpha' = 0$ by least-squares fitting the entire set of data. Then, two separate polynomials, one on each side of the peak, of the form $\alpha - \alpha_m = A_1x^2 + A_2x^3 + \ldots + A_Nx^{N+1}$ can be given zero slope and the same peak amplitude at this point.

Assume now that the motion is not planar but that the roll rate is small. Equations (7.148) and (7.149) then become

$$\xi = \frac{\alpha_{R_1}'' - \alpha_{R_2}''}{K(\alpha_{R_1}' - \alpha_{R_2}')} - \frac{\alpha_{R_1}\phi_1'^2 - \alpha_{R_2}\phi_2'^2}{K(\alpha_{R_1}' - \alpha_{R_2}')} \tag{7.150}$$

$$(C_m)_S = \frac{\alpha_{R_2}''\alpha_{R_1}' - \alpha_{R_1}''\alpha_{R_2}'}{K_S(\alpha_{R_1}' - \alpha_{R_2}')} - \frac{\alpha_{R_2}\phi_2'^2\alpha_{R_1}' - \alpha_{R_1}\phi_1'^2\alpha_{R_2}'}{K_S(\alpha_{R_1}' - \alpha_{R_2}')} , \tag{7.151}$$

where α_R again denotes the resultant angle of attack and ϕ' is the rotation rate of the resultant-angle vector in the α-β plane (Fig.7.12). The subscripts 1 and 2 on α_R and ϕ' are interpreted exactly as in Figure 7.11. At a given value of α_R on each side of the peak angle there will be corresponding values for ϕ_1' and ϕ_2' just as there are for α_{R_1}' and α_{R_2}'.

For motions governed by a linear static moment and constant damping, one can analyze $\alpha_R(x)$, $\alpha(x)$, or $\beta(x)$ separately and obtain equally valid results within the limits of experimental error in angle readings. For motions governed by a nonlinear moment where the minimum α_R is more than about 20% of the peak α_R, only the $\alpha_R(x)$ curve will yield meaningful results. However, since α_R does not go to zero as in a planar case, the range of α_R values to be analyzed should not go beyond the inflection points on either side of the $\alpha_R(x)$ curve.

The success of this method depends strongly on accurate angle readings. The damping coefficient is very sensitive to random error. The static pitching moment coefficient is much less sensitive and sometimes can be determined to a useful degree of accuracy even in the absence of a peak. However, without the motion history on both sides of a peak, one has no way of determining the dynamic moment. An example showing application of this method is given in Section 7.9.2.

7.6.3 Tricyclic Method

The methods discussed so far run into serious problems in cases where asymmetries are present or when an unknown roll rate exists. These cases require the more complete tricyclic equations of motion for proper treatment[7.5,7.16]. In discussing the tricyclic method, projected angles as defined in Section 7.3.3 will be used instead of modified Euler angles. To the order of the approximations that will be made, the two sets of angles are essentially identical.

The important assumptions of this method are:

(i) Basic axial symmetry with only slight asymmetry due to, for example, a control surface or offset center of mass.

(ii) Linear aerodynamics.

(iii) Constant roll rate.

(iv) Small angular displacements.

(v) Small linear displacements due to swerve.

(vi) Small velocity change.

The differential equation of angular motion has been given in (7.103) and (7.106) and is reproduced here as follows.

$$\vec{\alpha}_R'' - \left\{\frac{\rho A}{2m}\xi + i\frac{\rho A}{2m}pl\left[-C_{L_{\alpha p}} + \frac{ml^2}{I}\left(C_{m_{\dot{\alpha}p}} - C_{m_{qp}}\right)\right] + i\frac{I_{\tilde{x}}}{I}p\right\}\vec{\alpha}_R' -$$

$$- \left\{\frac{\rho Al}{2I}\left(C_{m_\alpha} + iC_{m_{\alpha p}}pl\right) - \frac{\rho A}{2m}\frac{I_{\tilde{x}}}{I}p\left(C_{L_{\alpha p}}pl - iC_{L_\alpha}\right)\right\}\vec{\alpha}_R = Re^{ipx}, \qquad (7.152)$$

where $\vec{\alpha}_R = \beta + i\alpha$

and $\xi = C_D - C_{L_\alpha} + \frac{ml^2}{I}\left(C_{m_q} + C_{m_{\dot{\alpha}}}\right)$.

Equation (7.152) can be written as

$$\vec{\alpha}_R'' - (\phi_1 + \phi_2)\vec{\alpha}_R' + \phi_1\phi_2\vec{\alpha}_R = K_3(\phi_3 - \phi_1)(\phi_3 - \phi_2)e^{\phi_3 x}, \qquad (7.153)$$

which has the solution

$$\vec{\alpha}_R = K_1e^{\phi_1 x} + K_2e^{\phi_2 x} + K_3e^{\phi_3 x}. \qquad (7.154)$$

This is called the tricyclic equation, since it is equivalent to three rotating vectors in the α-β plane. This is shown in Figure 7.13, with the following nomenclature defined:

$$\phi_1 = \eta_1 + i\omega_1 \qquad K_1 = b_1 + ia_1$$
$$\phi_2 = \eta_2 - i\omega_2 \qquad K_2 = b_2 + ia_2$$
$$\phi_3 = ip \qquad K_3 = b_3 + ia_3.$$

If we write the components of $\vec{\alpha}_R$ in (7.154) we get

$$\beta = e^{\eta_1 x}(b_1\cos\omega_1 x - a_1\sin\omega_1 x) + e^{\eta_2 x}(b_2\cos\omega_2 x + a_2\sin\omega_2 x) + (b_3\cos px - a_3\sin px)$$
$$\alpha = e^{\eta_1 x}(b_1\sin\omega_1 x + a_1\cos\omega_1 x) + e^{\eta_2 x}(-b_2\sin\omega_2 x + a_2\cos\omega_2 x) + (b_3\sin px + a_3\cos px).$$

Note that from (7.152) and (7.153) we get the expressions

$$\phi_1 + \phi_2 = \frac{\rho A}{2m}\xi + i\frac{\rho A}{2m}pl\left[-C_{L_{\alpha p}} + \frac{ml^2}{I}\left(C_{m_{\dot{\alpha}p}} - C_{m_{qp}}\right)\right] + i\frac{I_{\tilde{x}}}{I}p$$

$$\phi_1\phi_2 = \frac{-\rho Al}{2I}\left(C_{m_\alpha} + iC_{m_{\alpha p}}pl\right) + \frac{\rho A}{2m}\frac{I_{\tilde{x}}}{I}p\left(C_{L_{\alpha p}}pl - iC_{L_\alpha}\right)$$

$$K_3(\phi_3 - \phi_1)(\phi_3 - \phi_2) = R.$$

Also,

$$\phi_1 + \phi_2 = \eta_1 + \eta_2 + i(\omega_1 - \omega_2)$$
$$\phi_1\phi_2 = \eta_1\eta_2 + \omega_1\omega_2 + i(\eta_2\omega_1 - \eta_1\omega_2).$$

We therefore have

$$\eta_1 + \eta_2 = \frac{\rho A}{2m}\xi \qquad (7.155)$$

$$\omega_1 - \omega_2 = \frac{\rho A}{2m}pl\left[-C_{L_{\alpha p}} + \frac{ml^2}{I}\left(C_{m_{\dot{\alpha}p}} - C_{m_{qp}}\right)\right] + \frac{I_{\tilde{x}}}{I}p \qquad (7.156)$$

$$\eta_1\eta_2 + \omega_1\omega_2 = \frac{-\rho Al}{2I}C_{m_\alpha} + \frac{\rho A}{2m}\frac{I_{\tilde{x}}}{I}p^2lC_{L_{\alpha p}} \qquad (7.157)$$

$$\eta_2\omega_1 - \eta_1\omega_2 = \frac{-\rho A}{2m}\frac{I_{\tilde{x}}}{I}pC_{L_\alpha} - \frac{\rho Al}{2I}C_{m_{\alpha p}}pl. \qquad (7.158)$$

In order to obtain numerical values for the desired aerodynamic coefficients one must obtain the coefficients in (7.154). A least squares procedure using differential corrections (described in the appendix) can be used to fit (7.154) to the experimental data, α and β, at various values of x. The constants a_1, a_2, a_3, b_1, b_2, b_3, η_1, η_2, ω_1, and ω_2 are determined from the fit. If one examines (7.155) thru (7.158), it will be noted that there are more aerodynamic coefficients to be determined than there are equations, a seemingly impossible

situation. However, for most ballistic range tests of aerodynamically stable projectiles launched from non-rifled guns, the model experiences low roll rates and the Magnus terms can usually be ignored. It will be shown later, after development of the displacement equations of motion, how some of these Magnus coefficients can be obtained. When the Magnus terms are negligible, it is very simple to obtain the remaining coefficients. From (7.155) the dynamic stability parameter ξ is

$$\xi = \frac{\eta_1 + \eta_2}{\rho A/2m} , \tag{7.159}$$

while from (7.156) with $C_{L_{\alpha p}}$, $C_{m_{\dot{\alpha} p}}$, $C_{m_{qp}}$, and $C_{m_{\alpha p}} = 0$,

$$\omega_1 - \omega_2 = \frac{I_{\tilde{x}}}{I} p . \tag{7.160}$$

Thus, the roll rate p is not an independent parameter but is fully determined by ω_1 and ω_2. From (7.157), since $\eta_1\eta_2 \ll \omega_1\omega_2$, we obtain

$$C_{m_\alpha} = \frac{-2\omega_1\omega_2 I}{\rho A l} . \tag{7.161}$$

Equation (7.158) indicates that C_{L_α} can be obtained from

$$C_{L_\alpha} = \frac{\eta_1\omega_2 - \eta_2\omega_1}{\frac{\rho A}{2m}\frac{I_{\tilde{x}}}{I} p} . \tag{7.162}$$

However, the η's and ω's are usually not precise enough to define an accurate value of C_{L_α} from this expression. If C_{L_α} can be obtained from the swerve (displacement of the model trajectory) then one can express η_2 as a function of η_1, C_{L_α} and p (Equations (7.160) and (7.162)):

$$\eta_2 = \left(\eta_1 + \frac{\rho A}{2m} C_{L_\alpha}\right)\frac{\omega_2}{\omega_1} - \frac{\rho A}{2m} C_{L_\alpha} . \tag{7.163}$$

We therefore have to determine only nine independent coefficients rather than eleven. For the case where p is known from experimental measurements of the model roll rate, then from (7.160)

$$\omega_2 = \omega_1 - \frac{I_{\tilde{x}}}{I} p \tag{7.164}$$

and as a result

$$\eta_2 = \left(\eta_1 + \frac{\rho A}{2m} C_{L_\alpha}\right)\left(\frac{\omega_1 - (I_{\tilde{x}}/I)p}{\omega_1}\right) - \frac{\rho A}{2m} C_{L_\alpha} . \tag{7.165}$$

Then ω_2 and η_2 are functions of only ω_1 and η_1 and the measured values of p and C_{L_α}, and only eight unknown coefficients have to be determined.

7.6.3.1 Starting Solution

To initiate the least-squares-with-differential-corrections procedure, starting values for the unknown coefficients must be provided. The method used is a modification of Prony's method[7.17]. Fundamental to Prony's method is the following theorem: If

$$(\beta + i\alpha)_l = \sum_{j=1}^{3} K_j e^{\phi_j x_l} , \tag{7.166}$$

where

$x = x_1, x_2, \ldots x_n$ (x locations of equally spaced points, Δx apart)

$l = 1, 2, \ldots n$ (n = number of points, $\beta + i\alpha$),

then $\beta + i\alpha$ satisfies the linear difference equation

$$(\beta + i\alpha)_{l+3} + Q_2(\beta + i\alpha)_{l+2} + Q_1(\beta + i\alpha)_{l+1} + Q_0(\beta + i\alpha)_l = 0 , \tag{7.167}$$

where Q's are constants such that the roots of $h^3 + Q_2h^2 + Q_1h + Q_0 = 0$ are

$$h_j = e^{\phi_j \Delta x} .$$

This minimizes

$$\sum[(\beta + i\alpha)_{l+3} + Q_2(\beta + i\alpha)_{l+2} + Q_1(\beta + i\alpha)_{l+1} + Q_0(\beta + i\alpha)_l]^2 \tag{7.168}$$

instead of

$$\sum[(\beta+i\alpha)_{measured} - (\beta+i\alpha)_{calculated}]^2 , \tag{7.169}$$

which means simply that the coefficients derived from the procedure are not the "best possible" coefficients but are good first approximations. To obtain values for the coefficients K_j and ϕ_j, the first step is to solve the following set of equations by the method of least squares for Q_2, Q_1, and Q_0 (see Equation (7.167)).

$$\left.\begin{aligned}
(\beta+i\alpha)_4 + Q_2(\beta+i\alpha)_3 + Q_1(\beta+i\alpha)_2 + Q_0(\beta+i\alpha)_1 &= 0 \\
(\beta+i\alpha)_5 + Q_2(\beta+i\alpha)_4 + Q_1(\beta+i\alpha)_3 + Q_0(\beta+i\alpha)_2 &= 0 \\
\vdots \qquad\qquad & \\
(\beta+i\alpha)_n + Q_2(\beta+i\alpha)_{n-1} + Q_1(\beta+i\alpha)_{n-2} + Q_0(\beta+i\alpha)_{n-3} &= 0 .
\end{aligned}\right\} \tag{7.170}$$

With Q_2, Q_1, and Q_0 known, the cubic equation

$$h^3 + Q_2h^2 + Q_1h + Q_0 = 0 \tag{7.171}$$

is solved for roots h_1, h_2, and h_3, where

$$\begin{aligned}
h_1 &= e^{\phi_1\Delta x} \\
h_2 &= e^{\phi_2\Delta x} \\
h_3 &= e^{\phi_3\Delta x} .
\end{aligned} \tag{7.172}$$

Then Equations (7.172) are solved for ϕ_1, ϕ_2 and ϕ_3, which are substituted into (7.166) to obtain K_1, K_2, and K_3 by a second least squares operation. However, since ϕ_3 is not independent of ϕ_1 and ϕ_2 for the tricyclic equation in question (i.e., $p = f(\omega_1,\omega_2) \Rightarrow \phi_3 = g(\phi_1,\phi_2)$) the procedure is slightly modified.

We assume initially that $\phi_3 = 0$ and therefore $h_3 = e^0 = 1$. We therefore have

$$(\beta+i\alpha)_l = K_1e^{\phi_1x_l} + K_2e^{\phi_2x_l} + K_3 \tag{7.173}$$

and $h^3 + Q_2h^2 + Q_1h + Q_0 = 0$ has unity as a root and we get $1 + Q_2 + Q_1 + Q_0 = 0$. If we eliminate Q_0 between this equation and (7.167), we have

$$[(\beta+i\alpha)_{l+2} - (\beta+i\alpha)_l]Q_2 + [(\beta+i\alpha)_{l+1} - (\beta+i\alpha)_l]Q_1 = (\beta+i\alpha)_l - (\beta+i\alpha)_{l+3} . \tag{7.174}$$

This equation is now solved by least squares for the coefficients Q_1 and Q_2. The exponentials $e^{\phi_1\Delta x}$ and $e^{\phi_2\Delta x}$ are now found to be the roots of

$$h^2 + (Q_2+1)h + (Q_1+Q_2+1) = 0 . \tag{7.175}$$

So from

$$\left.\begin{aligned}
h_1 &= e^{\phi_1\Delta x} \\
h_2 &= e^{\phi_2\Delta x}
\end{aligned}\right\} \tag{7.176}$$

we can get ϕ_1 and ϕ_2. From ϕ_1 and ϕ_2 we can calculate ϕ_3 using the expression

$$\phi_3 = i\left[\frac{\mathcal{I}(\phi_1) + \mathcal{I}(\phi_2)}{I_{\tilde{x}}/I}\right],$$

where $\mathcal{I}$ denotes the imaginary part. The process is repeated with the new ϕ_3 until the coefficients remain essentially constant. The values of ϕ_j are then substituted into (7.166), and K_j solved for by a second least-squares procedure. Since equally-spaced data are required for Prony's method, they are either computed from the raw data using some interpolation scheme or obtained from hand fairings of the data.

7.6.3.2 Swerve Corrections

In ballistic range tests the angular measurements are normally made with respect to an earth-fixed axis system while the differential equations involve angles relative to the actual flight path. Hence a correction to the angular measurements may be required for the swerving of the trajectory. These corrections (which are usually small) can be computed by differentiating with respect to distance the $z(x)$ and $y(x)$ curves derived from the tricyclic lift analysis (Section 7.7.3). Figure 7.14 shows the relationship of the swerve trajectory, flight path angle, and measured angles in orthogonal planes.

$$\alpha = \theta + \tan^{-1}\frac{dz}{dx}$$

$$\beta = -\psi + \tan^{-1}\frac{dy}{dx} .$$

With this new set of angles the stability analysis could be performed again to give a better set of coefficients from the tricyclic analysis and then an iterative procedure set up between stability and lift analyses to obtain the best solution possible (that is, one would iterate until the angle corrections remained essentially constant).

7.6.3.3 Rotation of Coordinate Axes

One of the assumptions necessary in the derivation of the tricyclic equation (7.154) is that angular displacements are small so that the resultant angle of attack is simply the square root of the sum of the squares of the pitch and yaw angles:

$$\alpha_R = \sqrt{(\alpha^2 + \beta^2)} \quad . \tag{7.177}$$

The exact expression for the resultant angle of attack (with α and β regarded as projected angles) is

$$\alpha_R = \tan^{-1}\sqrt{(\tan^2\alpha + \tan^2\beta)} \quad . \tag{7.178}$$

These two equations agree closely for small angles. They agree exactly if either α or β equals zero. Thus, the error introduced by (7.177) can be reduced for near-planar motions by rotating the coordinate axes through an angle Φ to keep the angles in one plane small. To accomplish this, a peak amplitude near the middle of the flight is rotated into either the pitch or yaw plane, establishing the angle Φ, and then all data points are rotated through this angle. This concept is illustrated in Figure 7.15.

The error due to using the tricyclic analysis at large amplitudes (without rotating the data) is most evident in the dynamic stability parameter, ξ. Figure 7.16 demonstrates the magnitude of errors that are encountered for a typical case. Consider a test in a range which has 11 data stations at 1.22 meter intervals with test conditions such that $\rho A/2m = 0.002/m$ and the wavelength of oscillatory motion is 7.9 meters. Various values of ξ are considered at root-mean-square angles of attack of 20°, 30°, and 40° for a planar motion with $\Phi = 45°$ (the worst case). The figure shows the induced error $(\xi - \xi_{exact})$ as a function of ξ for the three values of α_{rms}. Note the near linear dependence of the induced error on ξ, and also the progressive increase in the error with increasing α_{rms}.

7.6.4 Nonlinear Static Restoring Moment

7.6.4.1 Introduction

One of the assumptions inherent in the tricyclic method (Section 7.6.3) is that the static pitching moment varies linearly with angle of attack. This is usually a good assumption at small angles of attack, but may not be true at larger angles of attack. In this section an examination will be made of nonlinear moments which contain various terms from a power series in angle of attack (or in resultant angle of attack).

$$M = -\Sigma M_n \alpha^{n+1} \quad . \tag{7.179}$$

The term represented by $n = 0$ will be referred to as a linear moment. Similarly, $n = 2$ will be called a cubic moment; $n = 4$, quintic moment; etc. Care must be taken in using even powers of α since they result in a moment curve unsymmetrical about the origin. For axially symmetric bodies, we want a moment which is an odd function of α, and hence use even exponents in the form $M_3\alpha^3|\alpha|$, etc. It will be shown that the results from the tricyclic method previously developed can be used as a first step in finding the nonlinear coefficients.

It is worthwhile to consider just how nonlinearities in the static moment can be detected in ballistic-range data. These nonlinearities affect both the shape and frequency (or wavelength) of the model oscillation. It is found, however, that moderate nonlinearities have only a second-order effect on the shape. In most instances, the resulting wave form differs very little from a damped sine wave. This is illustrated graphically in Figure 7.17, where the wave form for a pure cubic moment ($M = -M_2\alpha^3$) is compared to a sine wave having the same wavelength. This comparison is for planar motion with zero damping. It should be noted that the wave form corresponding to *all* nonlinear moments of the form $M = -M_0\alpha - M_2\alpha^3$, where both terms are stabilizing, would fall between the two curves shown in this figure.

Hence, the primary means for detecting nonlinearities in the static moment is by observing changes in the wavelength with amplitude of the pitching oscillation*. When the moment is nonlinear, the wavelength changes with amplitude as a consequence of the change in the mean slope of the pitching moment curve, C_{m_α} (see Equation (7.140)). Normally, the aerodynamic damping is small so the wavelength of the model oscillation is essentially constant during a given flight even though a nonlinear static moment exists. For this reason, a number of flights of a given configuration must be made having different peak amplitudes before the form of nonlinearity in the static moment can be determined.

A number of methods have been developed for analyzing ballistic-range data where a nonlinear static moment exists. Some of these methods will be detailed in the following sections. For clarity, the discussion will proceed from simple, very restricted systems toward a general solution with many of the restrictions dropped. First, however, it is useful to illustrate the influence of nonlinear static moments by considering a mechanical analogue.

* In at least one instance[7.18], the change in the wave form itself was used to determine the nonlinearities in the static moment.

7.6.4.2 Mechanical Analogue

The analogy between a spherical ball rolling over a contoured surface and the combined pitching and yawing motion of a model in flight is developed in Reference 7.19. A necessary assumption is that zero gyroscopic roll rate of the missile being simulated must be prescribed. Consider for simplicity an axially symmetric configuration. Then construct a bowl according to the equation

$$z = z_0 + A_0 r^2 + A_2 r^4 + \ldots .$$

or

$$\frac{dz}{dr} = 2A_0 r + 4A_2 r^3 + \ldots . ,$$

where z is the height of the bowl surface and r is the distance from the bowl center. A ball rolling over this bowl would execute a motion equivalent to the α versus β motion of a model in free flight which was governed by the static moment

$$C_m = B_0 \alpha_R + B_2 \alpha_R^3 + \ldots ,$$

where C_m denotes the moment coefficient at a given *resultant* angle of attack. In other words, C_m has the same form as $\frac{dz}{dr}$.

A number of bowls were made to check out the usefulness of this mechanical analogue. The contours of these bowls, and the static moments they correspond to, are shown in Figure 7.18. The bowls were placed directly below a motion-picture camera, and balls of different sizes and different materials were launched into them by rolling the balls down a chute. It was found that the surfaces of the bowls could be oiled in varying amounts to maintain a control on the damping in the system. Checks made with the "linear-moment" bowl, where an exact analytic solution exists, showed the bowl analogy to be valid.

The real interest in this analogy lay in examining the effect of a nonlinear static moment. One set of results for a linear-cubic moment where the linear term is destabilizing is shown in Figure 7.19. The two components of the resultant angle of attack make little sense by themselves, but the cross-plot of α versus β is completely understandable. The deflection away from the origin in this cross-plot is a characteristic of a nonspinning configuration that is statically unstable at small angles of attack. This mechanical analogue can often be helpful by intuitively revealing the type of static moment governing a particular model.

7.6.4.3 Static Moment Consisting of a Single Term

As an introduction to the treatment of nonlinear moments, we will consider a simple case where an exact solution exists. Consider the case of a single degree of freedom in pitch (planar motion), no aerodynamic damping, and a small velocity loss, and assume the static moment can be represented as

$$M = C_m \frac{\rho V^2 A l}{2} = -M_n \alpha^{n+1} , \qquad n \geq 0 , \tag{7.180}$$

so that

$$C_{m_\alpha} = \frac{-M_n (n+1) \alpha^n}{\frac{1}{2}\rho V^2 A l} . \tag{7.181}$$

The equation of motion to be considered is

$$I\ddot{\alpha} + M_n \alpha^{n+1} = 0 . \tag{7.182}$$

On multiplying this equation by $\dot{\alpha}$ and integrating, we obtain

$$\frac{I\dot{\alpha}^2}{2} + \frac{M_n \alpha^{n+2}}{n+2} = C .$$

To find C, we use the fact that $\dot{\alpha} = 0$ when $\alpha = \alpha_m$. Thus

$$C = \frac{M_n \alpha_m^{n+2}}{n+2}$$

and

$$dt = \left(\frac{(n+2)I}{2M_n}\right)^{\frac{1}{2}} \left(\frac{d\alpha}{\sqrt{(\alpha_m^{n+2} - \alpha^{n+2})}}\right) . \tag{7.183}$$

We can determine $\tau/4$ (where τ is the period of the oscillation) by integrating (7.183) from $\alpha = 0$ to $\alpha = \alpha_m$; that is,

$$\frac{\tau}{4} = \left(\frac{(n+2)I}{2M_n}\right)^{\frac{1}{2}} \int_0^{\alpha_m} \frac{d\alpha}{\sqrt{(\alpha_m^{n+2} - \alpha^{n+2})}} .$$

An expression for the period can be obtained in terms of gamma functions.

$$\tau = \left(\frac{2\pi I(n+4)^2}{(n+2)M_n\alpha_m^n}\right)^{\frac{1}{2}} \frac{\Gamma\left(\frac{n+3}{n+2}\right)}{\Gamma\left(\frac{n+3}{n+2}+\frac{1}{2}\right)} . \tag{7.184}$$

This is an exact relationship that shows the effect of the coefficients assumed in (7.180) and the maximum angle of attack. However, it does not provide much in the way of intuitive feel. This can be helped to some extent by introducing the concept of an "effective" angle of attack. First, consider the experimenter's situation. A number of firings have been made of a given configuration. The data have been analyzed as though the static moment were linear and the moment-curve-slope obtained. It is found that the moment-curve-slope is not a constant, but varies with the amplitude of the particular test. The question then arises, for what angles of attack are each of the moment-curve-slopes obtained true local values? That is, what is the effective angle of attack for each measurement?

Solving for M_n in (7.184) and substituting into (7.181) leads to the expression for C_{m_α},

$$C_{m_\alpha} = \frac{-2\pi(n+1)(n+4)^2}{n+2}\left[\frac{\Gamma\left(\frac{n+3}{n+2}\right)}{\Gamma\left(\frac{n+3}{n+2}+\frac{1}{2}\right)}\right]^2\left(\frac{\alpha}{\alpha_m}\right)^n \frac{2I}{\tau^2V^2\rho Al} . \tag{7.185}$$

For a linear moment, $n = 0$ and this equation reduces to (7.140):

$$C_{m_\alpha} \equiv C_{m_{\alpha_l}} = \frac{-8\pi^2 I}{\tau^2V^2\rho Al} . \tag{7.186}$$

We define the effective angle of attack α_{eff} as that angle at which the moment-curve-slope obtained from a linear analysis of a motion of amplitude α_m matches C_{m_α}. To obtain this angle of attack, we equate (7.185) and (7.186), substituting α_{eff} for α in (7.185). Thus,

$$\frac{\alpha_{eff}}{\alpha_m} = \left\{\frac{2\pi(n+2)}{(n+1)(n+4)^2}\left[\frac{\Gamma\left(\frac{n+3}{n+2}+\frac{1}{2}\right)}{\Gamma\left(\frac{n+3}{n+2}\right)}\right]^2\right\}^{1/n} . \tag{7.187}$$

This equation in effect gives the transformation from a plot of $C_{m_{\alpha_l}}$ versus α_m to a plot of C_{m_α} versus α, which can be integrated to obtain C_m. Figure 7.20 shows a plot of α_{eff}/α_m versus n. Note that for a cubic moment ($M = -M_2\alpha^3$), $C_{m_{\alpha_l}}$ should be applied at 0.489 α_m. This value will also arise when a linear-plus-cubic moment is considered.

The one-term moment represented by (7.180) has zero slope through the origin, and thus does not allow initial static stability or instability at $\alpha = 0^o$. Hence, this representation is not generally applicable, but was included as a simple introductory case.

7.6.4.4 Linear + Cubic Static Moment

Many real physical cases can be represented by the cubic case if a linear term is added to provide finite static stability or instability about the origin. We will still assume undamped angular motion, with only a small change in velocity, and consider a static moment represented by

$$M = C_m\frac{\rho V^2 Al}{2} = -M_0\alpha - M_2\alpha^3 \tag{7.188}$$

$$C_{m_\alpha} = -\frac{2}{\rho V^2 Al}(M_0 + 3M_2\alpha^2) . \tag{7.189}$$

It should be noted that three cases of interest exist depending on the signs of M_0 and M_2. These cases are shown in Figure 7.21.

Note that we are considering cases where a model in free flight is oscillating between $+\alpha_m$ and $-\alpha_m$. For a type 1 moment, α_m can be any value. For a type 2 moment, α_m must be less than α_1 or tumbling will occur, and for a type 3 moment, α_m must be greater than α_2 $\left(\text{defined by } \int_0^{\alpha_2} M\, d\alpha = 0\right)$ or the oscillation will take place about the trim angle (α_3) and never pass through zero.

Following the same approach as in the preceding section, we can obtain exact closed-form expressions for the effective-angle parameter, α_{eff}/α_m, in terms now of elliptic integrals. Defining $m_2 = M_2\alpha_m^2/M_0$, these expressions can be written as follows:

Type 1 and type 3 moments:

$$\frac{\alpha_{eff}}{\alpha_m} = \sqrt{\left(\frac{\pi^2(1+m_2)}{12m_2[K(k)]^2} - \frac{1}{3m_2}\right)} \tag{7.190}$$

K(k) = complete elliptic integral of the first kind

$$k = \sqrt{\left(\frac{m_2}{2(1+m_2)}\right)} .$$

Type 2 moment:

$$\frac{\alpha_{eff}}{\alpha_m} = \sqrt{\left(\frac{\pi^2(2+m_2)}{24m_2[K(k)]^2} - \frac{1}{3m_2}\right)} \tag{7.191}$$

$$k = \sqrt{\left(\frac{-m_2}{2+m_2}\right)} .$$

These solutions are shown graphically in Figure 7.22. It is interesting to note that the value of α_{eff}/α_m obtained in the previous section for a pure cubic moment (0.489), is representative of nearly all linear-cubic moments of both type 1 and type 3. In fact, except in the vicinity of the singular points for types 2 and 3, a value of α_{eff}/α_m of 0.5 would be a fairly close approximation.

What is most important to note at this point is that exact expressions have been obtained which allow a transformation from $C_{m_{\alpha_l}}$ (equivalent linear system) versus α_m to a local C_{m_α} versus α and the unknowns M_0 and M_2 can be obtained from experimental data by a simple iteration procedure, which proceeds as follows: Assume that $C_{m_{\alpha_l}}$ and α_m have been obtained from a number of tests (e.g., using the tricyclic method). First $(\alpha_{eff})_i$ is assumed equal to $[0.5\,(\alpha_m)_i]$ and a least squares fit is made to the equations

$$(C_{m_{\alpha_l}})_i = \left(\frac{-2}{\rho V^2 A l}\right)_i \left[M_0 + 3M_2(\alpha_{eff}^2)_i\right] ,$$

solving for M_0 and M_2. Depending on the type of moment, either (7.190) or (7.191) is then applied to yield better values of the transformation to apply to each of the $(\alpha_m)_i$ and the least squares procedure is repeated. It is found that the iteration process converges very rapidly for any of the three types of moment.

7.6.4.5 General Power-Series Moment

We will now relax some of the assumptions of the preceding sections and obtain an expression for the case of a spinning symmetric missile governed by an arbitrary nonlinear moment in the *resultant* angle of attack. It is still assumed that aerodynamic damping is negligible and that there is no swerve of the flightpath; therefore,

$$\alpha_R \equiv \sigma .$$

We start with a body-fixed coordinate system denoted by $\bar{x}, \bar{y}, \bar{z}$, with the origin at the center of gravity. This system is related to the inertial coordinate system (x,y,z) by the Euler angles θ_E, σ, and ψ_E (see Figure 7.23). The body has constant angular velocity p about the $\bar{x}$ axis. We will consider that the restoring moment is given by the expression

$$M(\sigma) = C_m \frac{\rho V^2 A l}{2} = -\sum_n M_n \sigma^{n+1} .$$

The moment is completely arbitrary in that any of the coefficients M_n may be set equal to zero*. Following the development in Reference 7.8, it is found that the following differential equation governs the resultant angle of attack σ.

$$\frac{1}{8}\left(\frac{d\sigma^2}{dt}\right)^2 = \left(\sigma^2 - \frac{\sigma_m^2 + \sigma_0^2}{2}\right)\sum_{n=0}^{\infty} \frac{\bar{M}_n}{n+2} \frac{\sigma_m^{n+4} - \sigma_0^{n+4}}{\sigma_m^2 - \sigma_0^2} + \sum_{n=0}^{\infty} \frac{\bar{M}_n}{n+2}\left(\frac{\sigma_m^{n+4} + \sigma_0^{n+4}}{2} - \sigma^{n+4}\right) . \tag{7.192}$$

Here σ_m and σ_0 are the maximum and minimum resultant angles of attack, and the $\bar{M}_n$ terms are the coefficients M_n modified to include the effect of spin. For the odd subscript terms $(\bar{M}_1, \bar{M}_3 \ldots)$, $\bar{M}_n = M_n/I$. For the even subscript terms, a general expression for $\bar{M}_n$ is exceedingly complicated. In most practical cases, however, the following expressions are essentially exact:

---

* It should be kept in mind that for the symmetric missile under consideration, the desired moment is an odd function of angle of attack. Since $\sigma \geq 0$, this poses no problem but for planar motion, note that terms like $M_1\alpha|\alpha|$ are implied.

$$\bar{M}_0 = \frac{M_0}{I} + \frac{P^2}{4}$$

$$\bar{M}_2 = \frac{M_2}{I} + \frac{P^2}{12}$$

$$\bar{M}_4 = \frac{M_4}{I} + \frac{17}{960} P^2$$

$$\bar{M}_{>4} = \frac{M_{>4}}{I} ,$$

where

$$P = \frac{I_{\bar{x}}}{I} p .$$

By integrating (7.192) from σ_0 to σ_m, an expression for the frequency of oscillation can be obtained. Evaluating the resulting integral in closed form can be done only in special cases. However, an excellent approximation for the frequency can be obtained[7.8]:

$$\omega^2(t) = \frac{8 \sum_{n=0}^{\infty} \frac{\bar{M}_n}{n+2} \left[\frac{\sigma_m^{n+4} + \sigma_0^{n+4}}{2} - \left(\frac{\sigma_m^2 + \sigma_0^2}{2} \right)^{(n+4)/2} \right]}{(\sigma_m^2 - \sigma_0^2)^2} . \tag{7.193}$$

This equation is least accurate for the case of planar motion. It becomes increasingly more accurate as more and more circular motions are considered, and is exact in the limit of circular motion.

Because the equation is least accurate for planar motion, it is interesting to compare it in this limit with exact results and also with approximate results obtained by the Kryloff-Bogoliuboff technique[7.20]. For planar motion ($\sigma_0 = 0$, $p = 0$), (7.193) assumes the form

$$\omega^2(t) = \frac{4}{I} \sum_{n=0}^{\infty} \frac{M_n}{n+2} \left[1 - \left(\tfrac{1}{2} \right)^{(n+2)/2} \right] \alpha_m^n . \tag{7.194}$$

The first comparison will be for the one-term moment of arbitrary power in angle of attack considered in Section 7.6.4.3 (i.e., $M = -M_n \alpha^{n+1}$). This comparison is shown in Figure 7.24. It is seen that the approximation given by (7.194) is superior to the Kryloff-Bogoliuboff approximation for all values of n greater than 2. It also agrees well with the exact results.

The other planar-motion comparison that will be shown is for a linear-cubic-quintic restoring moment:

$$M = -M_0 \alpha - M_2 \alpha^3 - M_4 \alpha^5 .$$

Exact results for this case are presented in Reference 7.21. For brevity, only the particular moment having stabilizing linear and quintic terms and a destabilizing cubic term will be considered. The comparisons are shown in the carpet plots (Fig. 7.25), where the dashes represent the exact solution and the solid lines a given approximation. Both approximations are fairly good, but results from (7.194) are clearly superior. Since (7.193) is least accurate for planar motion, it is apparently a very accurate representation.

7.6.4.6 Application to Free-Flight Data

Equation (7.193) shows the influence of maximum and minimum amplitudes, spinning rate, and an arbitrary set of restoring moment coefficients on the frequency of the motion. Before applying this equation to free-flight data, it is again convenient to transform from time to distance, which essentially removes velocity from the problem. If (7.193) is divided by V^2 and the terms of the series are written out explicitly, with only the dominant spin term retained, we obtain

$$\omega^2(x) = \frac{P^2(x)}{4} + \frac{1}{IV^2} \left\{ M_0 + \tfrac{8}{3} M_1 \left[\frac{\frac{\sigma_m^5 + \sigma_0^5}{2} - \left(\frac{\sigma_m^2 + \sigma_0^2}{2} \right)^{5/2}}{(\sigma_m^2 - \sigma_0^2)^2} \right] + \tfrac{3}{4} M_2 (\sigma_m^2 + \sigma_0^2) + \ldots \right\} .$$

Recall that each of the unknown M_n's contains V^2 (for example, $M_0 = -C_{m_\alpha} \rho V^2 A l/2$), so M_n/V^2 is independent of velocity. If we now define

$$\hat{M}_n = \frac{-M_n}{\rho V^2 A l/2} ,$$

the $\hat{M}_n$'s are coefficients in a power series in C_m,

$$C_m = \sum_n \hat{M}_n \sigma^{n+1} ,$$

and are assumed to be constants. Then the above equation becomes

$$\omega^2(x) = \frac{P^2(x)}{4} - \frac{\rho A l}{2I}\left\{\hat{M}_0 + \tfrac{8}{3}\hat{M}_1\left[\frac{\frac{\sigma_m^5+\sigma_0^5}{2} - \left(\frac{\sigma_m^2+\sigma_0^2}{2}\right)^{5/2}}{(\sigma_m^2-\sigma_0^2)^2}\right] + \right.$$

$$+ \tfrac{3}{4}\hat{M}_2(\sigma_m^2+\sigma_0^2) + \tfrac{8}{5}\hat{M}_3\left[\frac{\frac{\sigma_m^7+\sigma_0^7}{2} - \left(\frac{\sigma_m^2+\sigma_0^2}{2}\right)^{7/2}}{(\sigma_m^2-\sigma_0^2)^2}\right] +$$

$$+ \tfrac{1}{12}\hat{M}_4(7\sigma_m^4 + 10\sigma_m^2\sigma_0^2 + 7\sigma_0^4) + \tfrac{8}{7}\hat{M}_5\left[\frac{\frac{\sigma_m^9+\sigma_0^9}{2} - \left(\frac{\sigma_m^2+\sigma_0^2}{2}\right)^{9/2}}{(\sigma_m^2-\sigma_0^2)^2}\right] +$$

$$\left. + \tfrac{5}{32}\hat{M}_6(3\sigma_m^6 + 5\sigma_m^4\sigma_0^2 + 5\sigma_m^2\sigma_0^4 + 3\sigma_0^6) + \ldots\right\}. \qquad (7.195)$$

From a set of flights made at about the same test conditions, assume that a converged solution for each has been obtained with the tricyclic method of analysis. Then values of all the parameters except $\hat{M}_n$ are known for each flight for use in (7.195). A decision as to the number of terms to be retained is made, and then the $\hat{M}_n$ can be calculated from the set of m simultaneous equations (one for each test flight or portion thereof) by the method of least squares, provided $m >$ number of unknowns. Note that $\omega^2(x) - [P^2(x)/4]$ is essentially equal to the product $\omega_1\omega_2$ given by the tricyclic analysis.

Although damping has been assumed negligible in deriving (7.195), the procedure still gives good results when damping is present if values of σ_m and σ_0 are determined as follows:

$$\sigma_m^2 = \tfrac{1}{2}[\sigma_m^2\,(\text{first peak}) + \sigma_m^2\,(\text{last peak})]$$

$$\sigma_0^2 = \tfrac{1}{2}[\sigma_0^2\,(\text{first minimum}) + \sigma_0^2\,(\text{last minimum})]\ .$$

The question of which and how many terms to retain in (7.195) would seem to be critical. The possibilities are essentially unlimited, and there is no systematic way to make a choice a priori. Fortunately, however, a number of different assumed forms for the moment, when fit to the experimental data, turn out to yield nearly identical, $C_m(\alpha)$ curves. Hence, there is no unique representation for the moment that gives the "best fit" to the data but a number of choices which will give equally good fits.

This is illustrated by the following set of results, based on the experimental data of Reference 7.18. The data showed large nonlinearities, and it was decided that a four-term series representation of the moment was needed. The linear coefficient $\hat{M}_0$ was known from other sources and was not allowed to vary. All possible four-term moments, each containing $\hat{M}_0$, and three members of the set $(\hat{M}_1, \hat{M}_2, \hat{M}_3, \hat{M}_4, \hat{M}_5, \hat{M}_6)$ were fit to the experimental data using (7.195) and the method of least squares. The results are summarized as follows:

Powers of resultant angle of attack in assumed moment	*Sum of the squares of the residuals*
1-2-3-4	3.5×10^{-7}
1-2-3-5	4.9
1-2-3-6	6.6
1-2-3-7	8.5
1-2-4-5	6.6
1-2-4-6	8.4
1-2-4-7	10.4
1-2-5-6	10.2
1-2-5-7	11.6
1-2-6-7	12.4
1-3-4-5	2.4*
1-3-4-6	2.0*
1-3-4-7	1.9*
1-3-5-6	1.8*
1-3-5-7	2.0*
1-3-6-7	3.2
1-4-5-6	8.4
1-4-5-7	11.3
1-4-6-7	17.3
1-5-6-7	32.0×10^{-7}

Some of the moment representations have much larger error sums than others, and can be rejected as inferior. However, among several of the better fits, there is little to choose. Figure 7.26 shows the envelope from the five moments that gave the smallest sum of the squares of the residuals, marked in the above table with stars. The moment curves are close enough together, out to $\alpha \cong 36^{\circ}$, that no real choice between them need be made.

7.6.5 Effect of Nonlinear Static Moment on Deduced Damping

The study of nonlinearities in aerodynamic moments has been extended in Reference 7.22 to allow nonlinearities to exist in both the static moment and the damping moment, and nonlinear damping moments will be treated in the next section. The study revealed that a nonlinear *static* moment could lead to apparent nonlinearities (and large errors) in the deduced damping even when the actual damping was in fact linear. This effect will now be discussed.

For this purpose, it is assumed that the motion is planar and that there is no swerve in the trajectory. The equation of motion considered, with distance as the independent variable, is

$$\alpha'' + H_0\alpha' + \sum_{n\geq 0} \frac{M_n}{IV^2}\alpha^{n+1} = 0 . \tag{7.196}$$

Note again that since M_n contains V^2, M_n/V^2 is independent of velocity. The constant H_0 ($H_0 = -(\rho A/2m)\xi$) is a measure of the damping and we desire to determine its value. First, we consider the (idealized) case where we have exact values of the angle of attack α_m at every peak. If the static moment were linear, these peak angles would fall on the exponential envelope $e^{-(H_0/2)x}$ and the logarithmic decrement would be constant with the value

$$\log_e \left| \frac{(\alpha_m)_k}{(\alpha_m)_{k+1}} \right| = \frac{\pi}{2}\frac{H_0}{\omega} , \tag{7.197}$$

where the subscript k denotes the peak number and ω is the frequency of the motion defined by

$$\omega^2 = \frac{M_0}{IV^2} - \frac{H_0^2}{4} \approx \frac{M_0}{IV^2} .$$

The difficulty that arises is when the static moment is nonlinear, the logarithmic decrement is no longer a constant. However, it is useful to analyze the data as though it were constant and an effective linear damping H_{0_e} is defined by the expression

$$\log_e \left| \frac{(\alpha_m)_k}{(\alpha_m)_{k+1}} \right| = \frac{\pi}{2}\frac{H_{0_e}}{\omega_1} , \tag{7.198}$$

where ω_1 is now a function of α_m, M_n, and H_0. An approximate relationship between the apparent damping and the actual damping, which is in excellent agreement with numerical integrations, is derived in Reference 7.22, for arbitrary nonlinearities in both the static and damping moment and is expressed as the ratio of two power series. The complete expression will be given later, but the expression for a linear plus cubic static moment (and constant damping) is as follows*:

$$\frac{H_{0_e}}{H_0} = \frac{m_0 + (5/8)m_2}{m_0 + (15/16)m_2} . \tag{7.199}$$

Here m_0 is $+1$ if the linear static term is stabilizing and -1 if it is destabilizing. Note that the definition of m_2 is now modified slightly, becoming

$$m_2 = \frac{M_2\alpha_a^2}{M_0} ,$$

where α_a represents an "average" value of the maximum angle of attack; i.e., $\alpha_a^2 = \frac{1}{2}[(\alpha_m)_k^2 + (\alpha_m)_{k+1}^2]$. The physical import of (7.199) is shown in Figures 7.27-7.29, which give the variation of H_{0_e}/H_0 with m_2. The solid lines represent the case we are considering (exact knowledge of successive peak angles) and it is seen that a significant effect on the deduced damping is introduced by the nonlinear static moment. For the stable-stable case (Fig. 7.27), the deduced damping is always less than the true damping and in the most extreme case (pure cubic moment), it is 2/3 of the true damping. For the stable-unstable case (Fig. 7.28), the deduced damping is always greater than the true damping. The largest deviations of the deduced damping from true values occur with an unstable-stable static moment (Fig. 7.29), for which the error is never *less* than 33 percent.

It is, of course, unrealistic to presume exact knowledge of successive peak angles of attack. In the real case, the damping would probably be obtained using the tricyclic solution developed earlier (Equation (7.154)) fitted to the discrete data points measured along the trajectory. Results obtained in this manner are indicated by the circular symbols in Figures 7.27-7.29. To obtain these results, a number of exact trajectories were generated for a variety of linear-cubic static moments and these "data" (50 points for each run) were analyzed by the tricyclic method. There is scatter in the results, which is expected when discrete data are being

---

* A similar approximate formula was derived in Reference 7.23 and can be written

$$\frac{H_{0_e}}{H_0} = \frac{m_0 + (3/4)m_2}{m_0 + (9/8)m_2} .$$

This proves to be less accurate than (7.199).

analyzed, but the results show consistent trends. For each of the three types of nonlinear moments, the discrepancy from the true damping coefficient is greater than for the "exact-data-at-every-peak" case. What is noted is that the percent error is just about double that of the first case considered. Again the worst case is that with an unstable-stable static moment. It appears that if a static moment of this type governs, the deduced damping will differ from the true damping by a factor greater than 3. This statement holds whether the motion is damped or undamped.

For the case where exact values of the angle of attack are known at successive peaks, the true damping can be derived by a procedure to be given in the following section. However, when discrete data are analyzed by linear methods, no precise method exists to correct the deduced damping. An approximate correction would be to double the error calculated by assuming the peaks known.

7.6.6 Nonlinear Damping Moment

7.6.6.1 Approximate Solution

Since the aerodynamic damping is one of the most difficult aerodynamic parameters to determine from ballistic-range tests, the definition of "second-order" effects produced by nonlinearities in the damping is even more difficult. An important reason for studying the subject has been developed by Tobak and Pearson[7.24], who indicate that static nonlinearity should be accompanied by nonlinear damping. There are, of course, ample practical reasons for defining nonlinear damping in cases where the sign of the damping coefficient changes, introducing limit cycles and other major effects on the motion. With the recent advances in shadowgraph optics (particularly Kerr-cell shutters, see Chapter 6) and more sophisticated methods of reading the pictures obtained, far better data are becoming available for analysis; this should lead to less scatter in the experimental results and allow some coefficients previously lost in the scatter to be determined.

We will briefly consider nonlinear damping coefficients, confining the discussion to planar motion and zero swerve. The differential equation considered is

$$\alpha'' + \left(\sum_{n\geq 0} H_n \alpha^n\right) \alpha' + \sum_{n\geq 0} \frac{M_n}{IV^2} \alpha^{n+1} = 0 . \tag{7.200}$$

The middle term represents the damping moment, the last term, the static restoring moment. Note again that $n = 2$ will be referred to as a cubic moment, etc. As discussed in the previous section, if the static moment is nonlinear, the logarithmic decrement (determined from successive peaks) is not constant. We will consider that we have exact data at every peak in the angle of attack, and that we will analyze the data as though the logarithmic decrement were constant, which again introduces the concept of an "effective linear damping" (H_{0_e}). An approximate expression relating the effective linear damping to the linear term in the actual damping has been derived in Reference 7.22 and is given as follows*:

$$\frac{H_{0_e}}{H_0} = \sum_{k\geq 0} \frac{\sum_{n\geq 0} a_{kn} m_n}{\sum_{n\geq 0} b_{kn} m_n} h_k , \tag{7.201}$$

where

$$h_k = \left(\frac{1}{2+k}\right) \frac{H_k}{H_0} \alpha_a^k$$

and

$$m_n = \frac{M_n \alpha_a^n}{M_0} .$$

The constants a_{kn} and b_{kn} are given in the following tables.

Values of a_{kn}

n \ k	0	1	2	3	4	5	6	7	8
0	2.0000	1.2732	1.0000	0.8488	0.7500	0.6791	0.6250	0.5821	0.5469
1	1.5349	1.0095	0.8065	0.6913	0.6143	0.5582	0.5147	0.4797	0.4510
2	1.2500	0.8398	0.6797	0.5875	0.5250	0.4788	0.4428	0.4136	0.3895
3	1.0568	0.7208	0.5894	0.5130	0.4608	0.4218	0.3912	0.3663	0.3453
4	0.9167	0.6323	0.5213	0.4565	0.4118	0.3784	0.3519	0.3301	0.3118
5	0.8102	0.5639	0.4679	0.4118	0.3731	0.3439	0.3206	0.3014	0.2851
6	0.7266	0.5092	0.4249	0.3756	0.3415	0.3156	0.2950	0.2779	0.2633
7	0.6589	0.4645	0.3894	0.3456	0.3152	0.2920	0.2735	0.2581	0.2450
8	0.6031	0.4272	0.3596	0.3202	0.2928	0.2720	0.2552	0.2413	0.2294
∞	0	0	0	0	0	0	0	0	0

* Note that (7.199) is a special case of this expression.

Values of b_{kn}

n \ k	0	1	2	3	4	5	6	7	8
0	1.0000	1.0000	1.0000	1.0000	1.0000	1.0000	1.0000	1.0000	1.0000
1	0.9593	0.9575	0.9542	0.9505	0.9468	0.9434	0.9399	0.9364	0.9337
2	0.9375	0.9346	0.9297	0.9243	0.9188	0.9135	0.9084	0.9038	0.8997
3	0.9247	0.9211	0.9155	0.9091	0.9027	0.8964	0.8905	0.8850	0.8797
4	0.9167	0.9127	0.9067	0.8998	0.8929	0.8861	0.8797	0.8735	0.8677
5	0.9115	0.9073	0.9011	0.8940	0.8868	0.8798	0.8729	0.8665	0.8603
6	0.9082	0.9039	0.8975	0.8904	0.8831	0.8758	0.8688	0.8621	0.8558
7	0.9060	0.9016	0.8953	0.8882	0.8808	0.8735	0.8664	0.8596	0.8530
8	0.9047	0.9003	0.8940	0.8868	0.8795	0.8722	0.8650	0.8582	0.8516
∞	1.0	1.0	1.0	1.0	1.0	1.0	1.0	1.0	1.0

An example of what this equation looks like in expanded form is given as follows, where all terms relating to a 1-3-5 static moment together with a 1-3-5 damping moment have been retained.

$$\frac{H_{0_e}}{H_0} = \frac{m_0 + 0.6250\,m_2 + 0.4583\,m_4}{m_0 + 0.9375\,m_2 + 0.9167\,m_4} + \frac{m_0 + 0.6797\,m_2 + 0.5213\,m_4}{m_0 + 0.9297\,m_2 + 0.9067\,m_4}\,h_2 + \\ + \frac{0.7500\,m_0 + 0.5250\,m_2 + 0.4118\,m_4}{m_0 + 0.9188\,m_2 + 0.8929\,m_4}\,h_4 \,. \tag{7.202}$$

Equation (7.201) has been compared with the results from numerical integrations for many different nonlinearities in both the static and dynamic moments[7.22]. In all cases investigated, the approximate formula yielded results extremely close to the "exact" result. Of concern now is how the coefficients (M_n, H_n) in (7.200) can be extracted from experimental data.

7.6.6.2 Determination of Nonlinear Damping Parameters from Data

Equation (7.201) can be useful in determining the nonlinear damping parameters from a set of observed oscillations. Assume that a given oscillator is governed by (7.200). We wish to infer from observed oscillations the appropriate values of $H_0, H_2, H_4, \ldots$ and $M_0, M_2, M_4, \ldots$.

We assume that the frequency and maximum amplitudes for every half cycle of motion from each model flight can be accurately determined from the data. The effective linear damping for each half cycle is then computed by

$$H_{0_e} = \frac{2\omega}{\pi} \log_e \left| \frac{(\alpha_m)_k}{(\alpha_m)_{k+1}} \right| . \tag{7.203}$$

In addition, we assume that the damping is small so that $H_0/\omega \ll 1$. This assumption is normally satisfied in ballistic-range testing, and allows the simplification that the damping can be neglected in determining the static-moment parameters M_n.

By use of the approximation for the frequency developed earlier (Equation (7.194) transformed to distance), we can write

$$\omega^2(x) = \frac{M_0}{IV^2} + \sum_{n>0} A_n \frac{M_n}{IV^2}\,\alpha_a^n \,, \tag{7.204}$$

where

$$A_n = \frac{4}{n+2}\left[1 - \left(\tfrac{1}{2}\right)^{(n+2)/2}\right]$$

and

$$\alpha_a = \sqrt{\left(\frac{(\alpha_m)_k^2 + (\alpha_m)_{k+1}^2}{2}\right)} .$$

This formula is a good approximation for large and small nonlinearities, except in the vicinity of the singular points of static instability. By fitting this equation to a set of frequency versus amplitude data, the appropriate values of M_n can be obtained.

A similar but slightly more complicated situation exists for determining the damping parameters H_n. In this case, the static parameters play an important role, whereas in the determination of the static-moment parameters M_n, the effect of the damping parameters can be neglected. Rewriting (7.201) in a slightly different form, H_{0_e} is given by

$$H_{0_e} = B_0 H_0 + \sum_{k>0} B_k H_k \alpha_a^k , \tag{7.205}$$

where B_k $(k \geq 0)$ is

$$B_k = \frac{1}{2+k} \frac{\sum_{n\geq 0} a_{kn} M_n \alpha_a^n}{\sum_{n\geq 0} b_{kn} M_n \alpha_a^n} .$$

Equation (7.205) is analogous in form to (7.204). In this case, however, the coefficients B_k are functions of $M_0, M_1, M_2, \ldots\ldots$ and α_a, whereas the coefficients A_n were constants. In the determination of the damping, however, the static parameters can be regarded as already determined by the use of (7.204). Hence, the coefficients B_n are functions of only α_a insofar as determination of the damping is concerned.

It is now useful to divide both sides of (7.205) by B_0, obtaining

$$\frac{H_{0_e}}{B_0} = H_0 + \sum \frac{B_k}{B_0} H_k \alpha_a^k . \tag{7.206}$$

Because $B_0, B_1, B_2, \ldots$ all vary with α_a in a similar manner, the ratios B_k/B_0 vary slowly with α_a. Equation (7.206) can now be used to study a set of damping data in a manner analogous to studying frequency data with (7.204).

As a simple example, consider that a set of data for a given oscillator has been obtained and that the static moment, completely arbitrary, has been determined with the use of (7.204). Assume that the damping moment can be described by a linear term and a single arbitrary nonlinear term so that (7.206) appears as

$$\frac{H_{0_e}}{B_0} = H_0 + \frac{B_n}{B_0} H_n \alpha_a^n , \tag{7.207}$$

where n is not known. Choosing a particular value of n determines B_n/B_0. Then on a plot of H_{0_e}/B_0 versus $(B_n/B_0)\alpha_a^n$, when the right value of n is chosen, the data will fall on a straight line. The slope of the line yields H_n, and the intercept of the line with the H_{0_e}/B_0 axis yields H_0. This will be true without regard to the particular form of the static moment.

For an arbitrary damping moment described by a given set of data over an amplitude range, there may be many combinations of the parameters $H_0, H_1, H_2, \ldots$ that will fit the data. This situation also occurred in determining the static-moment parameters. One must often settle for a member of a class of moments that gives a good fit. Thus, a certain amount of experience is useful in analyzing the data. For a set of data including small angles of α_a as well as large, one should plot the damping data as H_{0_e}/B_0 versus $(B_2/B_0)\alpha_a^2$ (or as a first try against α_a^2 since B_2/B_0 varies slowly with α_a). If the data fall on a straight line, the damping moment is a cubic as described by (7.207) with $n = 2$. If the data deviate from a straight line, which might be expected to occur at larger values of α_a, one can estimate the magnitude and sign of the next higher order damping term needed to fit the data. In such a manner the appropriate form of damping polynomial tends to suggest itself.

7.7 LIFT ANALYSIS

A model in free-flight normally develops lift which causes the center of gravity to follow a trajectory that deviates from a straight line. For airplane-like configurations, this is often troublesome in that the lift can cause the model to quickly fly out of the field of view. Even for axisymmetric bodies the lift usually causes the model to depart from bore sight of the gun. This can be explained as follows. Consider the simplified form of (7.105)

$$z'' = -\frac{\rho A}{2m} C_{L_\alpha} \alpha , \tag{7.208}$$

where C_{L_α} is the lift-curve slope. Now assume for simplicity that the model emerges from the gun at zero angle of attack but is given an angular rate during separation from the sabot. A simple form for the angle of attack that satisfies these conditions is

$$\alpha = \alpha_m \sin \omega x .$$

Substituting this expression into (7.208) and integrating twice yields

$$z = \frac{\rho A}{2m} C_{L_\alpha} \frac{\alpha_m}{\omega^2} \sin \omega x + C_1 x + C_2 . \tag{7.209}$$

If we make the initial conditions $z = z' = 0$ at $x = 0$, then

$$z = \frac{\rho A}{2m} C_{L_\alpha} \frac{\alpha_m}{\omega^2} \sin \omega x - \frac{\rho A}{2m} C_{L_\alpha} \frac{\alpha_m}{\omega} x . \tag{7.210}$$

This equation indicates that even with zero vertical velocity upon emerging from the gun, a vertical velocity is acquired due to the lift. For this simplified case, the center of gravity oscillates about a straight line in phase with the angle of attack as shown in Figure 7.30. The presence of aerodynamic damping, gravity, etc. would cause the swerve oscillation to take place about a curved line. What is important to note here is that the magnitude of the deviation from some mean line is a measure of the lift. We will now consider various methods for determining the lift coefficient.

7.7.1 Determination from Displacement Variation Near a Peak

The most basic method for determining the lift coefficient as a function of angle of attack is by analysis of the lateral displacement history of the model mass center (which is caused by the lift). The deduced lateral acceleration is related to the angle of attack history to define $C_L(\alpha)$. For motions involving a small roll rate, an approach similar to that used for determining the moment coefficient in Section 7.6.2 can be used. For a planar motion in the x-z plane (ignoring gravity), the differential equation of motion is

$$z'' = -Kl(C_L)_D - K(C_L)_S \,, \tag{7.211}$$

where

$(C_L)_D$ = dynamic lift coefficient

$(C_L)_S$ = static lift coefficient

$K = \rho A/2m$.

As with the angle of attack data, a desirable segment of vertical displacement data is one which brackets a peak deviation, and which can be considered as two sets of data about this maximum or peak. (The swerving motion peaks at very nearly the same x position as the angular motion; they peak at exactly the same x if damping is zero.)

The development of the equations is exactly analogous to that for angles and we have, at any given α ,

$$-(C_L)_S = \frac{z_1'' + z_2''}{2K} - \frac{l}{2}\left[(C_L)_{D_1} + (C_L)_{D_2}\right] . \tag{7.212}$$

If we assume that $(C_L)_D = (C_{L_q} + C_{L_{\dot{\alpha}}})\alpha'$ we have

$$-(C_L)_S = \frac{z_1'' + z_2''}{2K} - \frac{l}{2}(C_{L_q} + C_{L_{\dot{\alpha}}})(\alpha_1' + \alpha_2') \,. \tag{7.213}$$

Usually, the contribution of the dynamic term to the lift coefficient is very small. Therefore, when z_1'' and z_2'' are determined (for points of equal angle of attack on either side of the peak), $(C_L)_S$ is effectively determined. If damping in lift is truly negligible, the two values of z'' are nearly identical. The deduced instantaneous values of $(C_L)_S$ are plotted against the instantaneous corresponding angles of attack to generate a curve of $C_L(\alpha)$. An example showing results from this method is given in Section 7.9.2.

7.7.2 Normal Force from Stability Data on Models with Different Centers of Mass

The normal-force-curve slope, C_{N_α} ($C_{N_\alpha} \approx C_{L_\alpha} + C_D$), and the center of pressure location, x_{cp} , are often found by testing models of fixed external shape but with two different (known) center of mass locations. The two bodies would have the same values of C_{N_α} and x_{cp} , but the moment-curve slope, C_{m_α} , would be different. Values of C_{m_α} can be obtained experimentally for each of the bodies by methods already described. Then using the relationship between C_m and C_N ,

$$C_{m_\alpha} = C_{N_\alpha}\left(\frac{x_{cg} - x_{cp}}{l}\right) , \tag{7.214}$$

where l is the reference length, we have a pair of simultaneous equations for the two unknowns, C_{N_α} and x_{cp} .

7.7.3 Tricyclic Method

When the angular motion is not planar and involves precession due to spin, the tricyclic method discussed in Section 7.6.3 can be used for the analysis of the swerve and the determination of lift coefficients. A trim lift force may be included in this analysis, defined as follows:

C_{y_0} lift coefficient in y direction for $\beta = 0$ at $x = 0$

C_{L_0} lift coefficient in z direction for $\alpha = 0$ at $x = 0$.

These are components of the $C_{L_{\delta_f}}$ term in (7.107). They rotate with the body at a rate, p , and their resultant represents the force at zero angle of attack due to small asymmetries in the model.

The equation for displacement acceleration is (see Equation (7.105))

$$y'' + iz'' = -K\{(C_{L_\alpha} + iC_{L_{\alpha p}} pl)(\beta + i\alpha) + l[(C_{L_q} + C_{L_{\dot\alpha}}) + i(C_{L_{\dot\alpha p}} - C_{L_{qp}})pl](\beta' + i\alpha') + (C_{y_0} + iC_{L_0})e^{ipx}\} +$$

$$+ ig/V^2 - 2\frac{\omega_E}{V}(\sin\theta_l + i\cos\theta_l \sin\theta_a) \quad . \qquad (7.215)$$

Note that the lift coefficients due to Magnus effects ($C_{L_{\alpha p}}, C_{L_{\dot\alpha p}}, C_{L_{qp}}$) are retained in this equation, but are exceedingly difficult to obtain experimentally unless very high roll rates are experienced. If these coefficients can be obtained, moment coefficients due to Magnus effects can be found from the stability analysis.

If we now integrate the above equation twice with respect to x we obtain

$$y + iz = -K\left\{C_{L_\alpha}\int_0^x\int_0^x (\beta + i\alpha)\,dx\,dx + ipl\,C_{L_{\alpha p}}\int_0^x\int_0^x (\beta + i\alpha)\,dx\,dx + \right.$$

$$+ l(C_{L_q} + C_{L_{\dot\alpha}})\int_0^x (\beta + i\alpha)\,dx - l(C_{L_q} + C_{L_{\dot\alpha}})(\beta_0 + i\alpha_0)x +$$

$$+ ipl^2(C_{L_{\dot\alpha p}} - C_{L_{qp}})\int_0^x (\beta + i\alpha)\,dx - ipl^2(C_{L_{\dot\alpha p}} - C_{L_{qp}})(\beta_0 + i\alpha_0)x +$$

$$\left. + (C_{y_0} + iC_{L_0})\left(\frac{1 + ipx - e^{ipx}}{p^2}\right)\right\} + (y_0' + iz_0')x +$$

$$+ (y_0 + iz_0) + \int_0^x\int_0^x i\frac{g}{V^2}\,dx\,dx -$$

$$- 2\frac{\omega_E}{V_0}(\sin\theta_l + i\cos\theta_l \sin\theta_a)\int_0^x\int_0^x \frac{V_0}{V}\,dx\,dx$$

which, after terms are rearranged, becomes

$$y + iz = -K\left\{(C_{L_\alpha} + ipl C_{L_{\alpha p}})\int_0^x\int_0^x (\beta + i\alpha)\,dx\,dx + \right.$$

$$+ l\left[(C_{L_q} + C_{L_{\dot\alpha}}) + ipl(C_{L_{\dot\alpha p}} - C_{L_{qp}})\right]\left[\int_0^x (\beta + i\alpha)\,dx - (\beta_0 + i\alpha_0)x\right] +$$

$$\left. + (C_{y_0} + iC_{L_0})\left(\frac{1 + ipx - e^{ipx}}{p^2}\right)\right\} + (y_0' + iz_0')x +$$

$$+ (y_0 + iz_0) + ig\int_0^x\int_0^x \frac{1}{V^2}\,dx\,dx -$$

$$- 2\frac{\omega_E}{V_0}(\sin\theta_l + i\cos\theta_l \sin\theta_a)\int_0^x\int_0^x \frac{V_0}{V}\,dx\,dx \quad . \qquad (7.216)$$

The term

$$ig\int_0^x\int_0^x \frac{1}{V^2}\,dx\,dx$$

is the displacement in the vertical plane due to gravity. It can be calculated separately and added to z algebraically. If the precise flight time is known for a specific x location, the displacement due to gravity is simply $z_g = \frac{1}{2}gt^2$. The Coriolis term can be integrated directly since $V_0/V = e^{KC_D x}$ (Equation (7.109)). The result is

$$-2\frac{\omega_e}{V_0}(\sin\theta_l + i\cos\theta_l \sin\theta_a)\left(\frac{e^{KC_D x} - KC_D x - 1}{(KC_D)^2}\right) \qquad (7.217)$$

and for small KC_D

$$\frac{e^{KC_D x} - KC_D x - 1}{(KC_D)^2} \simeq \frac{x^2}{2} \quad . \qquad (7.218)$$

This contribution to y and z can also be calculated separately and added algebraically to the y and z data.

If the Magnus terms are ignored, there are eight unknown coefficients in (7.216): C_{L_α}, $(C_{L_q}+C_{L_{\dot\alpha}})$, C_{y_0}, C_{L_0}, y_0', y_0, z_0', and z_0. All of these coefficients appear in a linear fashion and if the integrals of $(\beta+i\alpha)$ can be calculated in closed form and p is known, then the coefficients can be solved for by a standard least squares technique. The expressions for $(\beta+i\alpha)$ can be obtained in closed form from fitting (7.154) to the angle data in obtaining the static and dynamic stability. The roll rate p is also known from the stability reduction.

Some of the Magnus coefficients can now be found by using the stability and lift analyses together, provided the data are accurate and well-defined. From (7.216), values for $C_{L_{\alpha p}}$ and $(C_{L_{\dot\alpha p}}-C_{L_{qp}})$ can be obtained from a least-squares fit since they occur linearly as do the other coefficients. Then from (7.158), given C_{L_α}, we can calculate $C_{m_{\alpha p}}$. With (7.157), given $C_{L_{\alpha p}}$, we can calculate a slightly modified value of C_{m_α}. With (7.156), given $C_{L_{\alpha p}}$, we can obtain $(C_{m_{\dot\alpha p}}-C_{m_{qp}})$. Therefore, from the combined stability and lift analyses, we can derive all of the following coefficients: ξ, C_{m_α}, C_{L_α}, $C_{m_q}+C_{m_{\dot\alpha}}$, $C_{L_q}+C_{L_{\dot\alpha}}$, $C_{m_{\alpha p}}$, $C_{L_{\alpha p}}$, $C_{m_{\dot\alpha p}}-C_{m_{qp}}$, $C_{L_{\dot\alpha p}}-C_{L_{qp}}$, C_{y_0}, and C_{L_0}. For most ballistic range tests, however, the models are fired from smooth-bore guns so that the roll rates are small and the Magnus terms are negligible.

It is also possible to deduce the center of pressure, x_{cp}, and normal-force-curve slope, C_{N_α}, from measurements of a single model flight which define the lift, drag, and static stability coefficients. For small angles

$$C_{N_\alpha} \approx C_{L_\alpha} + C_D$$

and, as noted earlier,

$$C_{m_\alpha} = C_{N_\alpha}\left(\frac{x_{cg}-x_{cp}}{l}\right),$$

so that

$$\frac{x_{cp}}{l} = \frac{x_{cg}}{l} - \frac{C_{m_\alpha}}{C_{L_\alpha}+C_D}.$$

7.7.4 Nonlinear Lift

Another method for obtaining the lift coefficient, which can handle a case involving nonlinear lift, proceeds as follows. The lift coefficient is expressed as a polynomial in resultant angle of attack, α_R, as

$$C_L = \sum_{i=1}^{n} C_{L_{\alpha_i}}\alpha_R^i . \tag{7.219}$$

For simplicity in demonstration, we will use the two-term series

$$C_L = C_{L_\alpha}\alpha_R + C_{L_{\alpha_3}}\alpha_R^3 . \tag{7.220}$$

In the α-β plane, with the y and z coordinate axes also shown, we define an angle ϕ (see Figure 7.31) as the angle between the resultant angle of attack α_R and the β (or $-y$) axis. The lift in the z direction is

$$C_{L_z} = C_L\sin\phi = C_{L_\alpha}\alpha_R\sin\phi + C_{L_{\alpha_3}}\alpha_R^3\sin\phi \tag{7.221}$$

and in the y direction

$$C_{L_y} = C_L\cos\phi = C_{L_\alpha}\alpha_R\cos\phi + C_{L_{\alpha_3}}\alpha_R^3\cos\phi . \tag{7.222}$$

The differential equations of motion (with no damping) in the z and y directions are

$$z'' = -KC_{L_z} + \frac{g}{V^2} \tag{7.223}$$

$$y'' = -KC_{L_y} , \tag{7.224}$$

where $K = \rho A/2m$ and g is the acceleration due to gravity. Substituting (7.221) and (7.222) into these equations, we get

$$z'' = -K\left(C_{L_\alpha}\alpha_R\sin\phi + C_{L_{\alpha_3}}\alpha_R^3\sin\phi\right) + g/V^2 \tag{7.225}$$

$$y'' = -K\left(C_{L_\alpha}\alpha_R\cos\phi + C_{L_{\alpha_3}}\alpha_R^3\cos\phi\right) . \tag{7.226}$$

Integrating twice with respect to x we obtain

$$z = z_0 + z_0'x - KC_{L_\alpha}\int_0^x\int_0^x \alpha_R\sin\phi\,dx\,dx - KC_{L_{\alpha_3}}\int_0^x\int_0^x \alpha_R^3\sin\phi\,dx\,dx + \frac{gt^2}{2} \tag{7.227}$$

$$y = y_0 + y_0'x - KC_{L_\alpha}\int_0^x\int_0^x \alpha_R\cos\phi\,dx\,dx - KC_{L_{\alpha_3}}\int_0^x\int_0^x \alpha_R^3\cos\phi\,dx\,dx . \tag{7.228}$$

At each data station there are measured values for α, β, y, z; α_R can be calculated from

$$\alpha_R \cong \sqrt{(\alpha^2 + \beta^2)}$$

and ϕ can be obtained from

$$\phi = \tan^{-1}(\alpha/\beta) .$$

Thus, $\alpha_R \sin\phi$, $\alpha_R \cos\phi$, $\alpha_R^3 \sin\phi$, and $\alpha_R^3 \cos\phi$ can be plotted as functions of x and integrated graphically. With the integrals determined, a least squares technique can be used to find best values for all of the unknowns in (7.227) and (7.228).

7.8 NUMERICAL INTEGRATION OF EQUATIONS OF MOTION

The tricyclic method described earlier has been the most widely used means for obtaining aerodynamic coefficients from free-flight tests. Within the realm where the assumptions made in the derivation of the tricyclic equations were satisfied, the method was convenient and gave good results. Even when the assumptions were not satisfied, this method was normally applied first, and then the results were modified by some of the methods that have been described.

It is easy to see how this strong dependence on the tricyclic equations came about. The problem was to deduce the aerodynamic characteristics governing a body from discrete observations of its position and attitude in space. The complete differential equations governing the motion were presumed known. Since errors were certain to exist in the position and attitude data, a "best fit" of some kind was called for, preferably an iteration scheme that would search for this fit. A least-squares fit was the natural choice, and with it a differential correction technique would have to be used. For this to work, however, partial derivatives of each dependent variable (e.g. $\alpha, \beta, y, z, \ldots$.) with respect to each unknown coefficient in the differential equations of motion had to be known at every data station.

At that period in time, electronic computers were too slow to consider numerical determination of these partial derivatives. The remaining choice was to get a closed-form solution (e.g. $\alpha = f(x)$) so that the various partial derivatives would also have closed-form expressions. A least-squares fit is then straightforward, although convergence of the iteration procedure cannot be guaranteed. The tricyclic equations are the implementation of this approach. Enough approximations and assumptions are introduced into the differential equations of motion so that a closed-form solution can be obtained.

It would be beneficial if the need for having a closed-form solution could be by-passed, and the data fit instead by *numerical* solutions to the differential equations. This would allow far more generality in the problem of obtaining the aerodynamic coefficients because, at least theoretically, the exact differential equations of motion could be used. Two such methods will be described. The first (Section 7.8.1) is an approximate method which has been successfully applied in the past to small-amplitude motions of airplane-type configurations[7·25]. It does not require a very sophisticated computer, but does have the drawback that it yields results which cannot be improved except by trial and error. The second method described (Section 7.8.2) eliminates this drawback by providing an iterative scheme for seeking the "best fit" to experimental data[7·26]. In this case a high-speed digital computer is essential. In practice, the first method can be used to obtain a starting solution for the more powerful second approach.

7.8.1 Approximate Method

In Section 7.4.3.1 we obtained a set of differential equations to describe the motion of airplane-type configurations (Equations (7.95)-(7.98)). Simplifying the nomenclature, these equations appear essentially as follows:

$$y'' = B_1 y' + B_2 \bar{\alpha} \sin\phi + B_3 \bar{\beta} \cos\phi \tag{7.229}$$

$$z'' = B_1 z' - B_2 \bar{\alpha} \cos\phi + B_3 \bar{\beta} \sin\phi \tag{7.230}$$

$$\bar{\alpha}'' = B_4 \bar{\alpha}' + B_5 \bar{\alpha} + B_6 \bar{\beta}' + B_7 \bar{\beta} + B_8 \tag{7.231}$$

$$\bar{\beta}'' = B_9 \bar{\beta}' + B_{10} \bar{\beta} + B_{11} \bar{\alpha}' + B_{12} \bar{\alpha} + B_{13} . \tag{7.232}$$

Here ϕ is the angle of roll about the model's $\bar{x}$ axis measured from the pitch plane (see Figure 7.2b). Presumably it is a known function of distance. These four equations form the basis for determining the aerodynamic coefficients from the flight records. The following results are obtained after integrating twice with respect to distance (ζ and η are dummy variables):

$$y(x) = y_0 + (y_0' + B_1 y_0)x + B_1 \int_0^x y \, d\eta + B_2 \int_0^x d\eta \int_0^\eta \bar{\alpha} \sin\phi \, d\zeta + B_3 \int_0^x d\eta \int_0^\eta \bar{\beta} \cos\phi \, d\zeta \tag{7.233}$$

$$z(x) = z_0 + (z_0' + B_1 z_0)x + B_1 \int_0^x z \, d\eta - B_2 \int_0^x d\eta \int_0^\eta \bar{\alpha} \cos\phi \, d\zeta + B_3 \int_0^x d\eta \int_0^\eta \bar{\beta} \sin\phi \, d\zeta \tag{7.234}$$

$$\bar{\alpha}(x) = \bar{\alpha}_0 + (\bar{\alpha}_0' + B_4\bar{\alpha}_0 + B_6\bar{\beta}_0)x + B_4\int_0^x \bar{\alpha}\,d\eta + B_5\int_0^x d\eta\int_0^\eta \bar{\alpha}\,d\zeta + B_6\int_0^x \bar{\beta}\,d\eta + B_7\int_0^x d\eta\int_0^\eta \bar{\beta}\,d\zeta + B_8\frac{x^2}{2} \quad (7.235)$$

$$\bar{\beta}(x) = \bar{\beta}_0 + (\bar{\beta}_0' + B_9\bar{\beta}_0 + B_{11}\bar{\alpha}_0)x + B_9\int_0^x \bar{\beta}\,d\eta + B_{10}\int_0^x d\eta\int_0^\eta \bar{\beta}\,d\zeta + B_{11}\int_0^x \bar{\alpha}\,d\eta + B_{12}\int_0^x d\eta\int_0^\eta \bar{\alpha}\,d\zeta + B_{13}\frac{x^2}{2} . \quad (7.236)$$

To accurately evaluate the integrands in the above equations, a continuous history of $\bar{\alpha}$ and $\bar{\beta}$ must be obtained. Since the basic data $\psi_{ME}, \theta_{ME}, \phi, y, z$ are obtained only at discrete points along the trajectory, it must be assumed that a faired curve drawn through these observed points represents the true continuous trajectory of the model. For any x position, the angle of attack, $\bar{\alpha}$, and the angle of sideslip, $\bar{\beta}$, can then be determined from the observed parameters by use of the relationships defined in Figure 7.4.

$$\bar{\alpha} = (\theta_{ME} + z')\cos\phi + (\psi_{ME} - y')\sin\phi \quad (7.237)$$

$$\bar{\beta} = -(\psi_{ME} - y')\cos\phi + (\theta_{ME} + z')\sin\phi . \quad (7.238)$$

This method of obtaining a continuous record of $\bar{\alpha}$ and $\bar{\beta}$ is considered to be more accurate than to transform the measured points into $\bar{\alpha}$ and $\bar{\beta}$ and then fair the points.

Sets of redundant simultaneous equations are obtained by evaluating each of the equations (7.233) thru (7.236) at a number of x locations; since the required coefficients appear in a linear fashion, a straightforward application of a least-squares technique can be used to solve for them.

7.8.2 Iterative Approach[7.26]

As mentioned earlier, for a least-squares fit employing differential corrections to succeed, partial derivatives of each dependent variable with respect to every unknown coefficient must be known accurately at every data station. The problem of obtaining these partial derivatives can be successfully handled by the method of parametric differentiation. To illustrate the procedure, assume that the equations of motion governing a particular configuration are the two coupled nonlinear differential equations

$$\left.\begin{aligned} \alpha'' + C_1\alpha' + C_2\alpha + C_3\alpha^3 + C_4\beta' &= 0 \\ \beta'' + C_1\beta' + C_2\beta + C_3\beta^3 - C_4\alpha' &= 0 . \end{aligned}\right\} \quad (7.239)$$

Note that C_1 is related to the damping moment, C_2 and C_3 define a linear-cubic static moment, and C_4 is related to the roll rate.

The initial conditions at $x = 0$ are

$$\begin{aligned} \alpha(0) &= C_5 \\ \alpha'(0) &= C_6 \\ \beta(0) &= C_7 \\ \beta'(0) &= C_8 . \end{aligned}$$

We want to determine the four aerodynamic parameters (C_1 to C_4) and the four initial conditions such that we obtain a least-squares fit to experimental $\alpha(x)$ and $\beta(x)$ data. The method of differential corrections will be used to do this (described in the Appendix). Assume that initial values of the unknowns, required to start the differential correction procedure, are available (previous section). Next we need the partial derivatives of both α and β with respect to the eight unknowns. No closed-form solution exists for these derivatives, but they can be obtained numerically by the method of parametric differentiation. First define the following notation:

$$P_i = \frac{\partial\alpha}{\partial C_i}, \qquad P_i' = \frac{\partial P_i}{\partial x} = \frac{\partial\alpha'}{\partial C_i}, \qquad P_i'' = \frac{\partial^2 P_i}{\partial x^2} = \frac{\partial\alpha''}{\partial C_i}$$

$$Q_i = \frac{\partial\beta}{\partial C_i}, \qquad Q_i' = \frac{\partial Q_i}{\partial x} = \frac{\partial\beta'}{\partial C_i}, \qquad Q_i'' = \frac{\partial^2 Q_i}{\partial x^2} = \frac{\partial\beta''}{\partial C_i} .$$

Note that it is explicitly assumed here that the order of differentiation can be reversed and that

$$\frac{\partial}{\partial C_j}\left(\frac{\partial\alpha}{\partial x}\right) = \frac{\partial}{\partial x}\left(\frac{\partial\alpha}{\partial C_j}\right), \quad \text{etc} .$$

For well-behaved functions, this is normally true. Now differentiate (7.239) with respect to C_i, to obtain the following 16 differential equations.

$$
\left.\begin{aligned}
P_1'' + C_1P_1' + (C_2+3C_3\alpha^2)P_1 + C_4Q_1' &= -\alpha' \\
P_2'' + C_1P_2' + (C_2+3C_3\alpha^2)P_2 + C_4Q_2' &= -\alpha \\
P_3'' + C_1P_3' + (C_2+3C_3\alpha^2)P_3 + C_4Q_3' &= -\alpha^3 \\
P_4'' + C_1P_4' + (C_2+3C_3\alpha^2)P_4 + C_4Q_4' &= -\beta' \\
P_5'' + C_1P_5' + (C_2+3C_3\alpha^2)P_5 + C_4Q_5' &= 0 \\
P_6'' + C_1P_6' + (C_2+3C_3\alpha^2)P_6 + C_4Q_6' &= 0 \\
P_7'' + C_1P_7' + (C_2+3C_3\alpha^2)P_7 + C_4Q_7' &= 0 \\
P_8'' + C_1P_8' + (C_2+3C_3\alpha^2)P_8 + C_4Q_8' &= 0 \\
Q_1'' + C_1Q_1' + (C_2+3C_3\beta^2)Q_1 - C_4P_1' &= -\beta' \\
Q_2'' + C_1Q_2' + (C_2+3C_3\beta^2)Q_2 - C_4P_2' &= -\beta \\
Q_3'' + C_1Q_3' + (C_2+3C_3\beta^2)Q_3 - C_4P_3' &= -\beta^3 \\
Q_4'' + C_1Q_4' + (C_2+3C_3\beta^2)Q_4 - C_4P_4' &= +\alpha' \\
Q_5'' + C_1Q_5' + (C_2+3C_3\beta^2)Q_5 - C_4P_5' &= 0 \\
Q_6'' + C_1Q_6' + (C_2+3C_3\beta^2)Q_6 - C_4P_6' &= 0 \\
Q_7'' + C_1Q_7' + (C_2+3C_3\beta^2)Q_7 - C_4P_7' &= 0 \\
Q_8'' + C_1Q_8' + (C_2+3C_3\beta^2)Q_8 - C_4P_8' &= 0 .
\end{aligned}\right\} \qquad (7.240)
$$

The initial conditions are

$$
\left.\begin{aligned}
P_5 &= Q_7 = 1 \\
P_6' &= Q_8' = 1 \\
\text{all other} \quad P_i &= P_i' = Q_i = Q_i' = 0 .
\end{aligned}\right\} \quad \text{at} \quad x = 0
$$

Note that these are all linear differential equations with variable coefficients. However, both the variable coefficients and the right-hand sides are known from the numerical solution to (7.239). Hence numerical integration of (7.239) and (7.240) can yield values of α, β, and all partial derivatives. It is necessary to interpolate during the integration to obtain the values at the particular "x" locations where data exist. Corrections (ΔC_i) to the starting values of the eight unknown coefficients can then be obtained by solving the matrix equation

$$
\underset{8\times 8}{[A]}\ \underset{8\times 1}{[\Delta C]} = \underset{8\times 1}{[B]} ,
$$

where general elements of the A and B matrices are

$$
\left.\begin{aligned}
A_{ij} &= \sum_{\substack{\text{all data}\\ \text{stations}}} \left(\frac{\partial\alpha}{\partial C_i}\right)\left(\frac{\partial\alpha}{\partial C_j}\right) + \left(\frac{\partial\beta}{\partial C_i}\right)\left(\frac{\partial\beta}{\partial C_j}\right) \\
B_i &= \sum_{\substack{\text{all data}\\ \text{stations}}} (\alpha_{exp}-\alpha_{calc})\frac{\partial\alpha}{\partial C_i} + (\beta_{exp}-\beta_{calc})\frac{\partial\beta}{\partial C_i} .
\end{aligned}\right\} \qquad (7.241)
$$

The subscript "exp" denotes experimental values, while "calc" denotes calculated values obtained from the numerical integration. New values of the coefficients are obtained by adding ΔC_i to the present values, and the iteration process is continued until any prescribed degree of convergence is reached.

Some miscellaneous notes relating to this technique should be listed.

(i) As a starting solution, an approach as outlined in the previous section is best. In many cases, however, results from the tricyclic method or even educated guesses from a hand-fairing of the data can be used.

(ii) Although a large number of differential equations can become involved, the time to analyze a given flight is not prohibitive. With the foregoing example, the time to get a converged solution (five iterations) for a 200 ft flight is about 90 seconds on an IBM 7090.

(iii) Any known functions of distance (such as variable density) can easily be incorporated. For example, in (7.239) if C_i is replaced by $D_i f_i(x)$, C_2 by $D_2 f_2(x)$, etc., it is possible to solve for D_i exactly as C_i was solved for. The functions of distance may be either expressions or tabulations.

(iv) A number of different flights of a given configuration can be analyzed simultaneously to obtain the aerodynamic coefficients that best represent all flights. This would often be necessary to find terms that are nonlinear in angle of attack.

(v) Alternate approaches for numerically fitting differential equations to experimental data are discussed in References 7.27 and 7.28.

7.9 EXAMPLE CASES

7.9.1 Introduction

Examples showing application of some of the data reduction procedures that have been described will be given next. First the determination of aerodynamic coefficients from analysis of data points in the vicinity of a peak amplitude will be illustrated. This will be followed by examples illustrating the tricyclic analysis, and finally by an example applying the method of numerical integration of the equations of motion.

7.9.2 Analysis Using Angles and Displacements Near a Peak

An example application of the procedure described in Section 7.6.2 will now be given. A planar motion was generated numerically using nonlinear aerodynamic coefficients. A half cycle of motion bracketing a peak was then analyzed by the most complete version of the method in Section 7.6.2 (including damping) to see if the α versus x variation could be reduced to obtain the aerodynamic coefficients used to generate the motion. The α versus x segment analyzed is plotted in Figure 7.32. The center is found to be at $x = 18.4$ m where $\alpha = 24.89^\circ$. When both halves are plotted with the center as origin, the difference in the two curves can easily be seen as shown in Figure 7.33. Each curve is fitted with a polynomial of the form

$$\alpha - \alpha_m = A_1 x^2 + A_2 x^3 + A_3 x^4 + A_4 x^5 ,$$

where $\alpha_m = 24.89^\circ$. The C_m and ξ curves deduced are shown in Figures 7.34 and 7.35. With no random errors introduced into the α data, both results are very precise except at $\alpha < 10^\circ$, where the curvature in the angle data tends to vanish. With various degrees of random error (uniform error distribution), the deduced C_m curves remain fairly accurate but the ξ curves become poor rapidly as the maximum error is increased.

This example has also been used to illustrate the method for obtaining the lift coefficient as described in Section 7.7.1. The deduced C_L versus α curves are shown in Figure 7.36. Included are results for exact data (no random errors) and a case with random errors in both α and z. Above 10° both curves are very close to the exact curve.

7.9.3 Analysis Using Tricyclic Method

7.9.3.1 Data Reduction Procedure[7.29]

We will now discuss the overall procedure one might use for reducing data from a free-flight test utilizing the tricyclic analyses for stability and lift coefficients (Sections 7.6.3 and 7.7.3) and the direct t versus x analysis for drag coefficient (Section 7.5.1, Method 5). The emphasis here is on the interaction between the various reduction procedures which have previously been described.

A representative flow diagram for the order of the calculations in reducing ballistic range data is shown in Figure 7.37. The steps can be summarized as follows:

(i) Determination of drag coefficient by fitting x-t data with (7.110); correction of z and θ data for gravity effects.

(ii) Smoothing of experimental data. This smoothing procedure has not been discussed previously, but basically seeks to eliminate data points which lie well outside the standard deviation of the fit obtained. No exact criterion for rejection can be given but experience has shown that it is usually helpful to eliminate data points having residuals greater than about 2.25 standard deviations and replace them with the calculated values.

(iii) Determination of static and dynamic stability coefficients from angle data using tricyclic analysis (Equation (7.154)).

(iv) Rotation of orthogonal coordinate system to reduce inherent error in tricyclic analysis due to large angles.

(v) Determination of lift parameters from displacement data (Equation (7.216)) in conjunction with tricyclic analysis of angles.

(vi) Calculation of corrections to measured angles due to curvature (swerving) of the flight path.

(vii) Repeat stability analysis and continue with iterative scheme between stability and lift until angle corrections from swerve remain constant.

(viii) Smooth angle and displacement data and repeat any steps that are necessary.

7.9.3.2 Example, and Comparison of Free-Flight and Wind-Tunnel Results

An example of the application of the above procedures, and a comparison of results from free-flight and conventional wind tunnel tests of the same body shape at identical test conditions, is now made to illustrate the generally good agreement and to point up a common discrepancy in drag results[7.29]. The shape selected is the AGARD standard hypersonic ballistic correlation model HB-2. Free-flight data obtained in the Pressurized Ballistic Range at Ames Research Center[7.29] are compared to wind-tunnel data from Arnold Engineering Development Center (AEDC)[7.30,7.31] and some free-flight results from the Canadian Research and Development Establishment (CARDE)[7.32]. The model used in the Ames' tests (Fig.7.38) was ballasted at the nose to make it aerodynamically stable. The two pins on the base were used to measure the roll orientation and the small frustum on the base was gripped by the sabot during launch. The tests were conducted at a Mach number of 2.0 and a Reynolds number based on cylinder diameter of 1.7 million. A shadowgraph of this model in flight is shown in Figure 8.17.

Figure 7.39 shows a typical set of position, time, and angle data for the free-flight tests. Figure 7.39(a) shows the flight time as a function of distance and the resulting velocity decrease over the length of the range. Figures 7.39(b), and (c) show the displacement and angular measurements.

The total drag coefficient* as a function of angle of attack is shown in Figure 7.40. The Ames data are indicated by the circular symbols, through which a least-squares curve has been drawn, and the AEDC data are indicated by the dashed line. There is a significant difference in the level of C_D between the ballistic-range and wind-tunnel results although it is noted that the curves are roughly parallel. The wind tunnel total drag was obtained by combining the contributions of forebody and base drag measurements given in Reference 7.30. Sting effects on the base pressure were suspected to be the cause of the discrepancy (see, e.g., Reference 7.33). Therefore, the base drag coefficient was calculated from the flow-field configuration shown in shadowgraph pictures of the free flight models. More detail on base pressure estimation is given in Chapter 8, Section 8.5.4. This base drag coefficient, when added to the AEDC forebody drag, gave the shaded region in Figure 7.40 (the region brackets the results from four different flights analyzed in this manner). The agreement with the free-flight measurements of total drag is now excellent.

The lift-curve slope, as deduced from the swerving motion of each model, is shown in Figure 7.41 plotted against pitching amplitude. These data indicate that the lift coefficient is linear with angle of attack at least to 7 degrees. The wind-tunnel result for lift-curve slope (deduced from normal and axial force measurements) is shown, together with a value obtained using the Ames-deduced base pressure in the axial force contribution. The agreement between free-flight and wind-tunnel results is very good.

A curve of normal force versus angle of attack was calculated from the measured lift and drag data where $C_L = 3.40\alpha$ and $C_D = 1.239 + 0.00249\alpha^2$ and $C_N = C_L \cos\alpha + C_D \sin\alpha$. The results are plotted in Figure 7.42 and are compared to AEDC wind-tunnel data and to ballistic-range data obtained at CARDE[7.32]. The CARDE results fall slightly lower throughout the angle of attack range.

The nonlinear pitching-moment coefficient was calculated by the method described in Section 7.6.4.6 with linear and cubic terms in resultant angle of attack chosen as most representative of the data. (Higher order polynomials were examined but gave nearly identical results.) One flight at low amplitude ($\sigma_m = 1.8^o$) revealed a significant decrease in static stability, which is reflected in the lower initial slope of the Ames pitching-moment curve in Figure 7.43. The curves determined at AEDC and CARDE indicate slightly higher values for the pitching moment. Small differences in boundary-layer conditions or base pressure, as well as measurement inaccuracies, could contribute to the discrepancy.

As shown in Figure 7.39(c), the angular motions of these models were fairly heavily damped. The values obtained for the dynamic-stability parameter for unpowered flight at constant altitude,

$$\xi = C_D - C_{L_\alpha} + \frac{md^2}{I}\,(C_{m_q} + C_{m_{\dot\alpha}}) ,$$

are shown in Figure 7.44(a) while the values for $(C_{m_q} + C_{m_{\dot\alpha}})$ are given in Figure 7.44(b). The wind-tunnel result, from Reference 7.31, shows about 20% less dynamic stability than the free-flight results. The reduced frequencies ($\omega d/V$) for these two sets of tests were different (0.010 and 0.006, respectively) which might have an influence on the data.

It is concluded from these comparisons that ballistic range tests and wind tunnel tests will give closely comparable aerodynamic coefficients when the test conditions are similar, and that most discrepancies which occur can be explained in terms of known effects (e.g., sting interference effects, differences in boundary layer transition point, etc.).

---

* In the aerodynamic coefficients that are presented, the reference area is the cylinder cross-sectional area and the reference length is the cylinder diameter.

7.9.4 Analysis Using Numerical Integration of Equations of Motion

A series of ballistic-range tests of models of the Gemini capsule, conducted in 1962 in the Ames Pressurized Ballistic Range, indicated that both the static moment and the damping moment governing the model oscillations were nonlinear functions of angle of attack[7.34]. Four of these flights were found to be essentially planar and were analyzed simultaneously with the method described in Section 7.8.2 using one-degree-of-freedom simulation given by

$$\alpha'' + (H_0 + H_2\alpha^2)\alpha' + (M_0 + M_2\alpha^2)\alpha = 0 . \tag{7.242}$$

The constants H_0 and H_2 define the nonlinear damping moment, while the constants M_0 and M_2 define the nonlinear static moment. Twelve unknown coefficients were sought; four aerodynamic parameters, and eight initial conditions, two for each flight. The solution converged as follows: $SD(\alpha) = 2.29^o, 1.40^o, 0.88^o, 0.75^o, 0.7426^o, 0.7424^o, 0.7424^o$. The data points for the four flights together with the fit obtained by this method are shown in Figure 7.45. Values of the four coefficients are as follows:

$$H_0 = \frac{-0.0199}{m} , \qquad H_2 = \frac{0.000344}{m\ deg^2} , \qquad M_0 = \frac{0.224}{m^2} , \qquad M_2 = \frac{-0.000404}{m^2\ deg^2} .$$

Several points should be made at this time. The first is that the nonlinear static moment obtained by this analysis of four flights is in good agreement with that obtained using the method described in Section 7.6.4.6. This comparison is shown in Figure 7.46. No comparison with the nonlinear damping moment is possible; however, the value at $\alpha = 0^o$ is in good agreement with results in Reference 7.34.

Another point is that if one looks carefully at the fits to the experimental data shown in Figure 7.45, three of the motions are matched very well, while run 582 is not matched as well. For this run (although small-amplitude and hence small residuals) the fitted motion leads the data points at the early stations, reproduces the data well in the middle of the flight, and lags the data points at the end of the flight. When the analysis was first performed, it was not realized that any intentional difference existed between the models tested in the four flights. However, the model tested in run 582 turned out to have had no "simulated window cutouts", whereas the models for the three other flights did have these simulated windows. As discussed in Reference 7.34, the effect of the window cutouts was relatively minor, but when more than one flight is being analyzed at once as in the present case, minor differences in the aerodynamics can be detected. This kind of effect becomes more and more pronounced with increasing distance flown.

The three remaining runs, where the design model geometry *was* constant, were then analyzed together. As would be expected, the standard deviation in the fit did become better, ($SD(\alpha) = 0.7183^o$) but the improvement was small due to the small amplitude of run 582. The values of the coefficients are now: $H_0 = -0.0180$, $H_2 = 0.000315$, $M_0 = 0.220$, $M_2 = -0.000380$. These coefficients generate moments that differ only slightly from the previous set. The static moment obtained from these coefficients is also shown in Figure 7.46.

7.10 MISCELLANEOUS TOPICS

In this section, two topics will be considered. The first is the study of rolling motions. In particular, reference will be made to cases where a roll torque exists and hence the assumption made previously of a constant roll rate is invalid. It is sometimes of interest to study either roll acceleration due to control deflections, or roll damping. Interest in these properties can be stimulated by practical problems of missiles with fins, or even bodies without fins which sometimes acquire rolling velocity due to small asymmetries.

The other topic is the treatment of density variations along the flightpath. This has been mentioned briefly in Section 7.5.2.2 on drag determination and Section 7.8.2 on numerical integration. The motivation for considering it is the countercurrent ballistic facility (Chapter 5), in which the density encountered by a model is never absolutely constant. Density variations with respect to pitching motions will be emphasized and practical methods of handling them will be indicated.

7.10.1 Determination of Roll Derivatives

The equation for the angular momentum about the $\bar{x}$ axis in terms of Euler angles is given as follows. Using the expression for the kinetic energy given by (7.30) in the Lagrangian equations, one obtains

$$I_{\bar{x}}(\ddot{\psi}_E + \ddot{\theta}_E\cos\sigma - \dot{\theta}_E\dot{\sigma}\sin\sigma) + (I_{\bar{z}} - I_{\bar{y}})[\dot{\theta}_E^2\sin^2\sigma\sin\psi_E\cos\psi_E -$$
$$- \dot{\sigma}^2\sin\psi_E\cos\psi_E + (\dot{\sigma}\dot{\theta}_E\sin\sigma)(\cos^2\psi_E - \sin^2\psi_E)] = Q_{\psi_E} .$$

This applies to a general body. In this section, we are going to consider (near-) axisymmetric bodies, but are going to allow small roll-producing asymmetries, like canted fins. It can still be assumed that $I_{\bar{y}} = I_{\bar{z}}$, and then the above equation reduces to

$$I_{\bar{x}}(\ddot{\psi}_E + \ddot{\theta}_E\cos\sigma - \dot{\theta}_E\dot{\sigma}\sin\sigma) = Q_{\psi_E} = L . \tag{7.243}$$

The moment L is of aerodynamic origin. Retaining the most dominant terms in (7.74), we can write

$$L = \frac{\rho V^2 A l}{2}\left(C_{l_0} + C_{l_p}\frac{pl}{V} + C_{l_\alpha}\bar{\alpha} + C_{l_\beta}\bar{\beta}\right). \tag{7.244}$$

is the static rolling moment; it is normally produced by an asymmetry, like canted fins, deflected fins, etc. C_{l_p} is the damping due to roll, and C_{l_α} and C_{l_β} are changes in the rolling moment with of attack and sideslip.

Equation (7.243), with the moment given by (7.244), is difficult to solve in its present form since it is coupled to the motion in the other degrees of freedom. In practice, however, when rolling moment coefficients are to be determined, the model is rolled at a fairly rapid rate and, hence, the motion about the other axes tends to be small by comparison. It may then be permissible to assume that the terms in (7.243) involving θ_E and σ are small and can be neglected. With this assumption and a similar argument for terms with $\bar{\alpha}$ and $\bar{\beta}$, (7.243) and (7.244) are combined to obtain

$$\ddot{\psi}_E = \frac{\rho V^2 A l}{2 I_{\bar{x}}}\left(C_{l_0} + C_{l_p}\frac{pl}{V}\right) \tag{7.245}$$

For consistency with previous discussions a change will be made to x dependence. Equation (7.245) then becomes (note that $\psi'_E = p$)

$$\psi''_E - \frac{\rho A}{2m}\left(C_D + \frac{ml^2}{I_{\bar{x}}}C_{l_p}\right)\psi'_E = \frac{\rho A l}{2 I_{\bar{x}}}C_{l_0} . \tag{7.246}$$

The solution to this is

$$\psi_E = a_0 + a_1 x + a_2 e^{-a_3 x} , \tag{7.247}$$

where a_0 and a_2 are constants of integration, a_1 is the equilibrium roll rate given by

$$a_1 = \frac{-C_{l_0}}{\left(\frac{I_{\bar{x}}}{ml}C_D + lC_{l_p}\right)} \tag{7.248}$$

and

$$a_3 = -\frac{\rho A}{2m}\left(C_D + \frac{ml^2}{I_{\bar{x}}}C_{l_p}\right) . \tag{7.249}$$

There are several alternatives to the application of these equations to obtain rolling moment coefficients. The most general is to seek a least squares fit of (7.247) to ψ_E versus x data, and hence obtain C_{l_0} and C_{l_p}. Since a_3 appears as an exponent, a least-squares procedure using differential corrections is required (see Appendix). The disadvantage to this approach is that the data must be very accurate or extend over a long distance to yield accurate rolling-moment coefficients. The reason is apparent if one considers an expansion of (7.247) for small values of $a_3 x$; that is

$$\psi_E = (a_0 + a_2) + (a_1 - a_2 a_3)x + \frac{a_2 a_3^2 x^2}{2} - \frac{a_2 a_3^3 x^3}{6} + \ldots \tag{7.250}$$

In order to obtain the four coefficients (a_0 to a_3), terms to order of x^3 must be retained. This means to obtain accurate values of the a's, the data must be accurate to a small term cubed ($a_3^3 x^3$). This is equivalent to being able to determine the third derivative of ψ_E accurately.

If the roll rate changes only a small amount over the instrumented range ($\psi'_E \cong$ constant), the total rolling moment is essentially constant and hence the solution to (7.246) can be written as

$$\psi_E = C_0 + C_1 x + \left[\frac{\rho A l}{2 I_{\bar{x}}}C_{l_0} + \frac{\rho A}{2m}\left(C_D + \frac{ml^2}{I_{\bar{x}}}C_{l_p}\right)p_0\right]\frac{x^2}{2} , \tag{7.251}$$

where p_0 is the average roll rate over the length of the test flight not far different from the initial roll rate C_1. A least-squares curve fit of (7.251) to ψ_E versus x data will yield a value of the total rolling moment (since C_D is known from the drag reduction) but will not permit separation of C_{l_p} and C_{l_0} terms. If two tests are conducted, identical in all respects except roll rate, and they both satisfy the assumption of small roll rate change, then it is possible to separate the two terms.

Under special test conditions we can make one of the coefficients dominant and neglect the other. Near zero roll rate the C_{l_0} term will dominate and the data can be curve fit using (7.251) to determine C_{l_0}. Similarly, for certain model geometries and very accurate model construction, the C_{l_0} term can be made very small and a curve fit using either (7.251), or (7.247) with the $a_1 x$ term dropped, will yield C_{l_p}.

7.10.2 Variable Density

When testing in a counter-current ballistic facility, the possibility exists that the density of the test medium may vary with both time and position within the facility. This makes extraction of the aerodynamic coefficients more difficult. As noted in Section 7.8.2, the integral method can handle this problem quite generally. However, it is useful to consider some of the more traditional techniques that have been applied in the past[7.35,7.36].

Typically, the density encountered by the model changes slowly with distance flown. In most instances, the density can be represented simply by $\rho = \rho_0 - ax$, with a change in density of less than 20% between the first and last data station. Under these circumstances, an effective method of accounting for the density variation is as follows: the data are first analyzed by the constant-density methods already described (using the *average* density over the trajectory) and values of both the aerodynamic coefficients and initial conditions are obtained. These values are then used with the *measured* density variation, in the differential equations of motion. The equations are numerically integrated to generate a motion which roughly approximates the motion obtained experimentally. This generated motion is then analyzed by the constant-density program (again using the average density) and the computed coefficients compared with the input values.

The values of C_D, C_{m_α}, and C_{L_α} obtained by the constant density analysis have been found to show very close agreement with input values, and thus require no adjustment. The computed value of the dynamic stability parameter ξ, however (and hence $(C_{m_q} + C_{m_{\dot\alpha}})$), differs significantly from its input value. It is found by repeating the process of generating a motion, then analyzing it with the constant-density program, for different values of ξ that a simple relationship exists between the actual and calculated values, namely

$$\xi(\text{actual}) - \xi(\text{calculated}) = \text{const.}$$

Thus, the value obtained from analyzing the experimental data can be corrected to obtain the proper value.

Note that the constant in the above equation applies to a *specific* set of data. What the equation means is that the constant-density program, applied to a given set of experimental data where the density varied slowly, introduces a certain error in ξ that is independent of ξ. It is probable that the foregoing approach would be of little use if the density variation encountered were either very large or highly nonlinear.

With an arbitrary density variation, if the successive peak angles of attack are known, the following equations may be applied. It has been shown[7.36] that the envelope of the angle of attack of a coasting body in free flight can be written as

$$\alpha_{env}(x) = \frac{C_0 e^{\frac{1}{2}\int B(x)\,dx}}{[-C_{m_\alpha}(x)\rho(x)V^2(x)/2]^{1/4}} \tag{7.252}$$

where

$$B(x) = \frac{\rho A}{2m} C_D J$$

$$J = \frac{I}{C_D}\left[-C_{L_\alpha} + \frac{ml^2}{I}(C_{m_q} + C_{m_{\dot\alpha}})\right]$$

$$= \left[\frac{\xi}{C_D} - 1\right].$$

Note that C_D has been assumed constant in deriving this equation, but that any of the other aerodynamic coefficients, as well as the density, can be arbitrary functions of distance*.

When both the aerodynamic coefficients and density are constants, (7.252) reduces to (7.142b), namely

$$\alpha_{env}(x) = C_1 e^{(\rho A/4m)\xi x}.$$

When the aerodynamic coefficients are constants, but the density variation is arbitrary, a simple expression can again be obtained for α_{env}. Equation (7.108) is integrated once to give

$$\dot x = \dot x_0 e^{-\int(\rho A/2m)C_D\,dx} = \dot x_0 e^{-(1/J)\int B(x)\,dx}.$$

Then

$$\dot x^{-J/2} = \dot x_0^{-J/2} e^{\frac{1}{2}\int B(x)\,dx}$$

and (7.252) can be written

$$\alpha_{env}(x) = \frac{C_2(\dot x)^{-J/2}}{[\rho(x)V^2(x)/2]^{1/4}} = \frac{C_3(\dot x)^{-\xi/2C_D}}{[\rho(x)]^{1/4}}. \tag{7.253}$$

With peak angles of attack presumed known, together with velocity and density variations, the parameter J can be easily determined from ballistic range data. If the density variation is not extreme, C_D and C_{L_α} can be determined from the constant-density program and hence $(C_{m_q} + C_{m_{\dot\alpha}})$ follows. For more extreme density variations, an approach like that described in Section 7.8 would have to be used to find the components of the parameter J.

---

* Note also that (7.252) is an asymptotic solution, and hence would not be accurate in cases like the first few cycles of motion during atmospheric entry. Pertaining to ballistic ranges, however, it is essentially exact.

7.11 ERROR ANALYSIS*

In closing this chapter, we will undertake to discuss how accurately aerodynamic coefficients can be determined from ballistic range tests[7.37]. This is a difficult question to answer, even partially. In the first place, the problem is statistical in nature. Instead of talking about a coefficient being accurate to within plus or minus some number, statements must be made concerning parameters like the standard deviation in the coefficient. A further concern is that errors that degrade the results can enter from a variety of sources, and some of these are not amenable to analysis. Errors can be introduced by

(i) Incorrect determination of physical characteristics of the model.

(ii) Incorrect determination of test conditions (pressure, temperature, etc.).

(iii) Erroneous time measurements.

(iv) Erroneous measurements of model position or attitude angle on the film.

(v) Incorrect position reference system calibration (Chapter 6).

(vi) Incorrect mathematical model used in analyzing raw data.

These errors can be either random or systematic. The random errors come principally from misreading the film. To consider how random errors affect the deduced aerodynamic coefficients, a simplified approach will be followed and it is assumed that angle-distance data satisfy the equation

$$\alpha = Be^{Dx}\cos(2\pi x/\lambda) \ . \tag{7.254}$$

Note that the constant D is proportional to the dynamic stability parameter ξ and the wavelength λ is proportional to C_{m_α}.

7.11.1 Dynamic-Stability Parameter

An approximate expression for the standard deviation in the dynamic-stability parameter can be derived as follows. The sum of the squares of the angle residuals (SSR) is defined by

$$SSR = \sum_i (\alpha_i - \alpha_{exp_i})^2 \ ,$$

where α_i is the value of α calculated from (7.254) at point x_i, and α_{exp_i} is the experimental value of α at this point. Differentiating this equation with respect to D and setting the result equal to zero gives

$$\frac{\partial(SSR)}{\partial D} = 2\sum_i (\alpha_i - \alpha_{exp_i})\frac{\partial \alpha_i}{\partial D} = 0 \ . \tag{7.255}$$

Assume B and λ are known exactly and that α_{exp_i} is given by

$$\alpha_{exp_i} = B_E e^{D_E x_i}\cos(2\pi x_i/\lambda_E) + \Delta\alpha_i \ , \tag{7.256}$$

where the subscript E denotes exact values and $\Delta\alpha_i$ is the experimental error in α at x_i. Now let $D = D_E + \Delta D$, substitute (7.254) and (7.256) into (7.255), expand the exponentials involving ΔD retaining only linear error terms, and solve for ΔD. This gives

$$\Delta D = \frac{B_E \sum_i \Delta\alpha_i x_i e^{D_E x_i}\cos(2\pi x_i/\lambda_E)}{B_E^2 \sum_i x_i^2 e^{2D_E x_i}\cos^2(2\pi x_i/\lambda_E)} \ .$$

The variance of D, which is the same as the variance of ΔD, can now be obtained.

$$VAR(D) = \frac{VAR(\alpha)}{B_E^2 \sum_i x_i^2 e^{2D_E x_i}\cos^2(2\pi x_i/\lambda_E)} \ .$$

Now expand the exponential retaining terms linear in x, assume that the data points are close enough together to allow replacing the summation by an integration, and neglect all oscillatory terms after integrating. The result is

$$VAR(D) = \frac{6\ VAR(\alpha)}{B^2\lambda^2 N^3 n\,(1 + 3\lambda DN/2)} \ ,$$

---

* As a supplement to this section, the Appendix (Section 7.12) shows how a differential correction procedure can be used in estimating errors in the deduced coefficients.

where N is the number of cycles of motion being analyzed, and n is the number of data points per cycle. We want the standard deviation in the dynamic-stability parameter ξ. Since $\xi = 2D/K$ (Equation (7.139)) where $K = \rho A/2m$, the variance of ξ can be related to that of D as follows:

$$\text{VAR}(\xi) = \frac{4}{K^2}\,\text{VAR}(D) + \frac{4D^2}{K^4}\,\text{VAR}(K) .$$

The standard deviation is the square root of the variance, and the final result is

$$\text{SD}(\xi) = \sqrt{\left\{\frac{24\,[\text{SD}(\alpha)]^2}{B^2K^2\lambda^2N^3n\,(1 + 3K\lambda\xi N/4)} + \frac{\xi^2[\text{SD}(K)]^2}{K^2}\right\}} . \tag{7.257}$$

A number of approximations have been introduced in deriving this expression. Nevertheless, the expression yields results that are in very good agreement with results from a Monte Carlo analysis. This is shown in Figure 7.47, where the standard deviation in ξ is plotted versus the number of cycles of motion being analyzed (N) for a variety of number of data points per cycle (n). Each data point represents the results of analyzing 20 cases having random errors in the angle data (using the tricyclic method of analysis, Section 7.6.3). It is noted that $\text{SD}(\xi)$ increases rapidly below $N = 1\frac{1}{2}$ as would be expected, due to the difficulty in being able to differentiate between damping and trim angle. Results from (7.257) are shown for two values of n.

7.11.2 Static-Stability Parameter

A similar derivation for the standard deviation in the static-stability parameter C_{m_α} assuming that B and D in (7.254) are known exactly yields

$$\frac{\text{SD}(C_{m_\alpha})}{C_{m_\alpha}} = \sqrt{\left\{\frac{6\,[\text{SD}(\alpha)]^2}{\pi^2B^2N^3n\,(1 + 3K\lambda\xi N/4)} + \frac{[\text{SD}(K_1)]^2}{K_1^2}\right\}} , \tag{7.258}$$

where $K_1 = 2I/\rho Al$. This equation has also been investigated by analyzing many cases containing random errors. The results showed (7.258) to be valid and indicated similar trends to those shown in Figure 7.47, but the induced errors were exceedingly small (always less than 1%). An accurate measure of C_{m_α} is far easier to achieve than an accurate measure of ξ.

7.11.3 Lift-Curve Slope

The swerving deviations from straight-line flight are used to deduce the lift-curve slope. By treating the equation (simplified version of Equation (7.216))

$$z = z_0 + z_0'x - KC_{L_\alpha}\int_0^x\int_0^x Be^{Dx}\cos(2\pi x/\lambda)\,dx\,dx$$

in a similar manner as was done in the discussion of the dynamic stability parameter (presuming now that all constants except C_{L_α} are known exactly), the following equation for the standard deviation in the lift-curve slope is obtained:

$$\text{SD}(C_{L_\alpha}) = \sqrt{\left\{\frac{16\pi^4\,[\text{SD}(z)]^2}{K^2B^2\lambda^4(T_s + 1)} + \frac{2C_{L_\alpha}^2\,[\text{SD}(\alpha)]^2}{B^2(T_s + 1)} + \frac{C_{L_\alpha}^2[\text{SD}(K)]^2}{K^2}\right\}} .$$

Here T_s is the total number of observation stations. The results of this equation have also been confirmed by a Monte Carlo analysis.

7.11.4 Drag Coefficient

The time-distance equation which determines the drag coefficient is (Equation (7.110))

$$t = t_0 + \frac{1}{V_0KC_D}\left(e^{KC_Dx} - 1\right) .$$

To obtain the standard deviation in C_D, the exponential is expanded and terms to order x^2 are retained. Again the derivation is similar to that for $\text{SD}(\xi)$, except here all three unknowns (C_D, V_0, t_0) are allowed to contain errors, so the resulting expression is more accurate than those previously given. The result is

$$\text{SD}(C_D) = \sqrt{\left\{\frac{720(T_s - 3)!\,\{V_0^2[\text{SD}(t)]^2 + [\text{SD}(x)]^2\}}{K^2\Delta x^4\,(T_s + 2)!} + \frac{C_D^2[\text{SD}(K)]^2}{K^2}\right\}} . \tag{7.259}$$

Here Δx is the distance between data stations, assumed constant.

Some insight can be gained by considering a specific example.

T_s = 11 stations SD(x) = 0.000114 m

Δx = 1.22 m SD(t) = 0.02 μsec

K = 0.00041/m $V_0 \cdot SD(t)$ = 0.000122 m

C_D = 1.0 SD(K) = 0 .

V_0 = 6100 m/sec

Substituting these numbers into (7.259) leads to $SD(C_D) = 0.0187$. Twenty cases were generated using a uniform error distribution with standard deviations as listed. These cases were analyzed by Method 5 described in Section 7.5.1 and from these 20 cases, $SD(C_D) = 0.0198$, very close to 0.0187. The results for these cases, in order of increasing drag coefficient, follow.

C_D	$\Sigma(\Delta t)^2$ (sec^2)
0.953	0.58×10^{-14}
0.977	0.44
0.983	0.78
0.983	0.22
0.989	1.45
0.991	0.46
0.996	0.34
0.997	0.71
0.997	0.42
0.999	0.43
1.004	0.42
1.004	0.42
1.007	0.75
1.010	0.26
1.013	0.51
1.014	0.52
1.015	0.64
1.015	0.46
1.016	0.69
1.055	0.32×10^{-14}
Avg. 1.001 .	

Also listed is the sum of the squares of the residuals for each case (ascribing all the error to time, none to distance). In about half of the cases, the calculated drag coefficient is within 1% of the actual value. There are two cases, however, where the calculated drag coefficient is off by a significant amount, about 5%. Note that the sum of the squares of the residuals for these two cases would not indicate that bad answers had been obtained. It is cases like these that prove perplexing when real data are being analyzed. Re-reading the position data on the film would probably improve the answers, but nothing can be done to get different time measurements.

7.11.5 Facility Calibration

It is obvious that poor position and angle calibrations of a ballistic facility can introduce errors in deduced aerodynamic coefficients. Furthermore, these errors are more likely systematic than random, which is a worse situation. What is interesting to point out here is how the facility calibration can be monitored in the process of determining aerodynamic coefficients.

Every run analyzed yields, among other things, differences between measured and calculated values at every data station. The drag routine gives time residuals (or equivalent $\Delta x = V\Delta t$ residuals), the stability routine gives angle residuals, and the lift routine gives y and z residuals. If these residuals are saved, station by station, from every run analyzed until there are enough of them to be statistically meaningful, then errors (or changes) in the facility calibration can be detected. If the errors at each station are random, the residuals should scatter about zero. If they scatter about a non-zero value, in all likelihood there is a calibration error. From the error indicated, a correction can be made. This analysis is most meaningful if done for a number of tests of a single configuration at given test conditions, since the variation in film reading accuracy between different configurations and free stream conditions would be eliminated.

Figure 7.48 shows the y residuals versus station number from 32 tests of sphere-cone models conducted in the Ames Hypervelocity Free-Flight Aerodynamic Facility. It is obvious that at some stations the scatter is not symmetrical about zero. The fact that the amount of the scatter is about the same at every station indicates that this is probably the reading accuracy, in this case $SD(y) \approx 0.015$ cm . If the amount of scatter differed from station to station (stations assumed identical), it could be an indication that the equations used to analyze the motion were not sufficiently complete.

7.12 APPENDIX

7.12.1 Method of Least Squares Using Differential Corrections

The problem can be stated as follows: given a set of experimental data and the function relating the dependent and independent variables, find the unknown coefficients in the function such that a "best fit" to the experimental data is obtained. The method of least squares determines a best fit on the basis of minimizing the sum of the squares of the residuals (differences between experimental and calculated values).

The function can be written as

$$y = f(x; C_1, C_2, \ldots, C_r) , \tag{7.260}$$

where the C's are the unknown coefficients*. The sum of the squares of the residuals is then

$$SSR = \sum_{i=1}^{n} [y_{exp_i} - f(x_i; C_1, C_2, \ldots C_r)]^2 , \tag{7.261}$$

where n is the number of data points. Note that the errors have all been assumed to be in the dependent variable y. The minimization is achieved by taking the partial derivative of SSR with respect to each coefficient. These expressions are equated to zero, summed over all data points, and the resulting equations are solved simultaneously for the C's. This is straightforward if all the C's in the function, f, appear in a linear manner. A simple example is the case where f is a polynomial. Consider the three-term polynomial $y = C_1x^2 + C_2x + C_3$. The unknowns are obtained by solving the following three equations:

$$\begin{bmatrix} \sum_{i=1}^{n} x_i^4 & \sum x_i^3 & \sum x_i^2 \\ \sum x_i^3 & \sum x_i^2 & \sum x_i \\ \sum x_i^2 & \sum x_i & n \end{bmatrix} \begin{bmatrix} C_1 \\ C_2 \\ C_3 \end{bmatrix} = \begin{bmatrix} \sum_{i=1}^{n} x_i^2 y_i \\ \sum x_i y_i \\ \sum y_i \end{bmatrix} . \tag{7.262}$$

In many cases of practical interest, however, the coefficients appear in a nonlinear or transcendental manner. For these cases the straightforward approach does not work, but a technique employing what are commonly called differential corrections can be used instead. First an approximation to each coefficient must be available. The function f can then be expanded in a Taylor series about this approximate solution.

$$f(x; C_1, C_2, \ldots C_r) = f^0(x; C_1^0, C_2^0, \ldots C_r^0) + \sum_{j=1}^{r} \frac{\partial f^0}{\partial C_j} \Delta C_j .$$

The zero superscript refers to the approximate solution, and $\Delta C_j = C_j - C_j^0$. Substituting this into (7.261) yields

$$SSR = \sum_{i=1}^{n} \left[y_{exp_i} - f^0(x_i; C_1^0 \ldots C_r^0) - \sum_{j=1}^{r} \frac{\partial f_i^0}{\partial C_j} \Delta C_j \right]^2 . \tag{7.263}$$

Note that the ΔC_j's appear in a linear manner and the minimization of SSR with respect to them is straightforward. The partial derivative of SSR with respect to ΔC_k is

$$\frac{\partial (SSR)}{\partial \Delta C_k} = 2 \sum_{i=1}^{n} \left\{ \left[y_{exp_i} - f^0(x_i; C_1^0 \ldots C_r^0) - \sum_{j=1}^{r} \frac{\partial f_i^0}{\partial C_j} \Delta C_j \right] \frac{\partial f_i^0}{\partial C_k} \right\} = 0 . \tag{7.264}$$

In matrix form, then, we have

$$\underset{r \times r}{[A]} \; \underset{r \times 1}{[\Delta C]} = \underset{r \times 1}{[R]} , \tag{7.265}$$

where $[A]$ is a square matrix with elements

$$A_{jk} = A_{kj} = \sum_{i=1}^{n} \frac{\partial f_i^0}{\partial C_j} \frac{\partial f_i^0}{\partial C_k} , \tag{7.266}$$

---

* Note that some of the C's might represent initial conditions and not appear explicitly in f; for example, if $y = \int_0^x \int_0^w g(w)\, dw dw$, then $y(0)$ and $y'(0)$ would also be unknowns.

ΔC is a column vector containing the corrections to the coefficients

$$\Delta C \simeq \begin{bmatrix} \Delta C_1 \\ \Delta C_2 \\ \vdots \\ \Delta C_r \end{bmatrix} \tag{7.267}$$

and R is a column vector of the residuals

$$R = \begin{bmatrix} \sum_{i=1}^{n} (y_{exp_i} - f_i^0) \dfrac{\partial f_i^0}{\partial C_1} \\ \vdots \\ \sum_{i=1}^{n} (y_{exp_i} - f_i^0) \dfrac{\partial f_i^0}{\partial C_r} \end{bmatrix} . \tag{7.268}$$

Note that normally the partial derivatives that appear in the A and R matrices have closed form expressions and are hence easy to evaluate. A case was presented in Section 7.8.2, however, where numerical techniques were needed to obtain the partial derivatives.

Equation (7.265) may be solved by hand for simple cases or on a computer for complicated cases. Symbolically, the result is

$$\Delta C = [A]^{-1} R , \tag{7.269}$$

where $[A]^{-1}$ is the inverse of $[A]$. New values of the coefficients are obtained by adding ΔC_j to the present value.

$$C_j = C_j^0 + \Delta C_j . \tag{7.270}$$

This new solution can now be considered as an approximate solution and the entire process repeated to obtain a better solution*. This process continues until changes in the coefficients, ΔC_j, approach zero or in practice some small value. It is often easier to monitor the convergence process by computing the SSR for each iteration and when it stops changing within some prescribed limit, the solution is considered converged. When this point is reached, the best least squares set of coefficients has been obtained.

An additional benefit of a differential correction process of this type is the simplicity with which the accuracy of the various coefficients can be determined. It can be shown that after convergence, the elements of the $[A]^{-1}$ matrix are related to the variance (VAR) and covariance (COV) of the coefficients as follows:

$$\left.\begin{aligned} VAR(C_i) &= A_{ii}^{-1} \cdot VAR(y) \\ SD(C_i) &= [VAR(C_i)]^{\frac{1}{2}} \\ COV(C_i, C_j) &= A_{ij}^{-1} \cdot VAR(y) \qquad i \neq j . \end{aligned}\right\} \tag{7.271}$$

Here A_{ij}^{-1} denotes the ij^{th} element of the $[A]^{-1}$ matrix. Thus if one can estimate the accuracy of the measured quantity y, the accuracy of the coefficients can be obtained. Note that the standard deviation of the least squares fit to the experimental data ($SD = \sqrt{(SSR/n)}$) is normally better than the true measuring accuracy.

If the parameters of interest are related to the coefficients (C_i) by a routine relationship, the following equations can be used in conjunction with (7.271) to find the accuracy in these parameters. Let a and b be constants.

$$VAR(aC_1) = a^2 VAR(C_1)$$

$$VAR(aC_1 \pm bC_2) = a^2 VAR(C_1) + b^2 VAR(C_2) \pm 2ab\, COV(C_1, C_2)$$

$$VAR(aC_1^2) \approx a^2 [4C_1^2 VAR(C_1) + 2\, VAR^2(C_1)]$$

$$VAR(aC_1C_2) \approx a^2 [C_2^2 VAR(C_1) + C_1^2 VAR(C_2) + 2C_1C_2\, COV(C_1, C_2) + VAR(C_1)\, VAR(C_2) + COV^2(C_1, C_2)]$$

$$VAR\left(\frac{aC_1}{C_2}\right) \approx \frac{a^2}{C_2^2}\left[VAR(C_1) + \frac{C_1^2}{C_2^2} VAR(C_2) - \frac{2C_1}{C_2} COV(C_1, C_2)\right]$$

$$VAR(e^{aC_1}) \approx a^2 e^{2aC_1} [VAR(C_1) + \tfrac{3}{2}a^2 VAR^2(C_1) + \tfrac{7}{6}a^4 VAR^3(C_1) + \ldots\ldots] .$$

The two equations involving $VAR(aC_1^2)$ and $VAR(aC_1C_2)$ are exact if C_1 and C_2 are normally-distributed random variables.

* There is no guarantee that this iteration procedure will not diverge. However, with reasonable initial estimates of the coefficients, convergence is normally obtained.

REFERENCES

7.1	Lanchester, F.W.	*Aerial Flight*. Vol.1 – Aerodynamics; Vol.2 – Aerodonetics. Constable & Co. Ltd, London, England, 1907 and 1910.
7.2	Fowler, R.H. Gallop, E.G. Lock, C.N.H. Richmond, H.W.	*The Aerodynamics of a Spinning Shell*. Phil. Trans. Roy. Soc., London, 1920.
7.3	Fowler, R.H. Lock, C.N.H.	*The Aerodynamics of a Spinning Shell, Part II*. Phil. Trans. Roy. Soc., Vol.222, London, March 15, 1922, pp.227-247.
7.4	Bolz, R.E. Nicolaides, J.D.	*A Method of Determining Some Aerodynamic Coefficients from Supersonic Free-Flight Tests of a Rolling Missile*. J. Aeron. Sci., Vol.17, No.10, October 1950. (Also BRL No.711, 1949.)
7.5	Nicolaides, J.D.	*On the Free-Flight Motion of Missiles Having Slight Configurational Asymmetries*. Report 858, BRL, 1953.
7.6	Charters, A.C.	*The Linearized Equations of Motion Underlying the Dynamic Stability of Aircraft, Spinning Projectiles, and Symmetrical Missiles*. NACA TN 3350, 1955.
7.7.	Murphy, C.H.	*The Effect of Strongly Nonlinear Static Moment on the Combined Pitching and Yawing Motion of a Symmetric Missile*. Report No.1114, BRL, 1960.
7.8	Rasmussen, M.L. Kirk, D.B.	*On the Pitching and Yawing Motion of a Spinning Symmetric Missile Governed by an Arbitrary Nonlinear Restoring Moment*. NASA TN D-2135, 1964.
7.9	Murphy, C.H.	*Free Flight Motion of Symmetric Missiles*. Report 1216, BRL, 1963.
7.10	Timoshenko, S. Young, D.H.	*Advanced Dynamics*. McGraw-Hill, New York, 1948.
7.11	Curry, W.H. (Sandia Corp.) Uselton, J.C. (AEDC)	*Some Comments on the Aerodynamic Characteristics of the Tomahawk Sounding Rocket*. A Volume of Technical Papers Presented at AIAA Sounding Rocket Vehicle Technology Specialist Conference, Williamsburg, Va., 1967.
7.12	Maple, C.G. Synge, J.L.	*Aerodynamic Symmetry of Projectiles*. Quarterly of Appl. Math., Vol.VI, No.4, January 1949.
7.13	Seiff, A.	*A New Method for Computing Drag Coefficients from Ballistic-Range Data*. J. Aero. Sci., Vol.25, No.2, February 1958, pp.133-134.
7.14	Seiff, A. Wilkins, M.E.	*Experimental Investigation of a Hypersonic Glider Configuration at a Mach Number of 6 and at Full-Scale Reynolds Numbers*. NASA TN D-341, 1961.
7.15	Terry, J.E. Miller, R.J.	*Aerodynamic Characteristics of a Truncated-Cone Lifting Reentry Body at Mach Numbers from 10 to 21*. NASA TM X-786, 1963.
7.16	Kelley, J.L. McShane, E.J.	*On the Motion of a Projectile with Small or Slowly Changing Yaw*. BRL Report No.446, 1944.
7.17	Shinbrot, M.	*A Least Squares Curve Fitting Method with Applications to the Calculation of Stability Coefficients from Transient Response Data*. NACA TN-2341, 1951.
7.18	Kirk, D.B. Miller, R.J.	*Free-Flight Tests of Fifth-Stage Scout Entry Vehicle at Mach Numbers of 5 and 17*. NASA TN D-1425, 1962.
7.19	Canning, T.N.	*A Simple Mechanical Analogue for Studying the Dynamic Stability of Aircraft Having Nonlinear Moment Characteristics*. NACA TN 3125, 1954.
7.20	Kryloff, N. Bogoliuboff, N.	*Introduction to Nonlinear Mechanics*. Princeton University Press, 1947.
7.21	Kirk, D.B.	*A Method for Obtaining the Nonlinear Aerodynamic Stability Characteristics of Bodies of Revolution from Free-Flight Tests*. NASA TN D-780, 1961.
7.22	Rasmussen, M.L. Kirk, D.B.	*A Study of Damping in Nonlinear Oscillations*. NASA TR R-249, 1966.
7.23	Murphy, C.H.	*On the Quasi-Linear Substitution Method for Missile Motion Caused by a Strongly Nonlinear Static Moment*. BRL Memo No.1466, April 1963.

7.24 Tobak, M.
Pearson, W.
A Study of Nonlinear Longitudinal Dynamic Stability. NASA TR R-209, 1964.

7.25 Boissevain, A.G.
Intrieri, P.F.
Determination of Stability Derivatives from Ballistic Range Tests of Rolling Aircraft Models. NASA TM X-399, 1961.

7.26 Chapman, G.T.
Kirk, D.B.
A New Method For Extracting Aerodynamic Coefficients from Free-Flight Data. AIAA Paper 69-134, January 1969.

7.27 Bellman, R.
Kagiwada, H.
Kalaba, R.
Quasilinearization, System Identification, and Prediction. RAND Corporation RM-3812-PR, August 1963.

7.28 Goodman, T.R.
System Identification and Prediction – An Algorithm Using a Newtonian Iteration Procedure. Quarterly of Applied Mathematics, Vol.XXIV, No.3, October 1966, pp.249-255.

7.29 Malcolm, G.N.
Chapman, G.T.
A Computer Program for Systematically Analyzing Free-Flight Data to Determine the Aerodynamics of Axisymmetric Bodies. NASA TN D-4766, 1968.

7.30 Gray, J.D.
Lindsay, E.E.
Force Tests of Standard Hypervelocity Ballistic Models HB-1 and HB-2 at Mach 1.5 to 10. AEDC-TCDR-63-137, August 1963.

7.31 Gray, J.D.
Summary Report on Aerodynamic Characteristics of Standard Models HB-1 and HB-2. AEDC-TDR-64-137, July 1964.

7.32 Conn, H.
Ballistic Range Measurements of the Cubic Normal Force and Pitching Moment of a Nonrolling Symmetric Missile. CARDE TR 569/67, January 1967.

7.33 Hruby, R.J.
McDevitt, J.B.
Coon, G.W.
Harrison, D.R.
Kemp, J.H. Jr
FM Telemetry and Free-Flight Techniques for Aerodynamic Measurements in Conventional Wind Tunnels. NASA TN D-3319, 1966.

7.34 Kruse, R.L.
Malcolm, G.N.
Short, B.J.
Comparison of Free-Flight Measurements of Stability of the Gemini and Mercury Entry Capsules at Mach Numbers 3 and 9.5. NASA TM X-957, 1964.

7.35 Intrieri, P.F.
Experimental Stability and Drag of a Pointed and a Blunted 30° Half-Angle Cone at Mach Numbers from 11.5 to 34 in Air. NASA TN D-3193, 1966.

7.36 Sommer, S.C.
Tobak, M.
Study of the Oscillatory Motion of Manned Vehicles Entering the Earth's Atmosphere. NASA Memo 3-2-59A, 1959.

7.37 Chapman, G.T.
Kirk, D.B.
Obtaining Accurate Aerodynamic Force and Moment Results from Ballistic Tests. AGARD Conference Proceedings No.10, The Fluid Dynamic Aspects of Ballistics, September 1966, pp.381-401.

BIBLIOGRAPHY

Boissevain, A.G.
Experimental Investigation of the Damping in Roll of Cruciform Triangular Wing-Body Combinations at Mach Numbers from 1.5 to 6. NACA RM A54B15a, 1954.

Bolz, R.E.
Dynamic Stability of a Missile in Rolling Flight. J. Aeron. Sci., Vol.19, No.6, June 1952.

Canning, T.N.
DeRose, C.E.
Drag and Rolling Moment Effectiveness of Trailing-Edge Spoilers at Mach Number 2.2 and 5. NACA RM A55F15, 1955.

Coakley, T.J.
Laitone, E.V.
Maas, W.L.
Fundamental Analysis of Various Dynamic Stability Problems for Missiles. University of California, Inst. of Eng. Res. Series 176, Issue 1, June 1961.

Cranz, C.
Lehrbuch der Ballistik. Springer, Berlin, 1926.

Durand, W.F.
Aerodynamic Theory, Vol.V. Durand Reprinting Committee, CIT, 1943.

Friedrich, H.R.
Dore, F.J.
The Dynamic Motion of a Missile Descending Through the Atmosphere. J. Aeron. Sci., Vol.22, No.9, September 1955, pp.628-632, 638.

Jaffe, P. — *Obtaining Free-Flight Dynamic Damping of an Axially Symmetric Body (at All Angles-of-Attack) in a Conventional Wind Tunnel.* JPL Tech. Report 32-544, 1964.

Karpov, B.G. — *The Accuracy of Drag Measurements as a Function of and Distribution of Timing Stations.* BRL Report No.658, February 1948.

Kent, R.H. — *An Elementary Treatment of the Motion of a Spinning Projectile About Its Center of Gravity.* BRL Report No.85, 1937. (Revision by Kent and McShane, BRL Report No.459, 1944.)

Kopal, Z.
Kavanagh, K.E.
Rodier, N.K. — *A Manual of Reduction of Spinner Rocket Shadowgrams.* Technical Report No.4, M.I.T., 1949.

Malcolm, G.N. — *Stability and Drag Characteristics at Mach Numbers of 10 and 26 of a Proposed Slender Atmospheric Probe.* NASA TN D-3917, 1967.

McShane, E.J.
Kelley, J.L.
Reno, F.V. — *Exterior Ballistics.* The University of Denver Press, 1953.

Moulton, F.R. — *New Methods in Exterior Ballistics.* University of Chicago, 1926.

Murphy, C.H. — *Analogue Computer Determination of Certain Aerodynamic Coefficients.* BRL Report No.807, 1952.

Murphy, C.H. — *The Measurement of Non-Linear Forces and Moments by Means of Free-Flight Tests.* BRL Report 974, 1956.

Murphy, C.H. — *On Stability Criteria of the Kelley-McShane Linearized Theory of Motion.* BRL Report No.853, 1953.

Murphy, C.H.
Hodes, B.A. — *Planar Limit Motion of Nonspinning Symmetric Missiles Acted on by Cubic Aerodynamic Moments.* BRL Memo Report 1358, June 1961.

Nicolaides, J.D. — *Variation of the Aerodynamic Force and Moment Coefficients with Reference Position.* BRL Technical Note No.746, 1952.

Nicolaides, J.D.
Bolz, R.E. — *On the Pure Rolling Motion of Winged and/or Finned Missiles in Varying Supersonic Flights.* J. Aeron. Sci., Vol.20, No.3, March 1953, pp.160-168. (Also BRL Report No.799, 1952.)

Nielsen, K.L.
Synge, J.L. — *On the Motion of a Spinning Shell.* Quarterly of Appl. Math., Vol.4, No.3, October 1946.

Perkins, C.D.
Hage, R.E. — *Airplane Performance Stability and Control.* Wiley, New York, 1949.

Phillips, W.H. — *Effect of Steady Rolling on Longitudinal and Directional Stability.* NACA TN 1627, 1948.

Rankin, R.A. — *The Mathematical Theory of the Motion of Rotated and Unrotated Rockets.* Phil. Trans. of the Royal Soc., London, Series A, Vol.241, No.837, March 23, 1949, pp.457-485.

Rasmussen, M.L. — *Determination of Nonlinear Pitching-Moment Characteristics of Axially Symmetric Models from Free-Flight Data.* NASA TN D-144, 1960.

Redd, B.
Olsen, D.M.
Barton, R.L. — *Relationship Between the Aerodynamic Damping Derivatives Measured as a Function of Instantaneous Angular Displacement and the Aerodynamic Damping Derivatives Measured as a Function of Oscillation Amplitude.* NASA TN D-2855, 1965.

Rosser, J.B.
Newton, R.R.
Gross, G.L. — *Mathematical Theory of Rocket Flight.* McGraw-Hill, New York, 1947.

Schmidt, L.E.
Murphy, C.H. — *Effect of Spin on Aerodynamic Properties of Bodies of Revolution.* BRL Memo No.715, August 1953.

Smith, R.A. — *A Simple Non-Linear Oscillation.* J. London Math. Soc., Vol.36, 1961, pp.33-34.

Turetsky, R. — *Reduction of Spark Range Data.* BRL Report No.684, 1948.

Webster, A.G. — *The Dynamics of Particles and of Rigid, Elastic, and Fluid Bodies.* Stechert-Hafner, New York, 1920 (B.G.Teubner, Leipzig, 1904).

Whittaker, E.T. — *A Treatise on the Analytical Dynamics of Particles and Rigid Bodies.* 4th edition. Dover, New York, 1944.

Zaroodny, S.J. *On Jump Due to Muzzle Disturbances.* BRL Report No.703, 1949.

Zaroodny, S.J. *On the Mechanism of Dispersion and Short Ranges of Mortar Fire.* BRL Report No.668, 1948.

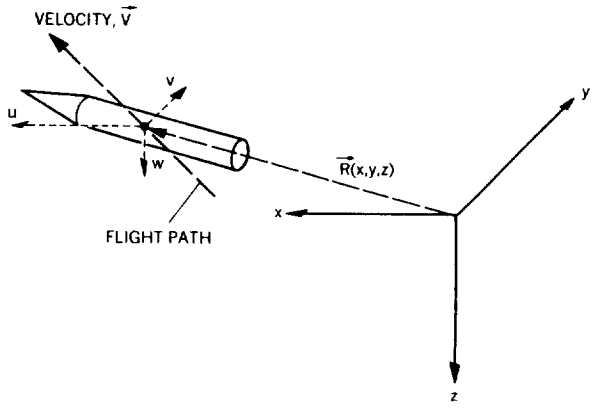

Fig. 7.1 Earth-fixed axes

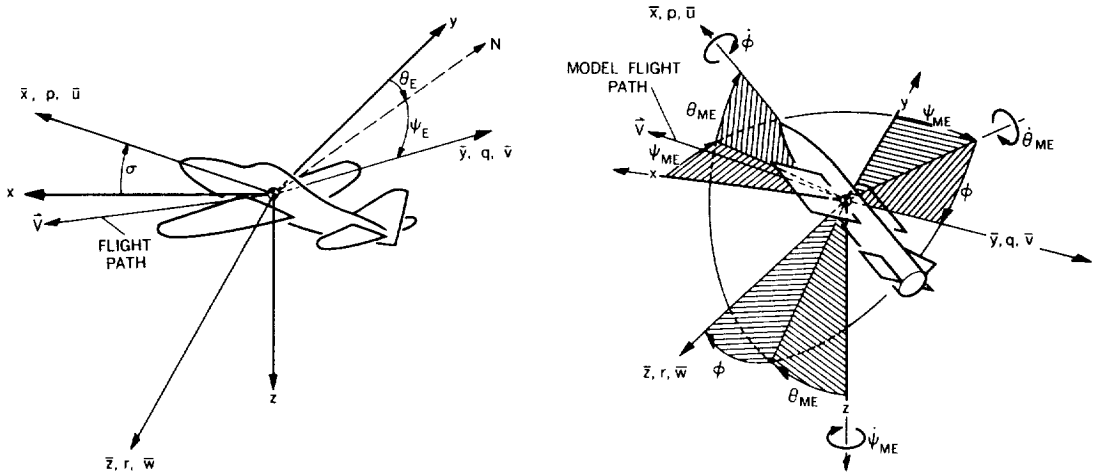

(a) Euler angles (b) Modified Euler angles

Fig. 7.2 Body-fixed axes

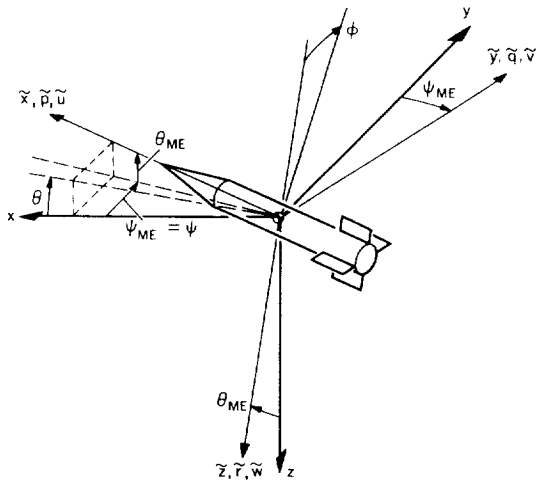

Fig. 7.3 Model-oriented fixed-plane axes

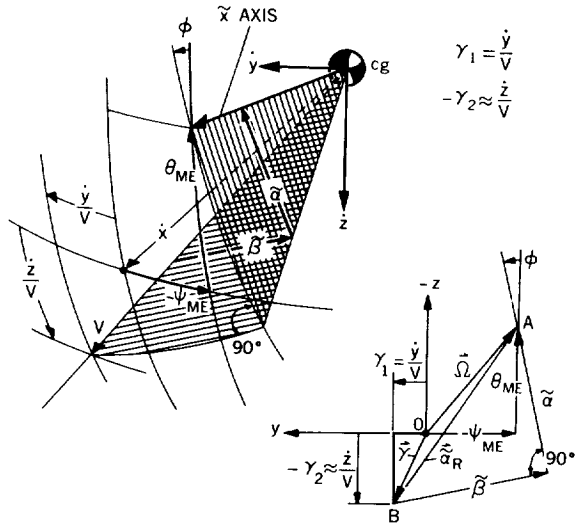

Fig. 7.4 Angular relationships between model axes and flight direction

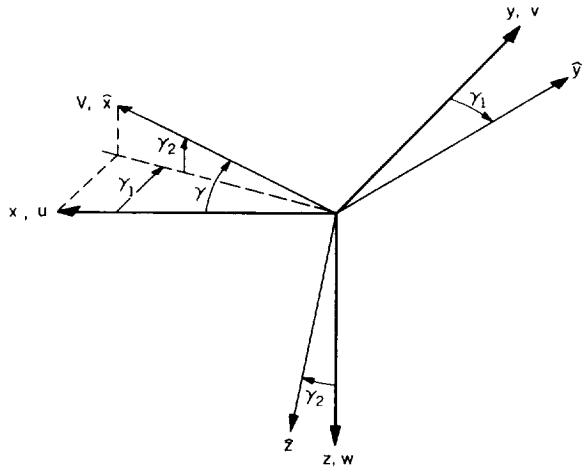

Fig. 7.5 Trajectory axes

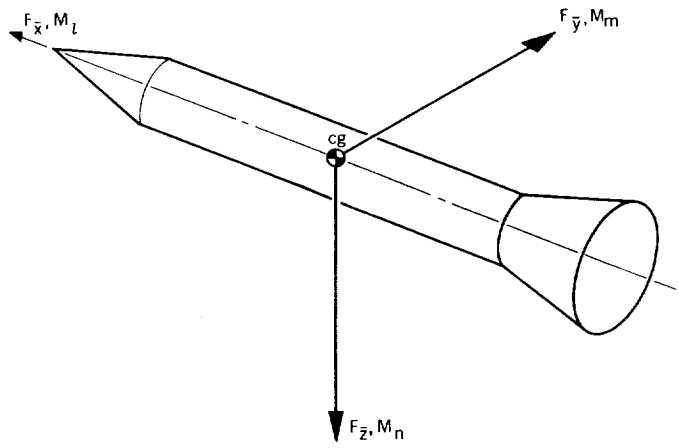

Fig. 7.6 Aerodynamic forces and moments

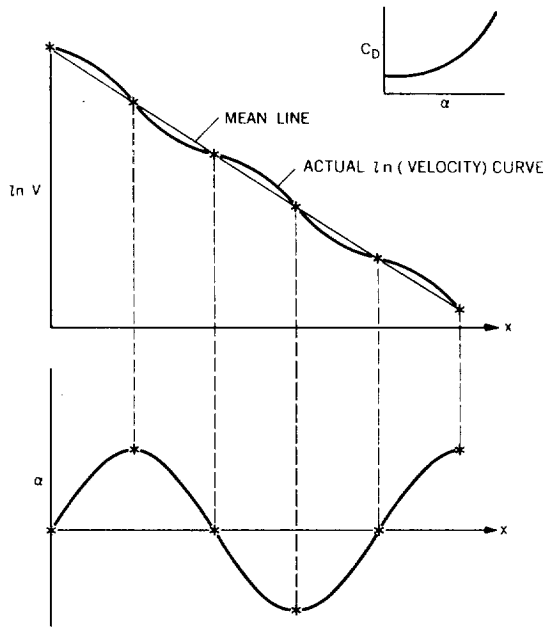

Fig. 7.7 Variation of $\log_e V$ and angle of attack with flight distance

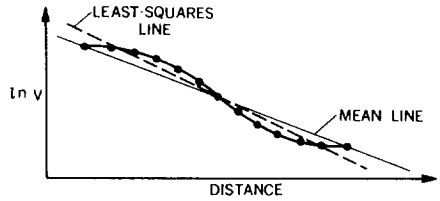

Fig. 7.8 Mean line relative to least-squares line

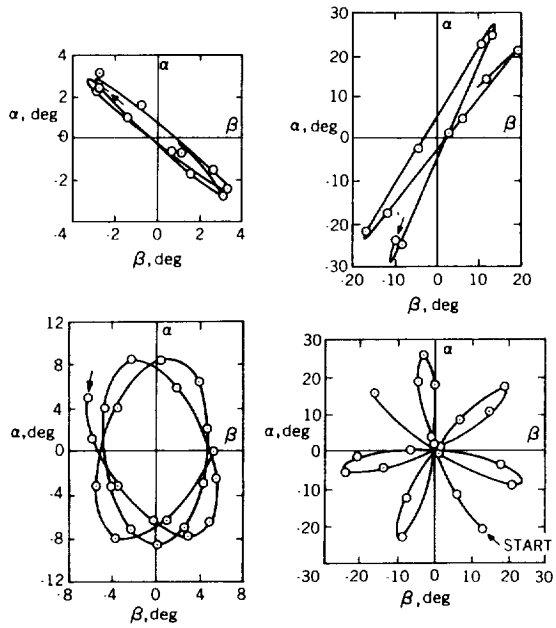

Fig. 7.9 Typical angular motions

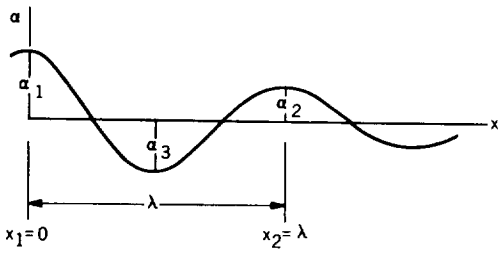

Fig.7.10 Angle variation with distance

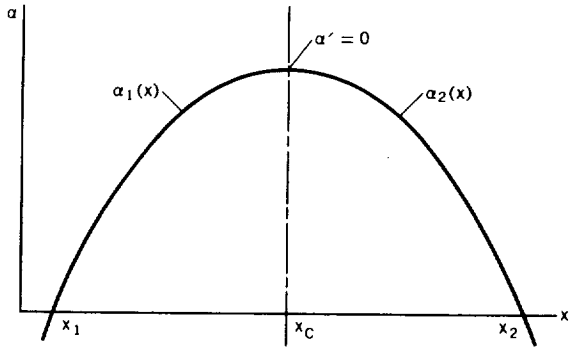

Fig.7.11 Sketch of peak

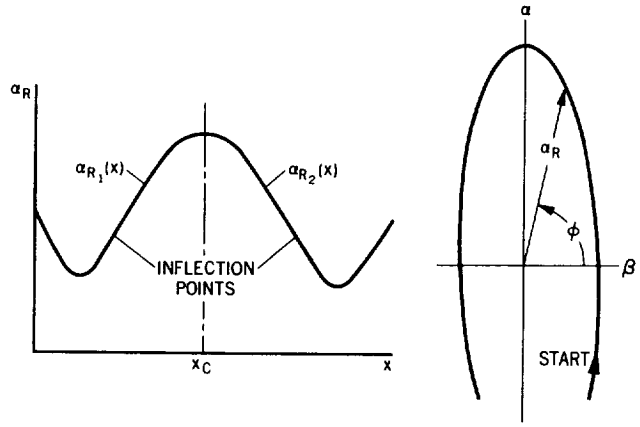

Fig.7.12 Sketch of resultant angle peak for a nonplanar motion

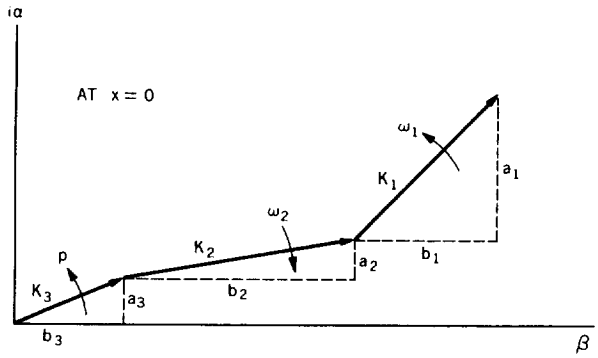

Fig.7.13 Three rotating vectors

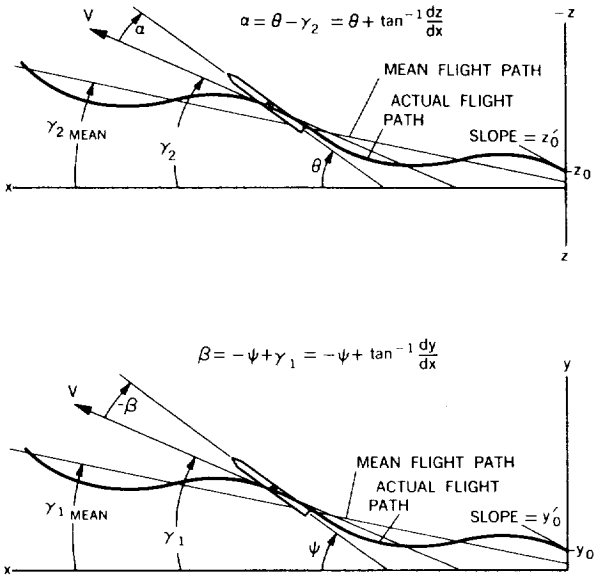

Fig. 7.14 Swerve corrections to measured angles

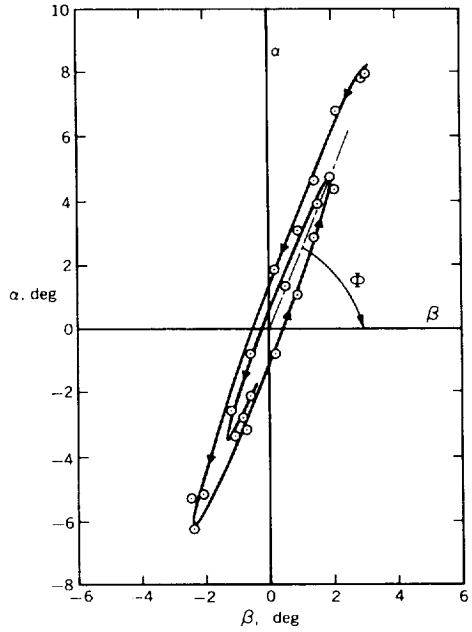

Fig. 7.15 Rotation of coordinate axes

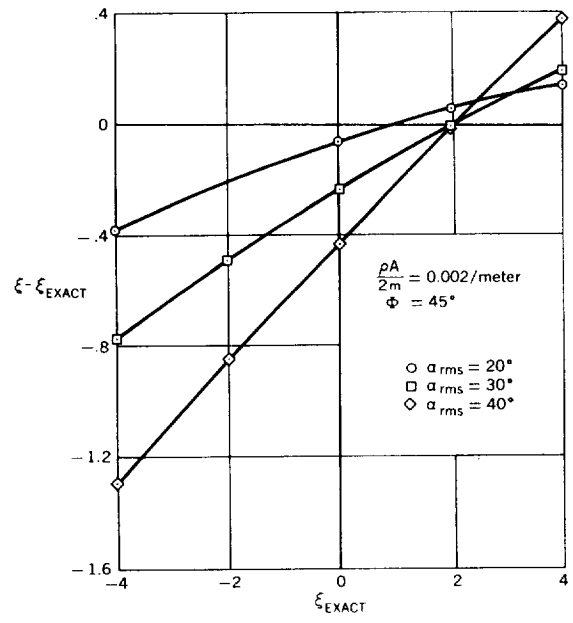

Fig. 7.16 Effect of large angles on deduced dynamic-stability parameter

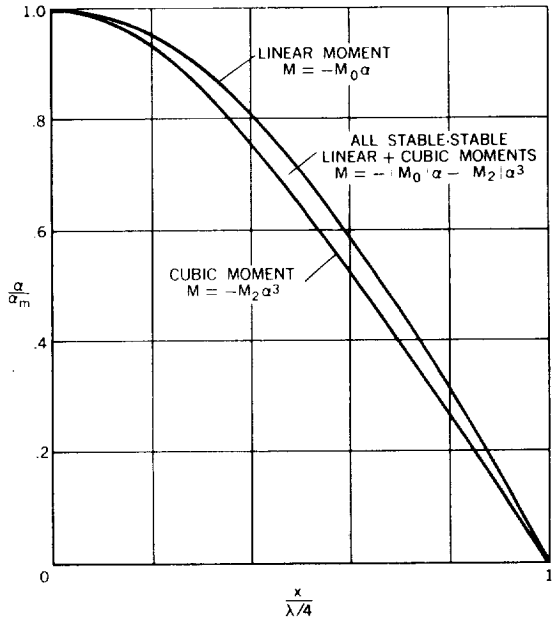

Fig. 7.17 Effect of nonlinear moment on wave-form of oscillation

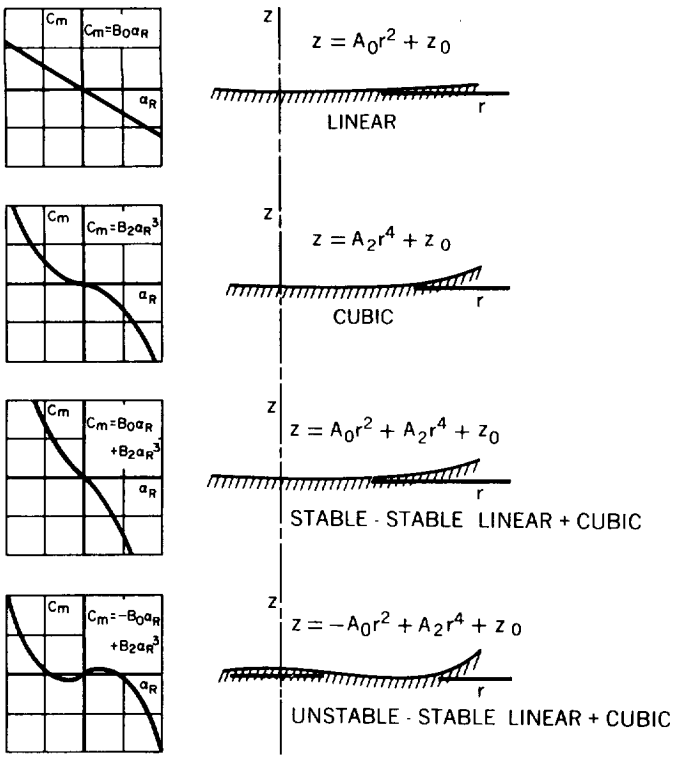

Fig. 7.18 Moment curves and surface profiles for analogue surfaces tested

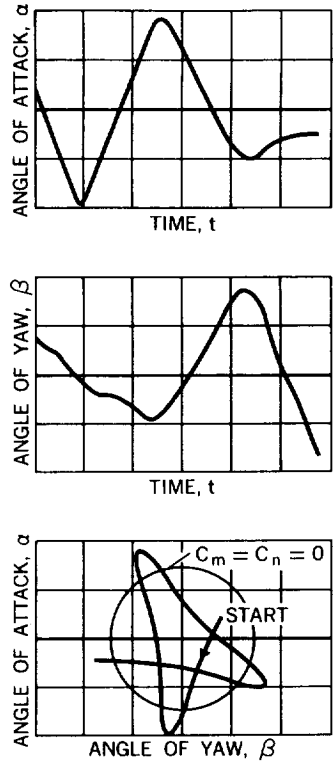

Fig. 7.19 Pitch and yaw histories for stable-unstable linear + cubic case

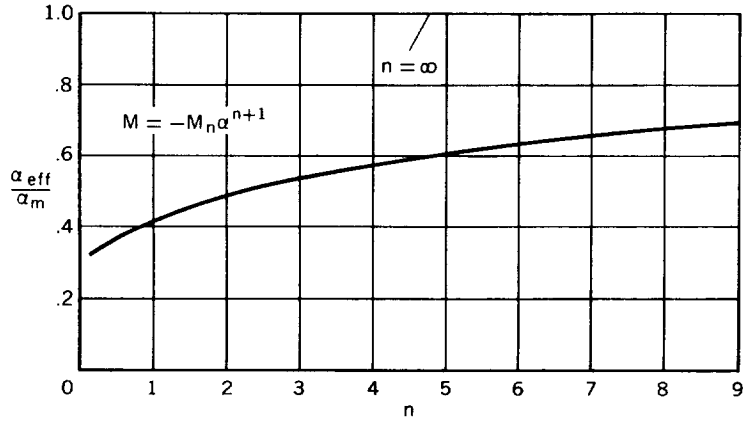

Fig. 7.20 Effective angle-of-attack parameter for a single-term nonlinear restoring moment

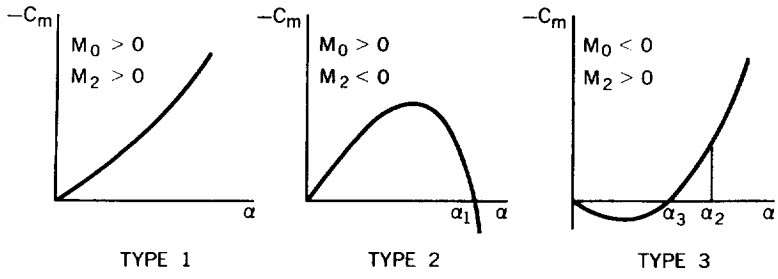

Fig. 7.21 Three types of linear + cubic moment

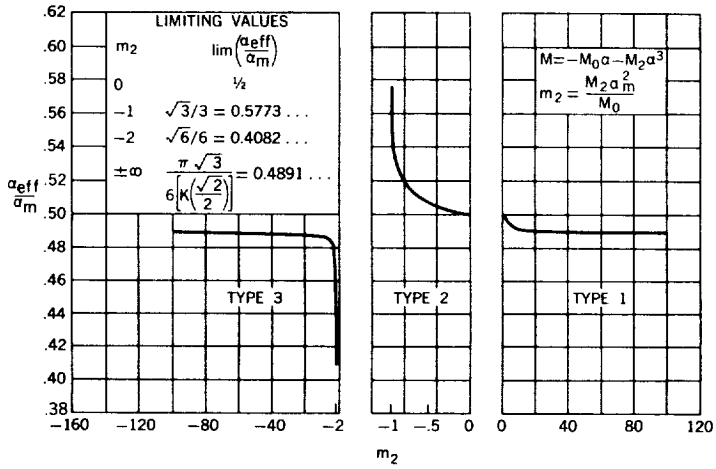

Fig. 7.22 Effective angle-of-attack parameter for a linear + cubic restoring moment

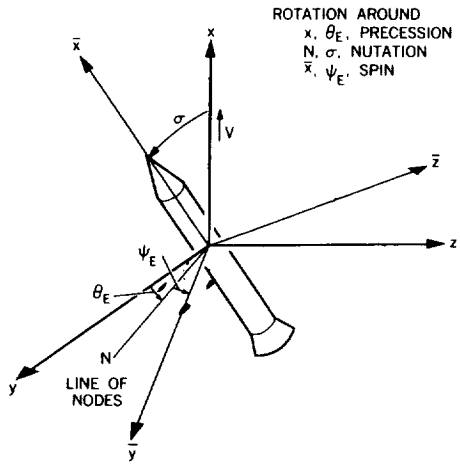

Fig. 7.23 Euler angles

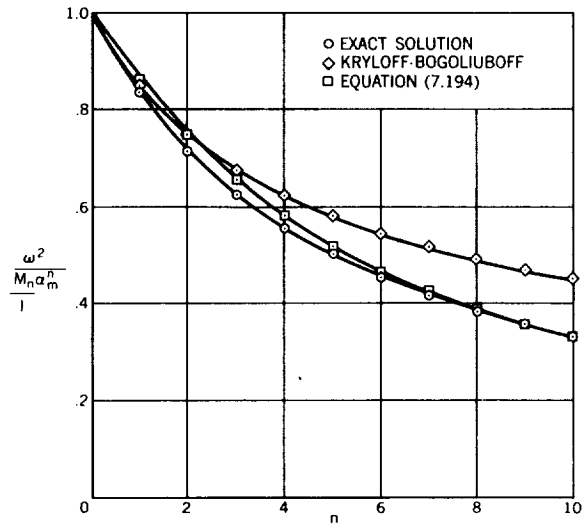

Fig. 7.24 Comparison of approximate solutions with exact solution; $M = -M_n\alpha^{n+1}$

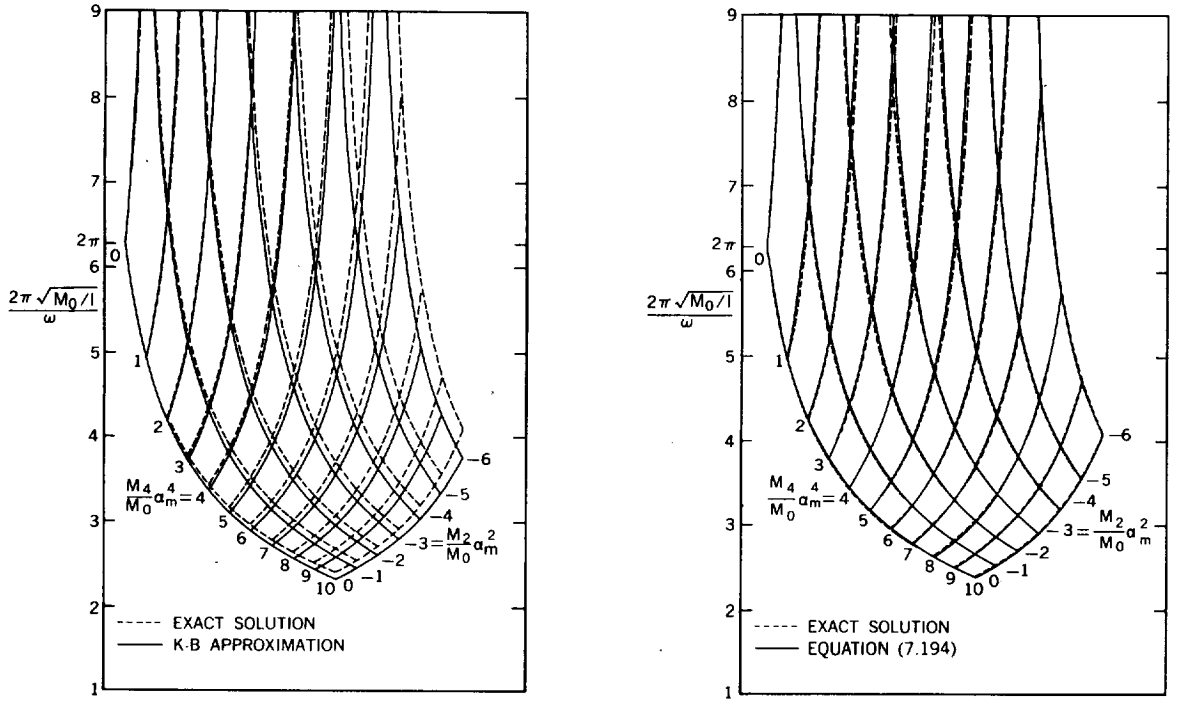

(a) K-B approximation versus exact solution

(b) Approximation of Reference 7.8 versus exact solution

Fig. 7.25 Carpet plots showing comparison of approximate solutions with exact solution; $M = -M_0\alpha - M_2'\alpha^3 - M_4\alpha^5$, $M_0 > 0$, $M_2 < 0$, $M_4 > 0$

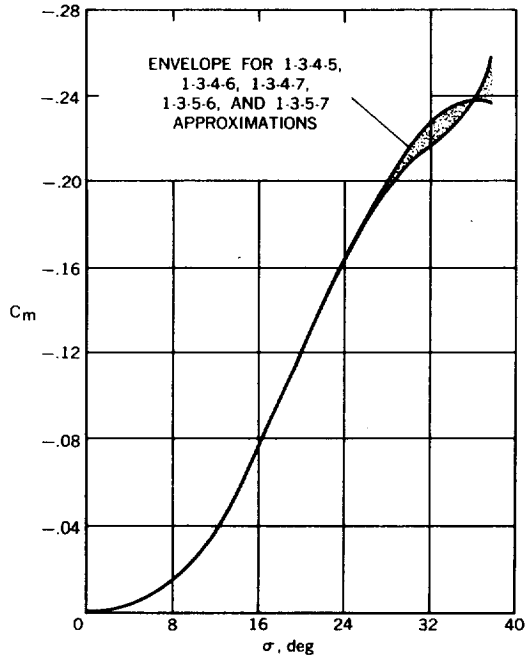

Fig. 7.26 Restoring-moment coefficients corresponding to various assumed moment representations

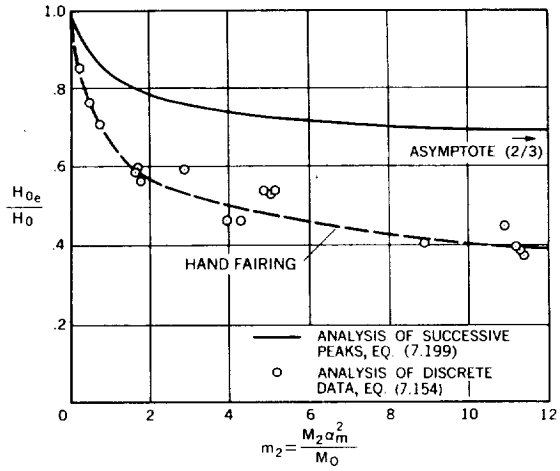

Fig. 7.27 Effective damping parameter for stable-stable linear + cubic static moments

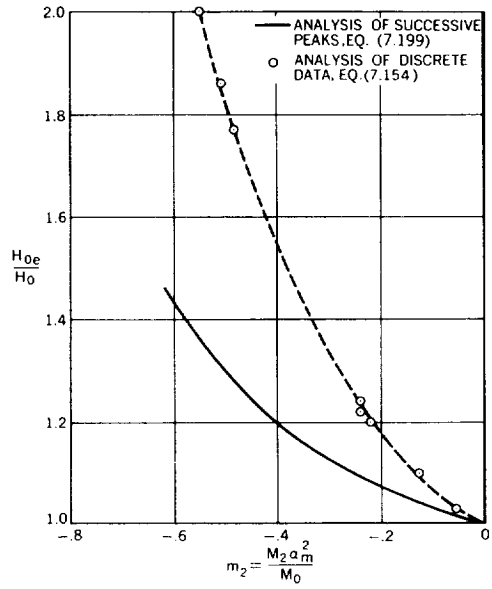

Fig. 7.28 Effective damping parameter for stable-unstable linear + cubic static moments

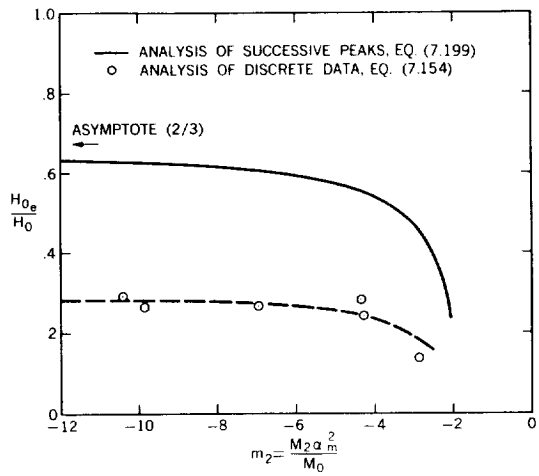

Fig. 7.29 Effective damping parameter for unstable-stable linear + cubic static moments

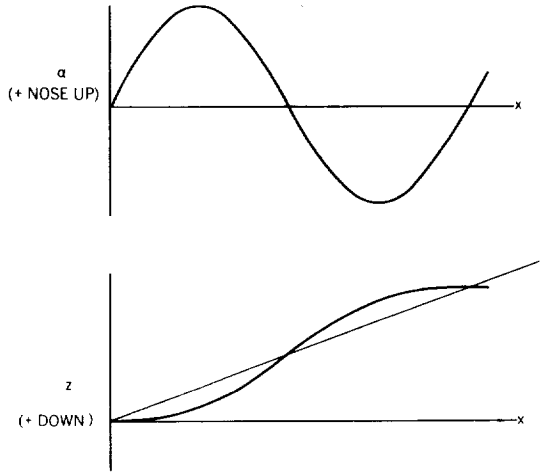

Fig. 7.30 Angle and displacement history

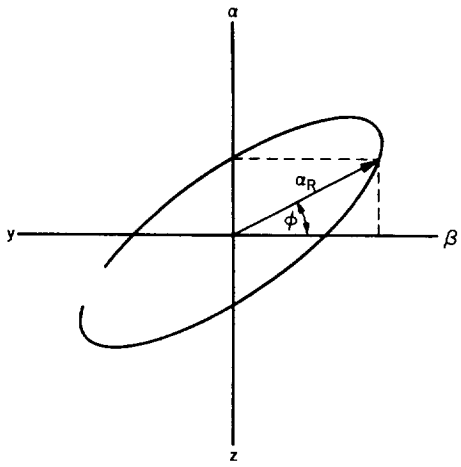

Fig. 7.31 Definition of angle ϕ

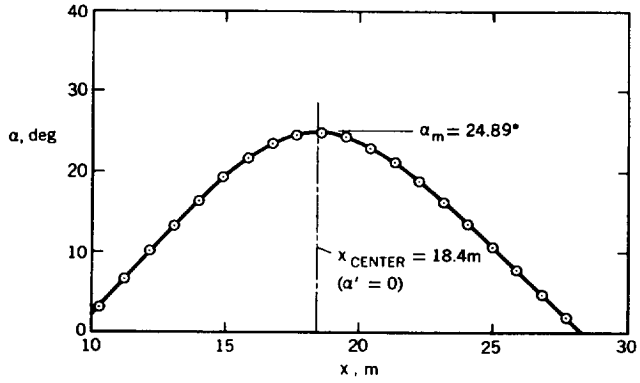

Fig. 7.32 Angle of attack versus flight distance

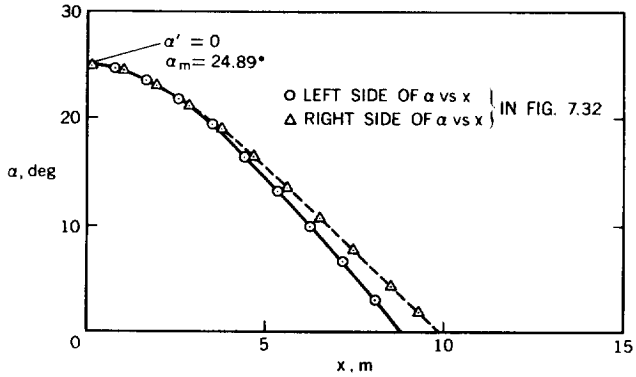

Fig. 7.33 Angle of attack versus flight distance (folded about x_{center})

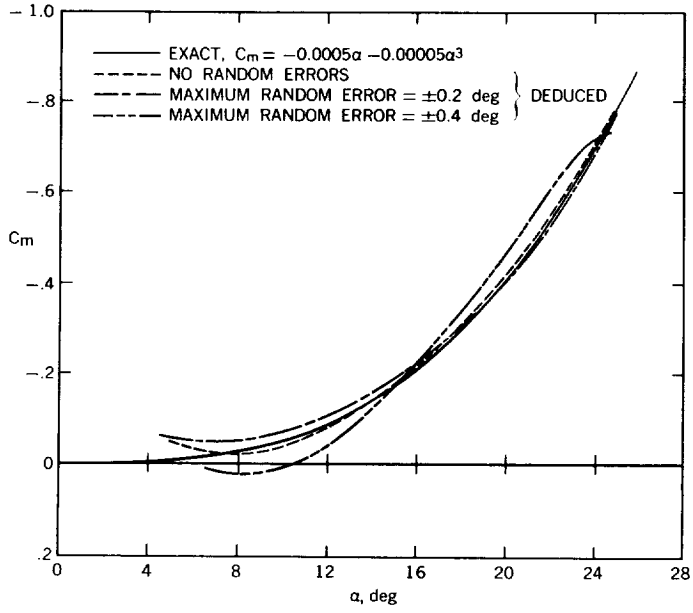

Fig. 7.34 Pitching-moment coefficient versus angle of attack

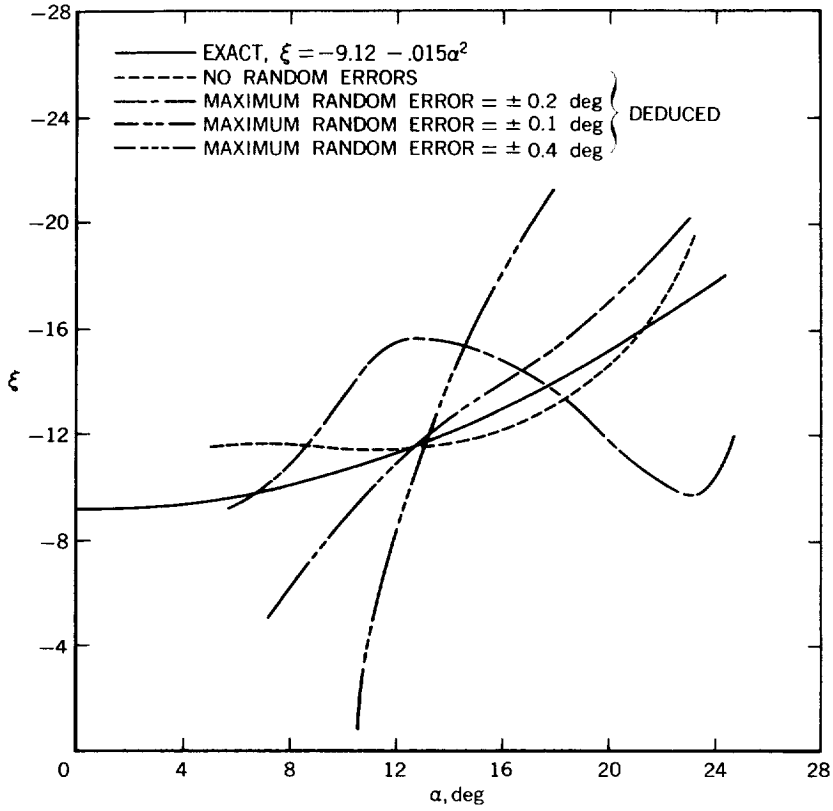

Fig. 7.35 Dynamic-stability parameter versus angle of attack

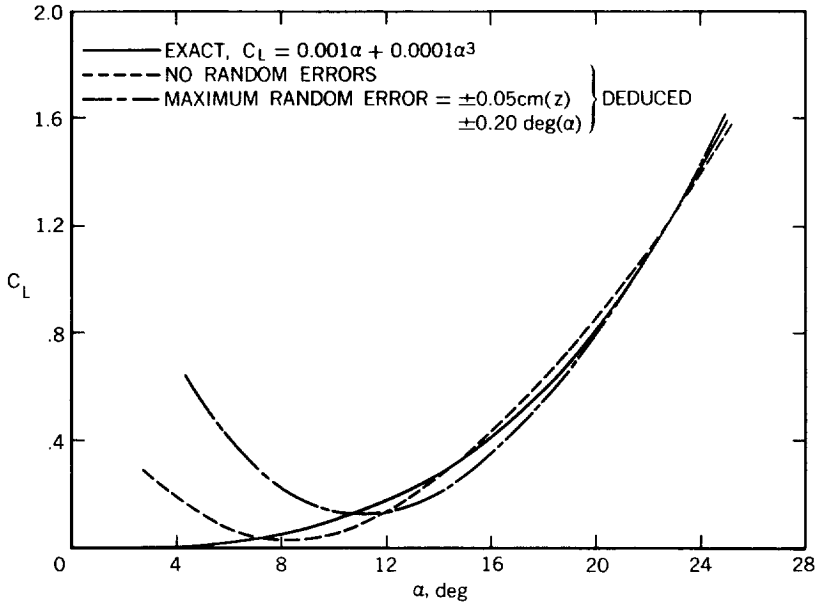

Fig. 7.36 Lift coefficient versus angle of attack

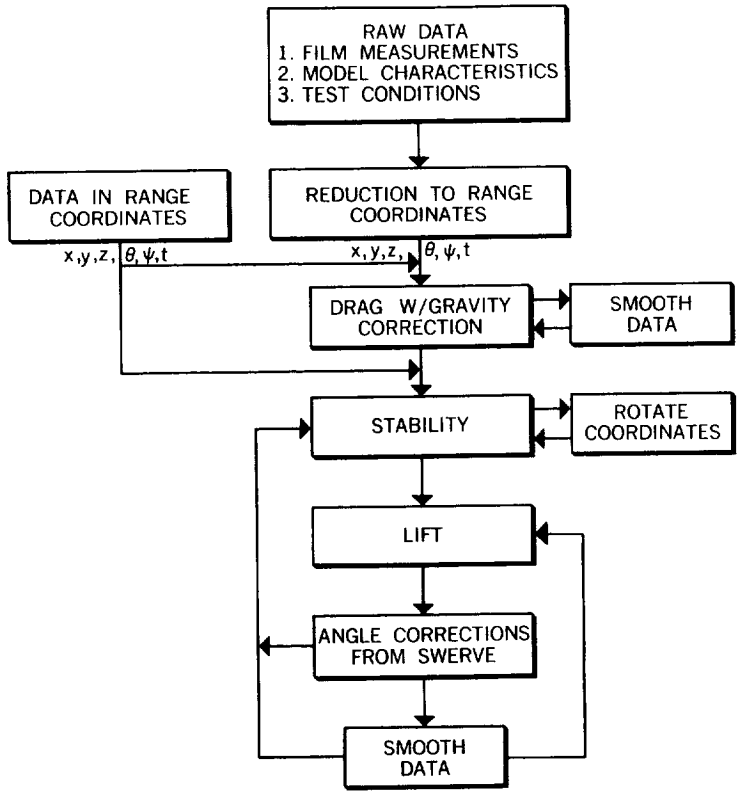

Fig.7.37 Flow chart of data-reduction procedure

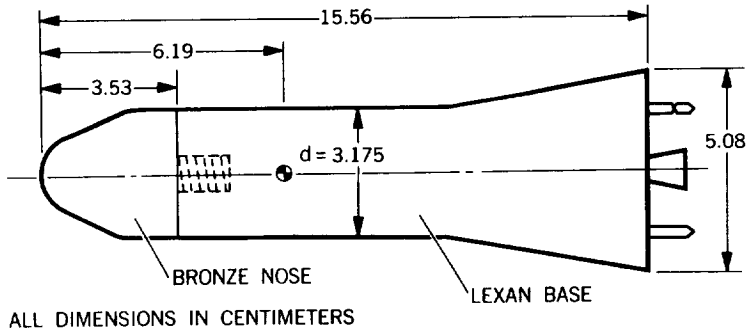

Fig.7.38 Model tested (AGARD HB-2)

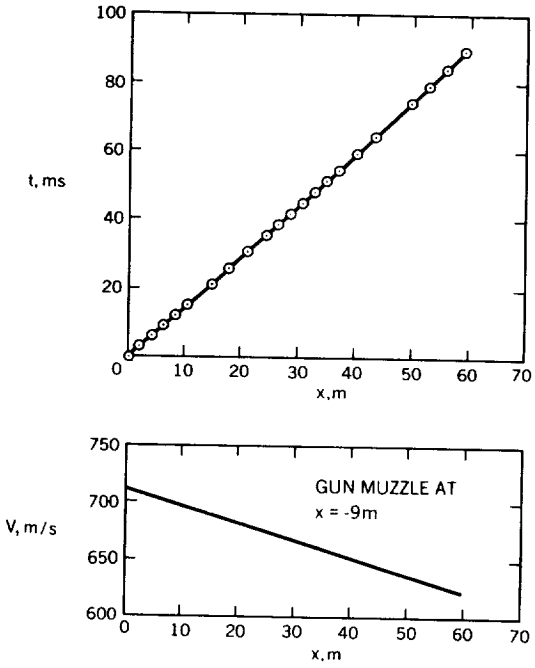

(a) Time and velocity versus distance

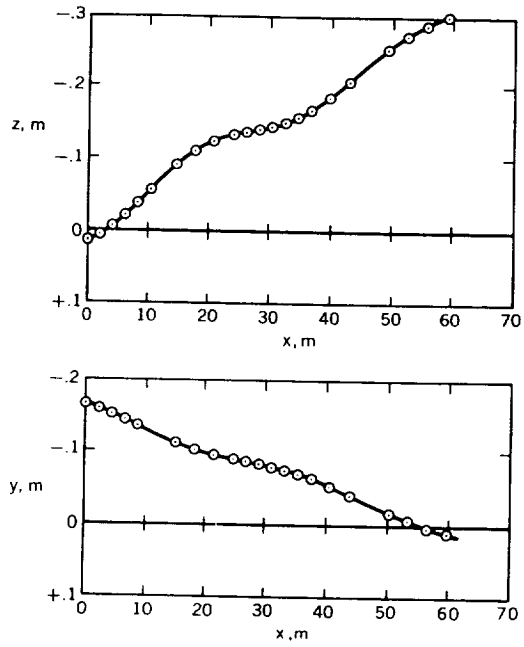

(b) Displacement versus distance

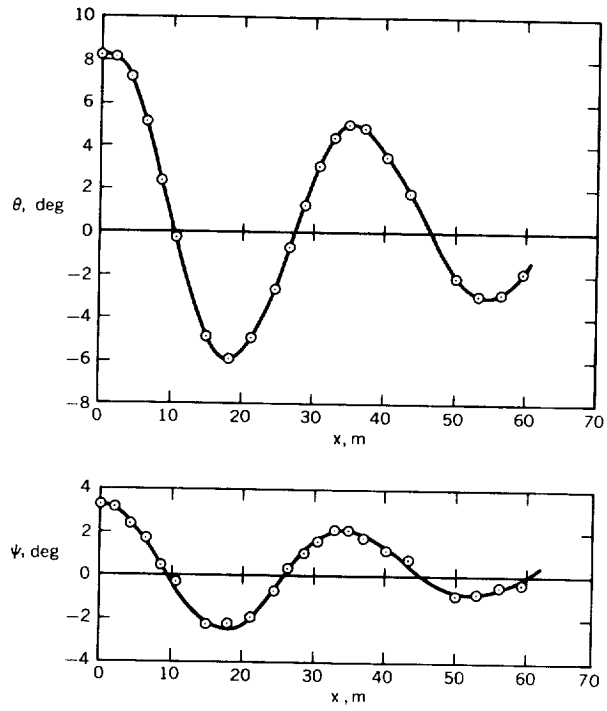

(c) Angular measurements versus distance

Fig. 7.39 Typical ballistic-range data

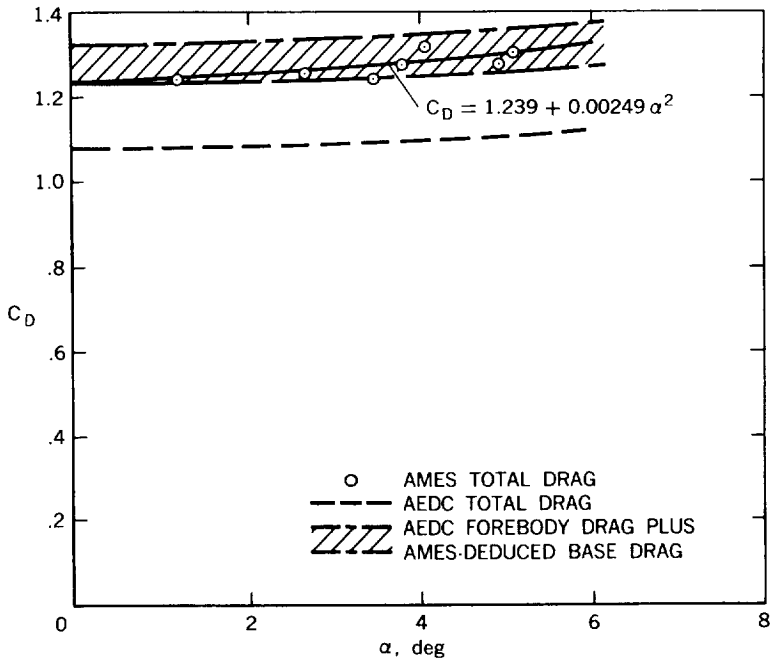

Fig. 7.40 Variation of drag coefficient with angle of attack

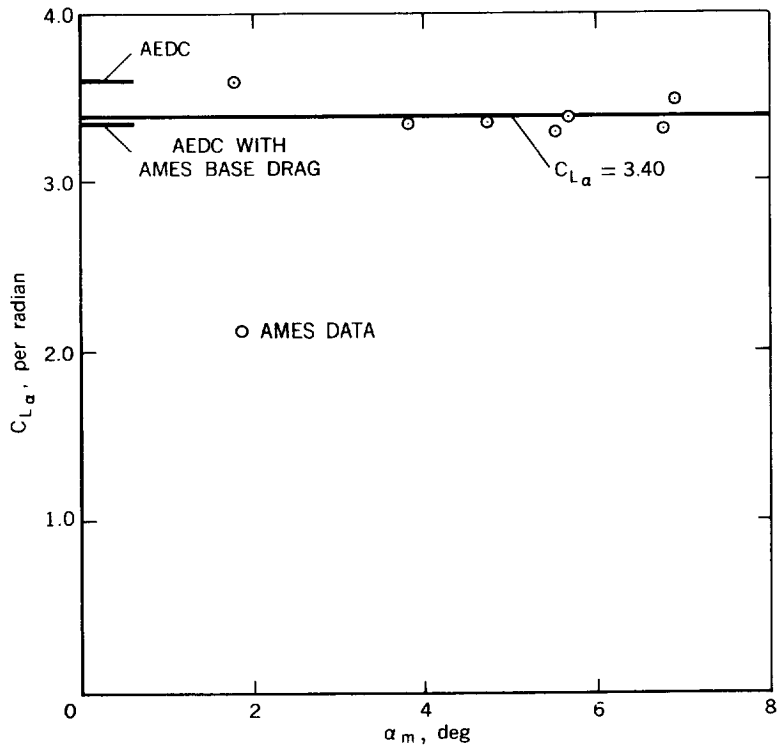

Fig. 7.41 Lift-curve slope

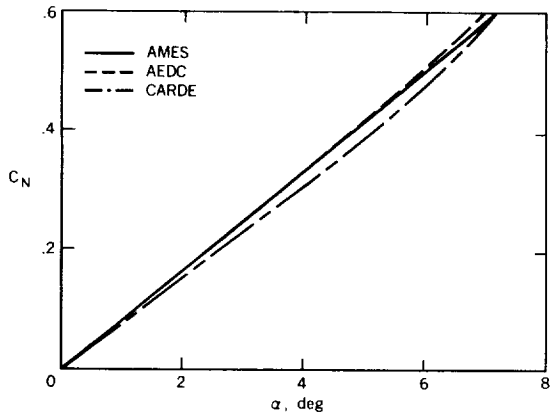

Fig. 7.42 Variation of normal-force coefficient with angle of attack

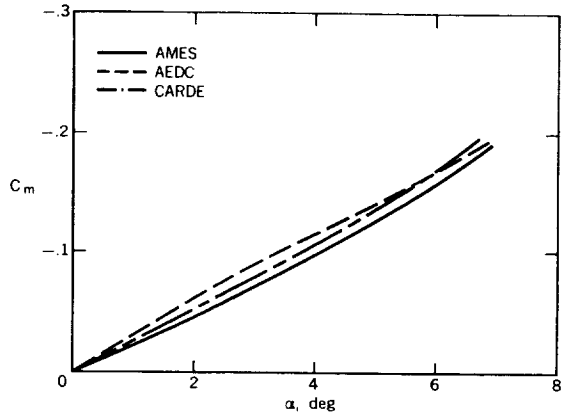

Fig. 7.43 Variation of pitching-moment coefficient with angle of attack

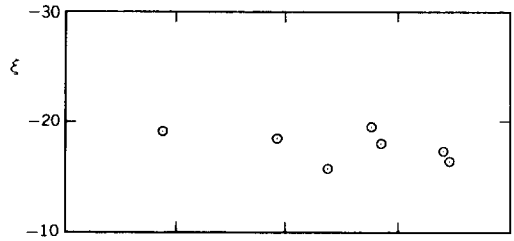

(a) Dynamic-stability parameter

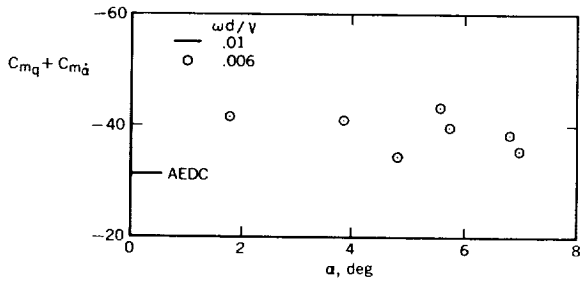

(b) Damping-in-pitch derivative

Fig. 7.44 Aerodynamic damping parameters

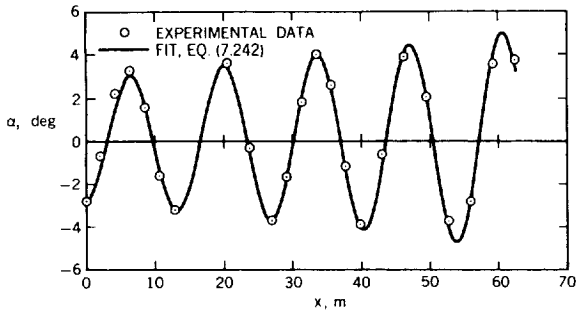

(a) Run 575

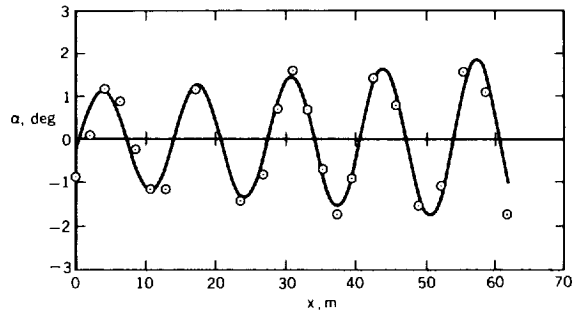

(b) Run 582

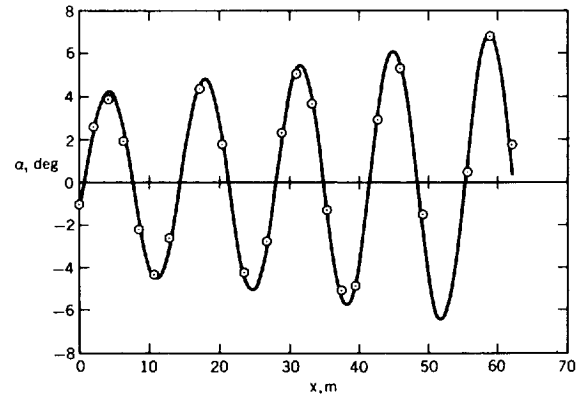

(c) Run 584

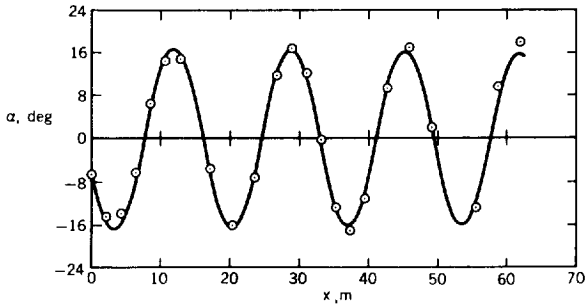

(d) Run 585

Fig. 7.45 Angle-of-attack histories for four Gemini flights